Modeling and Control of Plate Mill Processes

Pedersen, Lars Malcolm

1999

Document Version:
Publisher's PDF, also known as Version of record

Modeling and Control of Plate Mill Processes

Modeling and Control of Plate Mill Processes

Lars Malcolm Pedersen

Lund 1999

Published by Department of Automatic Control
Lund Institute of Technology
Box 118
SE-221 00 LUND
Sweden

ISSN 0280–5316
ISRN LUTFD2/TFRT–1053–SE

Printed in Sweden by Lunds Offset AB
Lund 1999

Contents

Preface

This thesis is the result of four years work at The Danish Steel Works Ltd., Frederiksværk, Denmark and the Department of Automatic Control, Lund Institute of Technology, Sweden. The first three years from 1992 to 1995 on full time and the last two years from 1997 to 1999 on half time. The first period has been supported financially by The Nordic Fund for Technology and Industrial Development and The Danish Steel Works Ltd. The last period has been financed exclusively by The Danish Steel Works Ltd. The thesis is directed towards control engineers with interest in the hot rolling and reheating processes, but might also be of interest for other technicians working with the two processes.

Beside this thesis the work has been published in the technical reports [Pedersen, 1993], and [Pedersen, 1998], my licentiate thesis [Pedersen, 1995b], and the conference papers and journal articles [Pedersen, 1994], [Pedersen, 1995a], [Pedersen and Wittenmark, 1996], [Pedersen, 1996], [Pedersen and Wittenmark, 1998a], [Pedersen and Wittenmark, 1998b], [Pedersen and Wittenmark, 1999], [Pedersen and Wittenmark, 1998d], and [Pedersen and Wittenmark, 1998c]. Furthermore 80 course credits equivalent to two years of study time have been collected as a necessary part of the Swedish PhD degree.

I would like to thank Kaj Groth and Niels Uhrbrand at The Danish Steel Works Ltd, Birgitte Rolf Jacobsen at the Danish Academy of Technical Sciences, and professors Björn Wittenmark and Karl Johan Åström at the Department of Automatic Control for making this project possible and for the freedom I have had in planning and carrying out the project work. I would furthermore like to thank all my colleagues at The Danish Steel Works and at The Department of Automatic Control for making these nice places to work. I would also like to direct a special thanks to the employees in the Plate Mill at The Danish Steel Works Ltd. for their cooperation and feedback in the experiments with the implementation of one of the control laws designed in this thesis.

At the Department of Automatic Control I would like to thank my advisor Björn Wittenmark for all his work in connection with this project and Bo Bernhardsson for proof reading this thesis several times. At MEFOS, which is the Swedish research institute for the steel industry, I would like to thank Bo Leden for his help in my work on the furnace modeling and control, and Hans Erik Wennerberg and Carsten Villadsen for always being prepared to help and discuss problems related to the project.

1

Introduction

The reheat furnace and the rolling mill can be considered two of the main processes in a plate mill. The reheat furnace is used for heating steel blocks, which is the raw material for the rolling mill and the rolling mill is used for turning the steel block to a plate by making it wider, thinner and longer.

The rolling mill and the furnace are quite different. The reheating is a thermal process, while the rolling mill is a mechanical process. The main items of interest in the operation of the furnace is the production capacity, the energy consumption and the temperature distribution of the steel blocks when they leave the furnace. The key variables of the rolling mill are production capacity, dimensional tolerances, plate flatness, and metallurgical parameters.

Naturally, the two processes interact. The production capacity of the rolling mill affects the operation of the reheat furnace and vice versa and to obtain proper flatness and thickness accuracy in the rolling mill a proper heating quality is important. Actually the two processes have even more in common:

- They are both large industrial processes where relatively small improvements of the performance can lead to large economical benefits.
- It is not feasible to measure the main variables of interest: slab temperature and plate thickness.
- The processes are multivariable, which implies that several variables should be handled simultaneously.
- Proper operation of the processes is crucial to the product quality and the capacity of the plate mill.

The above characteristics have made the reheat furnace and the plate mill to two of the key processes for automatic control in the steel industry and this is the reason for considering them in this thesis which consist of two separate parts

- Modeling and control of the plate thickness in a hot rolling mill.
- Modeling and control of the temperature of the steel blocks heated in the reheat furnace.

For more information on the two processes please refer to [Pedersen, 1993], and [Pedersen, 1998]. Further details on the control of the two processes will be given in Chapters 2, 3, and 8. Throughout the thesis data and specifications from the rolling mill and reheat furnace no. 2 at The Danish Steel Works Ltd. will be used in the work with the models and control algorithms. The design for the furnace control system is furthermore implemented at The Danish Steel Works Ltd.

1.1 Problem Formulation

The modeling in this thesis is made from a control engineer's point of view. Normally, control engineers work with relatively simple dynamical models for the processes. The relatively simple models make it possible to use some more or less advanced mathematics for analysis and design. The point of view in this work will therefore be different from the traditional approach, where either large and complex models are use for the furnace control or static nonlinear models typically are used for the rolling mill.

To be able to design better controllers, better models are needed. Therefore, development of suitable models and methods to determine the parameters of these models will be a key subject. To design an advanced control strategy we need a dynamical multivariable model. To minimize the number of parameters of the model and to ensure a good understanding, a physical model will be derived. Using the model it will be possible to evaluate the performance of the new control strategy using computer simulations and to analyze the stability of the processes. The digital control system on the reheat furnace makes it possible to perform experiments with the design for this process and therefore to evaluate the result of the design in practice.

We thus arrive at the following problem formulation:

> *The purpose of this thesis is to improve the performance of the slab temperature control for a reheat furnace and the plate thickness control for a hot rolling mill. The improvement will done by:*
>
> - *deriving dynamical multivariable models*
> - *designing control strategies on the basis of the models*

The performance of the improved control strategies will be evaluated by computer simulations and implementation of the slab temperature controller. The stability of the control loops will also be investigated in connection with the controller design.

It is usually hard to find a good mathematical model for a process at the first attempt. Process modeling therefore often is an iterative procedure. An initial modeling is necessary to decide which input and output signals to collect for the system identification where the parameters of the model are found. Using the results from the identification, the model is adjusted. Usually it is not necessary to collect new data. The controller will be designed when the model is ready. Sometimes the model is also changed in the controller design when the characteristics of the model are evaluated again. Inspired by [Gustavsson, 1975] we can illustrate the modeling, design, and implementation procedure by Figure 1.1.

1.2 Outline of the Thesis

The task of this thesis is to develop models and control strategies for the thickness control for a hot rolling mill and for the slab temperature control of a reheat furnace. The first part of the thesis is about thickness control and is more or less similar to my licentiate thesis. The last part of the thesis is about temperature control and has not been published before. This implies that the work of the thesis is presented in chronological order.

To give a background for this, three introductory chapters are included as an introduction to the modeling and design. The contents of the thesis are as follows:

Chapter 2: **The Thickness Control Problem**. This chapter gives a basic description of the hot rolling mill and the thickness control problem.

Chapter 3: **Thickness Control of Hot Rolling Mills**. Here it is described how the plate thickness is controlled today. The state of the art solution is analyzed and an example of where the traditional control fails is given.

Chapter 4: **Modeling of the Rolling Mill**. In this chapter the new mathematical models for the rolling mill are derived. The models are later used for the system identification, the controller design, and the computer simulations.

Chapter 5: **Thickness Control—Data Collection**. To find the parameters of the models, measurements of the input and output

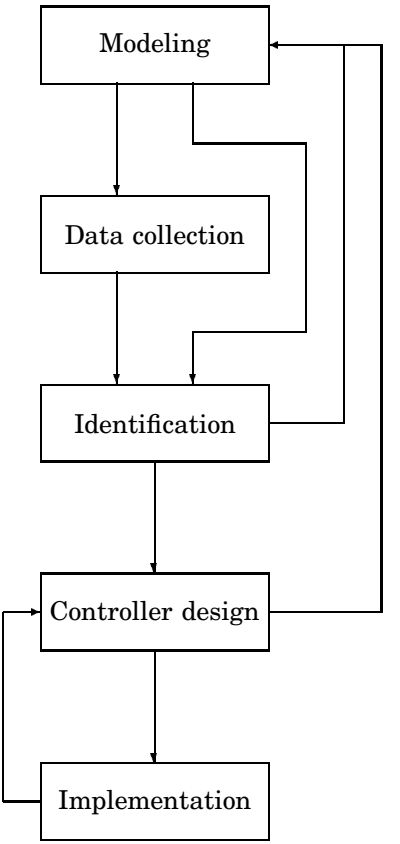

Figure 1.1 Flow diagram for the work in connection with the modeling and controller design. The figure illustrates the iterative nature of the modeling and design process.

variables are needed. The measurement procedure and the processing of the measurements are described here.

Chapter 6: **Thickness Control—System Identification**. The parameters of the model are determined. When this is done the models are ready for controller design, and computer simulations.

Chapter 7: **Thickness Control—Design**. The control law for the thickness control is designed and performance of the controller is evaluated using computer simulations. The stability and the effect of the time varying material characteristics are also

investigated.

Chapter 8: **The Slab Temperature Control Problem**. Here a basic description of the reheat furnace and the furnace control system is given. Some basic process characteristics are also analyzed.

Chapter 9: **Temperature Control—Data Collection**. In this chapter the data collection device is described and an example of the data is given.

Chapter 10: **Temperature Control—System Identification**. Contains descriptions of the models for the furnace and slab temperatures and results from the system identification of the model parameters.

Chapter 11: **Temperature Control—Design**. Includes design of the linear control law for the control system on the furnace at The Danish Steel Works Ltd. and a new nonlinear control algorithm for the slab temperatures.

Chapter 12: **Temperature Control—Simulations**. Evaluation and comparison of the performance of the linear and nonlinear controllers designed in the previous chapter.

Chapter 13 **Temperature Control—Experimental Results**. Contains a description and results from the experiments of the linear controller at the furnace no. 2 at The Danish Steel Works Ltd.

The conclusions on the work done in this thesis are given in Chapter 14. The important variables used throughout the thesis are listed in the last chapter: **Notations**.

2

The Thickness Control Problem

In this chapter a more detailed description of the hot rolling process is given. The description will serve as a basis for the work in the following chapters. The main purposes are to give the reader a feeling for the problem and to introduce the necessary concepts. It should here be noted that this is a description of the rolling process seen from a control engineer's point of view and therefore a lot of details are left out. For more detailed descriptions of the process the reader should read the references as a supplement.

In the following, hot rolling is first described in general and a short introduction to the planning of the rolling sequence is given. The functionality of the rolling mill, relevant for the thickness control, is also described. After this the thickness control problem is described in more detail.

2.1 Hot Rolling of Steel Plates

The purpose of the hot rolling process is to turn preheated steel blocks into plates, that is to make them longer and thinner. The steel blocks are called *slabs*. The thickness of the slabs is reduced by pulling them through two parallel rolls, see Figure 2.1.

Each time the plate is pulled through the rolls is called a *pass* and the difference between the ingoing and outgoing thickness is called the *thickness reduction*. As indicated in Figure 2.1 it is possible to change the outgoing thickness by moving the upper roll. Due to physical limitations the thickness reduction in one pass is limited. It is therefore necessary with several passes before the plate has obtained the desired thickness. In practice this is done by reversing the rolls when the pass is finished and

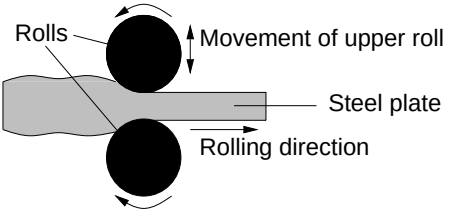

Figure 2.1 The principle of the hot rolling process. The thickness of the steel plate is reduced by pulling it through two parallel rolls.

then rolling the plate in the other direction. The series of passes from slab to finished plate is called a *pass schedule*. The above process is called *hot rolling* and the equipment performing the deformation of the steel plate is called a *hot rolling mill*.

The thickness of the slabs at The Danish Steel Works Ltd. are 100, 210, or 260 mm before the rolling is started. Before rolling the slab temperature is around 1120°C and after rolling the plate temperature is between 1000°C and 800°C. Normally the width of a finished plate is between 2 m and 3 m, the length is between 10 m and 25 m, and the thickness is between 6 mm and 100 mm. The weight of one plate varies between 1,000 kg and 13,000 kg. The forces obtained during rolling are quite large, the maximal permitted vertical force, the *rolling force*, is 37.3 MN. This is equivalent to the weight of 1900 Volvo cars! To be able to handle these large forces the hot rolling mill is quite a solid construction, it is 13 m high, 5 m wide and the diameter of the rolls used for deforming the plate is 1 m. Even if the equipment is large it is possible to obtain quite accurate dimensions of the rolled plates, typical thickness tolerances for thin plates are in the range of ± 0.2 mm.

A schematic diagram of the rolling mill is shown in Figure 2.2. When comparing to Figure 2.1 it is seen that a number of things are added. The work rolls are the rolls used for deforming the steel plate, while the backup rolls are used for supporting the work rolls. This is to prevent excessive bending of the work rolls. The mill frame is used for holding the rolls and the equipment used for positioning the *upper roll pack*, which consists of the upper backup and work rolls. There are two ways of adjusting the position of the upper roll pack:

- using the screws;
- using the hydraulic positioning systems.

The screws are, as the name indicates, two large screws driven by two dc-motors while the hydraulic positioning systems are two grease cylinders

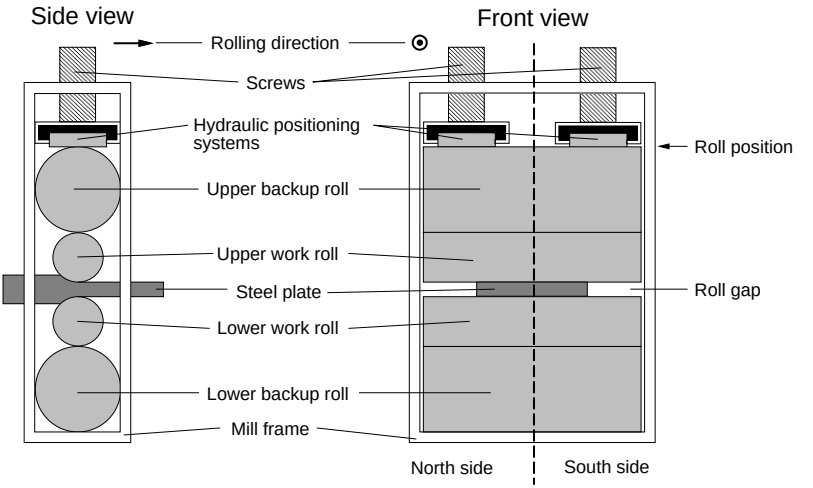

Figure 2.2 Principal diagrams of the rolling mill seen from the side and the front. The main thing to note here is the functionality of the positioning systems for the upper rolls.

placed between the screws and the upper roll pack. The screws are used for large position changes between passes while the hydraulic systems are used for small position changes between and during the passes. There are screws and hydraulic systems at both sides of the rolls. The two sides are in the thesis called the north and the south sides respectively, due to the geographical layout at The Danish Steel Works Ltd. Note that it is possible to adjust the position of the roll pack independently at the north and south sides and we therefore have a multivariable system.

The main limitation of the rolling mill is the magnitude of the supply pressure of the hydraulic systems. If the pressure due to the rolling force exceeds this limit it is not possible for the hydraulic systems to operate and the rolling is terminated. This has to be taken into consideration when planning the thickness reductions of the pass schedule.

Using a minimum of time for rolling a plate has several advantages. One is that the rolling is finished while the plate still is hot and therefore soft. Another advantage is that the rolling mill capacity is maximized. Careful planning of the pass schedule to ensure maximal utilization of the rolling mill capacity is therefore an important matter. Here maximal utilization implies that all passes should be rolled with a rolling force as close to the limit as possible. Today the planning is handled by a computer

control system which optimizes the thickness reduction in each pass to ensure that the rolling is done as fast as possible, for a description of a similar system see [Davies *et al.*, 1983]. The computer control system finds the desired set-points for the roll position, rolling force, and plate thickness. These set-points are transferred to the thickness control system, which operates in two modes:

- *relative control*, used the first 5 to 15 passes dependent on plate length, width and thickness
- *absolute control*, used in the last 4 passes.

The main difference between the absolute and relative control modes is the way the thickness reference is generated. In relative control the task of the thickness control system is to keep the thickness close to the value obtained without thickness control in the beginning of the pass. The goal of the absolute control is to keep the thickness as close as possible to the value specified by the planning system. The purpose of the relative control is to prepare the plate for the absolute control. The absolute control part is the one relevant for the thickness accuracy.The thickness control algorithm is analyzed in Chapter 3.

2.2 Controlling the Plate Thickness

The reason why it is necessary to control the plate thickness during a pass is that the vertical forces obtained in connection with the deformation of the steel plate are sufficiently large for elastic deformation of the rolling mill. At the maximal rolling force the deformation of the rolling mill is 7 mm, which is of the same order of magnitude as the plate thickness for the thin plates in the final passes. Due to the elastic deformation of the rolling mill, two different concepts for the roll gap, see Figure 2.2, are used, the *unloaded roll gap*, which is the roll gap between the passes, and the *loaded roll gap*, which is the roll gap during the pass.

The zero point of the unloaded roll gap varies with time. This is because of the thermal expansion of the rolls due to heating by the steel plates and wear of the work rolls. It is therefore necessary to find the zero point for the unloaded roll gap regularly. This can be done is by pressing the rolls together with a large force. When the measured position is corrected for the mill deflection we have a reliable mean value for the zero point of the unloaded roll gap. Another thing that affects the zero point of the unloaded roll gap is the roll eccentricity and ovalness. These phenomena vary considerably faster with time than the wear and thermal expansion. Therefore more advanced methods are needed to compensate for the roll ovalness and eccentricity.

Due to the bending of the rolls the plate is always thicker at the center than at the edges, this phenomenon is called *plate crown*. This results in an unnecessary use of material. To cancel this effect, to some extent, the work rolls are made thicker at the center than at the edges. This is referred to as *roll crown*.

If the rolling force during the pass was constant it would be possible to preset the position of the upper roll pack to ensure that the loaded roll gap was equal to the desired plate thickness. Unfortunately, the rolling force is hard to predict and it varies during the pass. These variations are due to different characteristics of the steel plate along the plate length:

- variation of the ingoing plate thickness;
- variation of the plate hardness.

The variations of the ingoing plate thickness are due to imperfect thickness control and the variations of the plate hardness are mainly induced by variations of the plate temperature. The temperature variations are due to inhomogeneous heating by the reheating furnaces and cooling by the roller tables used for transporting the plate. As will be seen in the data collection in Chapter 5 these disturbances have a significant influence on the plate thickness. In general the dynamics of the hydraulic systems are considerably slower than the dynamics of the mill stand. This is one of the reasons why it is difficult to eliminate the high frequency variations of the plate thickness. The steady state gain and the dynamics of the rolling process vary with material properties, this will be investigated in Chapter 7. Apart from the material properties the rolling force also varies with the thickness reduction, see [Roberts, 1983].

The thickness of the steel plate is controlled by varying the position of the hydraulic systems during the pass, that is, the hydraulic systems are the actuators of the thickness control system. A main difficulty in connection with the thickness control is that until now it has not been possible to measure the plate thickness during the rolling. The reason is that it is difficult to build reliable equipment for measuring the plate thickness because of the heat radiation from the steel plate and the steam from the water used for cleaning the plate surface during rolling. Since it is not possible to measure the thickness during the the pass it is necessary to estimate it. This estimate can then be updated using a value of the thickness measured after the last pass, see [Ferguson *et al.*, 1986].

The available measurements for the thickness control are:

- the positions of the screws;
- the positions of the hydraulic systems;
- the rolling forces at the north and south sides.

The rolling force is interesting because it is an internal variable which is closely related to the plate hardness. Since it is possible to get a reliable measurement of the rolling force it is often used for the thickness control, see [Wood *et al.*, 1977].

2.3 Conclusions

With the above basic description of the control problem in mind we conclude that the thickness control mainly is a regulator problem where the main task of the thickness control is to eliminate the effects of process disturbances. An additional difficulty, which makes the thickness control problem non-standard, is that it is not possible to measure the process output in connection with the control.

A natural question to be asked now is: *How is the thickness control problem solved today?* This question will be treated in the following chapter.

3

Thickness Control of Hot Rolling Mills

The purpose of this chapter is to describe the state of the art (1995) of thickness control for hot rolling mills. This is done to prepare the reader for the fundamental ideas used in the following chapters.

First a general statement of the thickness control problem is given and a general controller structure is derived. After this one of the state-of-the-art models is described and using this model the structure of a thickness controller is found. The performance and stability of this control structure is then analyzed. The thickness control laws rely on a fundamental symmetry assumption and in the last section an example is presented of what happens if the symmetry assumption is not fulfilled. This is done to illustrate the potential advantages of a multivariable control strategy.

3.1 What is Needed?

Inspired by Chapter 2 we formulate the thickness control problem for hot rolling mills:

> *The purpose of the thickness control for a hot rolling mill is to maintain the specified thickness despite:*
>
> - *variations of the plate hardness;*
> - *variations of the ingoing thickness.*
>
> *Since the plate thickness can not be measured during rolling it has to be estimated.*

We conclude that we need a model for the controller design, a controller able to cancel the above disturbances, and an observer for estimating the

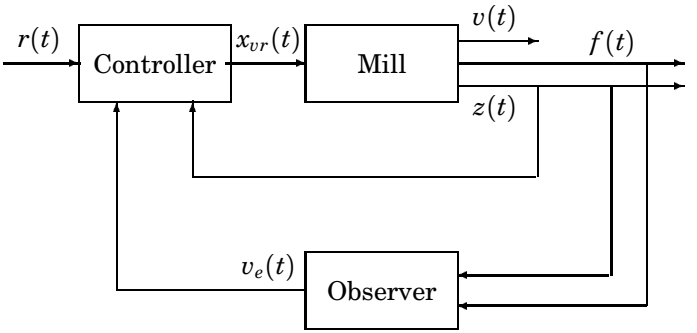

Figure 3.1 General structure of the thickness controller. Here f is the rolling force measurement, z is the roll position measurement, v is the plate thickness, r is the thickness reference, v_e is the estimate of the plate thickness, and x_{vr} is the control signal for the positioning systems. The observer is necessary since it is not possible to measure the plate thickness during rolling.

plate thickness during the rolling. Later on two models will be used. One for the controller design and one used in the observer for estimating the plate thickness. The reason for using two different models is that the rolling force measurement is available when implementing the controller, but is not of much use when designing the controller since it is just an internal variable of the rolling mill and not an independent input of the process. As will be seen later the rolling force is of good use when the thickness is to be estimated, and it is therefore used as an input for the observer.

At our disposal we have the signals, see Figure 2.2,

- the upper roll positions at the north and the south sides, which are the sums of the screw and the hydraulic positions, $z^T = [\, z_n \quad z_s \,]$;
- the rolling force measurements at the north and south sides, $f^T = [\, f_n \quad f_s \,]$.

The variables we want to control are

- the plate thickness at the north and south sides $v^T = [\, v_n \quad v_s \,]$.

The principal structure of the thickness controller is shown in Figure 3.1. Usually the same controller structure is used for absolute and relative control. The controller parameters can be adjusted dependent on the mode of operation if necessary. The controller structure is used both for the existing control strategy and the new control strategy developed in this report.

3.2 What is Done Already?

Looking at the existing thickness control strategies described in various articles and papers we conclude that the models and observers used for control purposes for the rolling stand are static and scalar, see for instance [Choi *et al.*, 1994], [Edwards, 1978], [Asada *et al.*, 1986], [Bryant *et al.*, 1975], [Ferguson *et al.*, 1986], [Ginzburg, 1984], [Atori *et al.*, 1992], [Nakagawa *et al.*, 1990], [Saito *et al.*, 1981], [Teoh *et al.*, 1984], and [Yamashita *et al.*, 1976]. The scalar models are found by using the mean values of the variables at the north and south sides.

Normally the rolling mill is modeled as a nonlinear spring $K(f,w)$ where w is the plate width f are the rolling forces. The plate is modeled as a time varying spring $a_m(t)$. Since a_m and K are spring constants they are real and positive.

Assuming that the plate thickness is equal to the loaded roll gap we find that the mean value of the deflection of the rolling mill is the difference between the mean value of the plate thickness after pass $\overline{v}$ and the mean value of the roll positions $\overline{z}$ and ovalness o, see Figure 3.2,

$$\overline{v}(t) - \overline{z}(t) - o(t),$$

where $\overline{z} = \frac{1}{2}(z_n + z_s)$, , and $\overline{v} = \frac{1}{2}(v_n + v_s)$. v_n is the plate thickness at the north edge and v_s is the plate thickness at the south edge.

The deflection of the plate is equal to the thickness reduction, see Figure 3.2

$$\overline{v}_{-1}(t) - \overline{v}(t),$$

where $\overline{v}_{-1} = \frac{1}{2}(v_{-1n} + v_{-1s})$. Here v_{-1n} is the ingoing thickness at the north edge and v_{-1s} is the ingoing thickness at the south edge.

Since the rolling mill and the plate are modeled as springs we find the mean value of the rolling force $\overline{f}$ by multiplying the deflection of the rolling mill by the mill spring coefficient K and the deflection of the plate by the plate hardness a_m. As illustrated by Figure 3.2 these two forces are equal and we therefore arrive at the equation

$$\overline{f}(t) = a_m(t)(\overline{v}_{-1}(t) - \overline{v}(t)) = K(f,w)(\overline{v}(t) - \overline{z}(t) - o(t)), \tag{3.1}$$

where $\overline{f} = \frac{1}{2}(f_n + f_s)$. We are now able to derive the equations for the mean value of plate thickness $\overline{v}$ after pass, where we suppress the arguments for convenience

$$\overline{v} = \frac{1}{K}\overline{f} + \overline{z} + o \tag{3.2}$$

$$= \frac{K}{K + a_m}(\overline{z} + o) + \frac{a_m}{K + a_m}\overline{v}_{-1}. \tag{3.3}$$

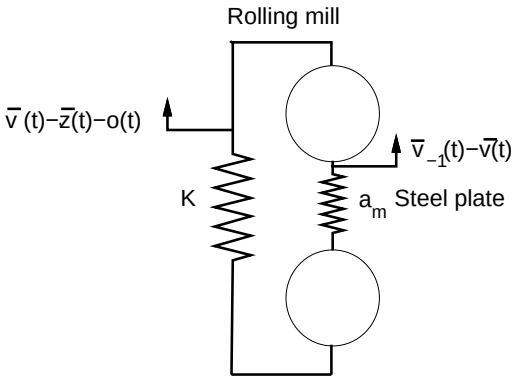

Figure 3.2 One of the state-of-the-art models used for thickness control today. The steel plate and the rolling mill are modeled as interconnected springs. a_m is the spring coefficient of the material and K is the mill spring coefficient of the mill. Note that the representation of the thickness reduction in the figure is a bit unphysical to obtain a simpler representation in the illustration.

We now see why the mean value of the force $\overline{f}$ is used for the thickness estimation. Using the rolling force it is possible to estimate the plate thickness without knowing the plate hardness a_m and the ingoing thickness $\overline{v}_{-1}$. The roll eccentricity and ovalness o still enters (3.2) as an unmeasurable disturbance. Eq. (3.2) is often referred to as the *gaugemeter equation*. Note that the gain of the relation between mean value of the thickness $\overline{v}$ and the mean value of the position $\overline{z}$ in (3.3) is time varying due to the variations of the plate hardness a_m and the mill spring coefficient K.

The two hydraulic systems are usually controlled using two inner loops, one for the south side and one for the north side, see for instance [Huzyak and Gerber, 1984], [Ginzburg, 1984], [Saito *et al.*, 1981], and [Nakagawa *et al.*, 1990]. We model the hydraulic systems as a second order system, with unit steady state gain

$$\overline{z}_h = G_h \overline{z}_r = \frac{\omega_h^2}{p^2 + 2\zeta_h \omega_h p + \omega_h^2} \overline{z}_r \tag{3.4}$$

where $\overline{z}_r$ is the reference for the positioning system from the thickness controller and $\overline{z}_h$ is the mean position of the hydraulic systems found using G_h. For a perfect model fit we have $\overline{z} = \overline{z}_h$. Here $p = \frac{d}{dt}$ is the differential operator, and G_h is the transfer function for the hydraulic system.

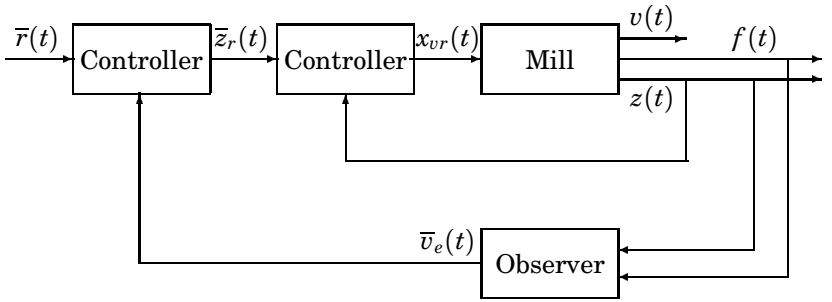

Figure 3.3 The state-of-the-art thickness control. Here $\overline{r}$ is the reference for the mean value of the plate thickness $\overline{v}$, $\overline{v}_e$ is the estimate of the mean value of the thickness, $\overline{z}_r$ is the reference for the position controllers, and x_{vr} are the control signals for the positing systems. The output signals are the roll positions z, the rolling forces f, and the plate thicknesses v. In this solution the hydraulic positioning systems are controlled by separate controllers.

Using (3.2) we obtain the observer for the thickness estimation

$$\overline{v}_e = \frac{1}{\overline{K}}\overline{f} + \overline{z} + o_e,$$

where $\overline{K}$ is an estimate of the mean value of the mill spring coefficient for the north and south sides, o_e is an estimate of the roll eccentricity and ovalness o, and $\overline{v}_e$ is an estimate of the mean value of the thickness $\overline{v}$. Using this for estimating the plate thickness we have the control law

$$\overline{z}_r = C_v(p)\,(\overline{r} - \overline{v}_e) = C_v(p)\left(\overline{r} - \frac{1}{\overline{K}}\overline{f} - \overline{z} - o_e\right), \tag{3.5}$$

where C_v is the transfer function for the thickness controller and $\overline{r}$ is the reference for the mean thickness $\overline{v}$.

The structure of the control system is shown in Figure 3.3. For more detailed descriptions of the thickness control problem, see [Middleton and Goodwin, 1990] and [Grimble and Johnson, 1988].

3.3 Analysis of the State-of-the-Art Solution

Introducing $\overline{z}_h$ for $\overline{z}$ in (3.5) and using (3.4) and (3.1) we find that

$$\overline{z}_h = \frac{G_h C_v}{1 + G_h C_v}\left(\overline{r} - \frac{a_m}{\overline{K}}(\overline{v}_{-1} - \overline{v}) - o_e\right).$$

Inserting this for $\overline{z}$ in (3.3) and assuming that the material hardness a_m varies slowly and that the estimate of the mill spring coefficient $\overline{K}$ is kept constant during the pass we find that

$$(1-\varphi G_t)\overline{v} = \frac{K}{a_m+K}G_t\overline{r} + \frac{K}{a_m+K}(o - G_t o_e) + \frac{a_m}{a_m+K}\left(1-\frac{K}{\overline{K}}G_t\right)\overline{v}_{-1}, \quad (3.6)$$

where $G_t = (G_h C_v)/(1+G_h C_v)$ and $\varphi = (K/\overline{K})a_m/(a_m+K)$. Normally an integrator is included in the thickness controller C_v and therefore the steady state gain of G_t will be 1.

Performance

Several things can be concluded from (3.6). If $\overline{K} = K$ we will have full compensation for the mill deflection ($\overline{v} = \overline{r}$) at steady state, since $1-\varphi G_t$ reduces to $K/(a_m+K)$ and the term on v_{-1} vanishes. However, if $o_e = 0$ then the roll eccentricity and ovalness o affects the mean value of the plate thickness $\overline{v}$ with a gain of 1 if $\overline{K} = K$. It can be seen from (3.3) that without the thickness control o is reduced by a factor $K/(a_m+K)$. The thickness control therefore tends to amplify the effect of roll eccentricity and ovalness. For a more detailed analysis of the accuracy of the thickness control, see [Kokai *et al.*, 1985].

It is not easy to see the dynamic effects of a change of the material hardness a_m on the plate thickness $\overline{v}$ from (3.6). We only dare to conclude that $1-\varphi G_t$ and hereby the closed loop dynamics of the thickness control system will be affected by such a disturbance.

The left side of (3.6) shows that the thickness control uses positive feedback. This stems from the fact that if the plate thickness for some reason becomes too large it is necessary to close the roll gap which increases the rolling force and thereby the plate thickness by a factor φG_t. Since $\varphi < 1$, for $\overline{K} = K$ the plate thickness $\overline{v}$ will, however, still be reduced by closing the roll gap in this case. The positive feedback can also be seen from the fact that a too large rolling force makes it necessary to close the roll gap which makes the force even larger—this also illustrates the fact that the thickness control tends to amplify the rolling force variations.

The problem of eliminating the effects of the roll eccentricity and ovalness o has been given much attention. There are two main groups of methods to reduce the impact of o

- Traditional methods, where it is exploited that o can be observed as small periodic variations in the rolling forces f. Here band-stop

filters and dead-zones are used to prevent the thickness control to react to these variations in the rolling force. These two methods only compensate partly for the roll eccentricity. Another possibility is to add an inner force control loop to ensure that the small variations of the rolling are cancelled. This method is able to compensate fully for the roll eccentricity and ovalness. For a comparison of these methods see [Edwards, 1978].

- Advanced methods, where o_e is estimated and used in the thickness control, as in (3.5).

Quite advanced methods have been used for the last alternative, see for instance [Kitamura *et al.*, 1987], [Yeh *et al.*, 1991], and [Edwards *et al.*, 1987].

Stability

To illustrate the stability problem we represent the characteristic polynomial on the form shown in Figure 3.4. Assuming that G_t is stable, and using the small gain theorem, see [Desoer and Vidyasagar, 1975], we find that the closed loop will be stable if

$$\begin{aligned} \gamma_1 &\geq \sup_{s=j\omega} |G_t(s)| \\ \gamma_2 &\geq \sup_{t} |\varphi(t)| \\ \gamma_1\gamma_2 &< 1. \end{aligned}$$

Even if it by the controller design is ensured that $\gamma_1 \leq 1$, the mill spring coefficient K can vary approximately $\pm 20\%$, which makes it necessary to increase the value of the estimate of the mill spring coefficient $\overline{K}$ to ensure that $\gamma_2 < 1$. Normally $\overline{K}$ is made 20% larger than K, this is called *detuning* and deteriorates the performance of the thickness control system. Note that the problem with the instability is introduced by the fact that it is necessary to estimate the plate thickness using an observer.

3.4 What Can Be Improved?—An Example

A general comment to the way thickness control is done today could be that the rolling mill is quite a complex structure which is modeled by a spring which is a simple mechanical structure. Several questions about the dynamics and multivariable structure of the process can be asked. We concentrate on this and will therefore not look at the compensation for roll

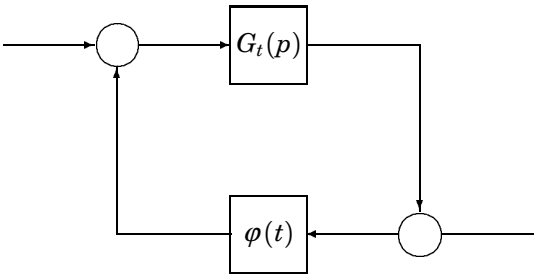

Figure 3.4 Standard representation of thickness control problem for using the small gain theorem to determine the stability.

eccentricity and ovalness, since this subject is considered well developed already.

The models described above use the mean values of the variables of the north and south sides. The implicit assumption is that the rolling process is symmetric around the vertical symmetry line of the rolling mill. This symmetry can be disturbed if the plate is not centered in the mill or if the temperature of one side of the plate deviates from the temperature of the other side. The variations of the plate hardness is typically induced by inhomogeneous heating by the reheating furnaces and inhomogeneous cooling by the roller tables.

The consequence of such asymmetric effects are shown in the simulations in Figure 3.5. Here the traditional thickness controller is combined with a more advanced model derived in the following chapters. In the simulations the plate hardness across the plate width is asymmetric. In the simulations asymmetric conditions in the plate hardness of ± 20 % between the plate edges are introduced at $t = 0.5$. For more details we refer to Chapter 7.

As seen from the figure the traditional control system does not react properly. The reason is that the mean value of the plate thickness is not changed. Worse is the fact that the plate length of the two sides will be different due to the different thickness reductions—this will give the plate an undesired curved shape.

To compensate for the hardness asymmetry we need:

- a multivariable model;
- a multivariable observer;
- a controller that can handle the multivariable case.

Due to the nonzero mass of the roll pack and the damping of the rolling

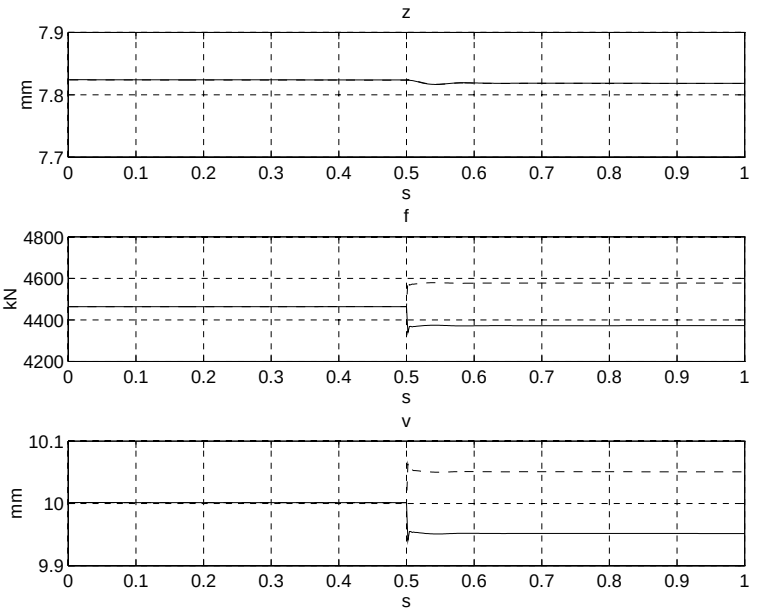

Figure 3.5 The effect of asymmetric material hardness using the traditional thickness controller. Top plot, full: roll position north side z_n and dashed: roll position at the south side z_s. These curves coincide. Middle plot, full: rolling force north side f_n and dashed: rolling force at the south side f_s. Bottom plot, full: plate thickness at north edge v_n and dashed: plate thickness at south edge v_s. It is seen that the thickness errors due to the asymmetric material conditions remains unaffected. The small change in the roll position is due to a slight change of the sum of the rolling forces.

process the rolling mill is also a dynamical system. We will thus develop dynamical multivariable models for the rolling mill in Chapter 4.

Since we are not able to measure the plate thickness we use the principle illustrated by Figure 3.1—the main difference will be that we increase the complexity of the observer, and the model used for the thickness control. Since we can not measure the process output we are not able to use a standard observer. We will therefore use an open loop observer for estimating the plate thickness from the roll positions z and the rolling forces f.

3.5 Conclusions

We have now described how the thickness control problem is solved today. The state of the art is a controller and an observer based on static scalar models. Investigating the thickness control system we find that special stability and performance problems occur since it is necessary to estimate the controlled output.

Since the thickness controllers today rely on a symmetry assumption, asymmetric rolling conditions cause errors in the control of the plate thickness. More complex models and controllers are necessary to handle this case. The derivation of these models and control strategies are the purposes of the work presented in the first part of this thesis.

4

Modeling of the Rolling Mill

The purpose of this chapter is to derive physical models for the rolling mill, which is divided into two subsystems:

- the hydraulic systems used for positioning the roll pack;
- the rolling stand used for deforming the steel plate.

The model for the hydraulic systems is more or less standard, see [Gou, 1991], while the other is developed by the author and it will therefore be described in more detail.

In the beginning of this chapter the model for the hydraulic systems is derived. This is done by explaining how the real systems work and which variables we can measure and from this determine a physical model that describes the main characteristics of interest. The nonlinear differential equations for the hydraulic systems are found from a physical model.

A model for the controller design and an observer for the thickness estimation are derived. The difference is that the rolling forces, which contain important information about the material properties of the plate, are available for the observer. A physical model is used to find energy functions for the rolling stand. The partial differential equations for the stand are found from the energy functions and ordinary differential equations are derived using modal truncation of the solution to the PDE.

The models for the hydraulic systems and the model for the rolling stand are combined to a total model for the entire system in the final part of the chapter.

Aspects connected with the system identification, such as parameterization and identifiability, will be treated later, since they depend on which realization of the models that is appropriate for describing the real system.

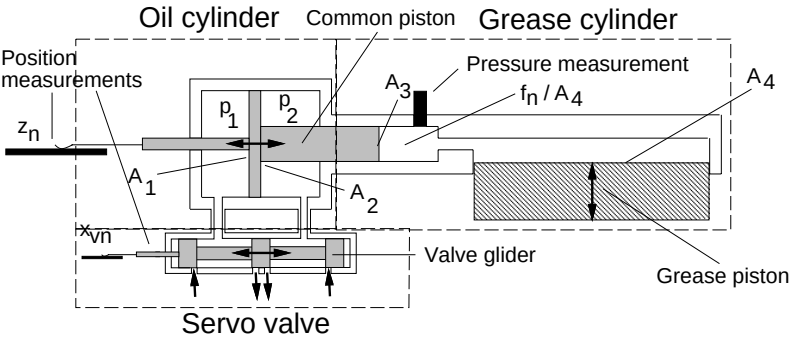

Figure 4.1 Schematic diagram of the main parts of the hydraulic system. The servo valve controls the oil flow to the oil cylinder. The oil cylinder is connected to the grease cylinder by the common piston. The grease piston moves the roll pack. In the figure z_n is the position measurement, x_{vn} is the valve glider position, A_1, A_2, A_3, and A_4 are areas of the hydraulic system, and f_n is the rolling force measurement.

4.1 Hydraulic System

The modeling of the hydraulic systems has already been done by several authors. The suggested nonlinear models do not differ much. For application to rolling mills see, for instance, [Ginzburg, 1984], [Paul, 1975], and [Gou, 1991].

There are two hydraulic systems on the rolling mill, one for each side. The two systems are identical and therefore only the north system is considered in the following. The hydraulic system can be divided into three main parts, see Figure 4.1:

- servo valve—controls the oil flow to the system;
- oil cylinder—positioning of common piston;
- grease cylinder—positioning of grease piston and roll pack.

Since the compressibility of grease is smaller than the compressibility of oil it is possible to use a higher working pressure in the grease cylinder. This makes it possible to reduce the area of the grease piston, which increases the stability of the mechanical construction. The common piston, which connects the oil and grease cylinders, reduces the pressure from the grease to the oil side and works as a mechanical amplifier.

The servo valve is used for controlling the velocity of the common piston. This is done by varying the flow “through" the oil cylinder. The velocity of the grease piston is controlled by adjusting the level in the grease cylinder using the common piston. To ensure a low back pressure

when adjusting the roll pack downwards the right side of the oil cylinder is drained for oil. Note that since the grease system is single acting the entire system is single acting. That the system is single acting implies that it is only possible to push the roll pack downwards with a large force.

The available measurements are, see Figure 4.1:

- position of valve glider of the servo valve x_{vn},
- position of the common piston z_n,
- rolling force f_n.

Note that even if it is the position of the grease piston we want to control it is the position of the common piston that is measured. The two positions can though easily be related by assuming that the grease is incompressible and using the ratio of the areas of the common piston.

The measurement of the grease pressure is used as a rolling force measurement. The load on the hydraulic system is not directly included in the model, it enters through the north rolling force f_n. The most significant part of the load is the friction between the work rolls and the mill frame. This implies that the rolling force measurement also includes the frictional forces from the movement of the upper roll pack, see [Zeltkalns *et al.*, 1977]. Generally, backlash is not a problem when the plate is in the mill since the mechanical system is pressed together with a large force. Furthermore, the positioning system is lubricated with grease. Backlash and friction will therefore not be considered here.

Physical Model

To be able to derive a mathematical model we first build a physical model, which includes the properties of the hydraulic systems we want to model, see Figure 4.2. Since it is not possible to measure the position of the grease piston only the oil side is included in the physical model. The mass and friction of the rest of the hydraulic system will therefore be included in the load. Furthermore, the function of the servo valve is not considered since it is not essential for the functionality of the hydraulic system.

The positive direction of the flow Q_1 of the left side of the oil cylinder is into the cylinder and the positive direction of the flow Q_2 of the right side of the oil cylinder is out of the cylinder. Note the leak flow between the piston and the cylinder wall. Note furthermore that the pressures of the return paths of the servo valve are set to zero and the supply pressure P_s is assumed constant.

To derive a model we need to know the pressure at both sides of the oil piston. To model the oil compressibility it is also necessary to know the time derivative of these pressures. Since the pressure is measured at

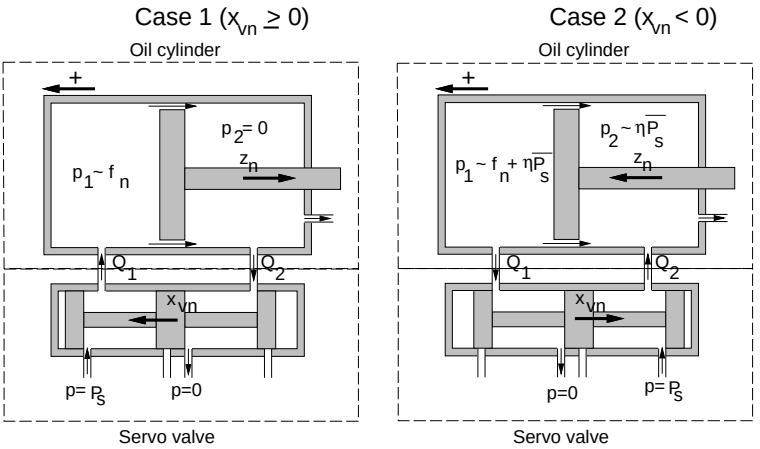

Figure 4.2 The physical model for the hydraulic systems. The model illustrates the situations when the piston is moved to the left and to the right. In the figure Q_1 and Q_2 are the flows into the left and right side of the cylinder respectively, p_1 and p_2 are the pressures at the left and right sides of the piston respectively, P_s is the supply pressure, and f_n is the rolling force at the north side of the mill. When the servo valve glider position x_{vn} is positive oil flows into the left side of the cylinder and the piston moves to the right, when the valve glider position is negative the piston is moved to the left. Note that the right side of the cylinder is drained for oil to reduce the pressure at the right side of the piston when it is moved to the right.

the grease side only a linear combination of the pressures at the oil side can be measured, neglecting mass and friction of the common piston the relation is

$$\frac{A_3}{A_4} f_n(t) = A_1 p_1(t) - A_2 p_2(t), \tag{4.1}$$

where p_1 and p_2 are the pressures at the left and right sides of the oil cylinder, respectively, and f_n is the rolling force. A_1, A_2, and A_3 are the areas of the common piston corresponding to p_1, p_2, and f_n/A_4 and A_4 is the area of the grease piston.

Since the oil is drained from the right side of the oil cylinder, we have an additional leak flow. This makes it hard to find the values of the flow Q_2 and the pressure p_2. When the valve glider position x_{vn} is positive and the positioning system in Figure 4.2 is moving to the right there is no flow Q_2 into the right side of the cylinder and we might assume that the

this side is drained for oil in this case. This leads us to the assumption

$$\begin{aligned} A_1 p_1(t) &\approx \frac{A_3}{A_4} f_n(t) \\ A_2 p_2(t) &\approx 0. \end{aligned} \tag{4.2}$$

When the valve glider position x_{vn} is negative and the positioning system therefore moves upwards there is an oil flow into the right side of the cylinder and we can no longer assume that it is drained for oil. We here make the simple assumption that the pressure $A_2 p_2 \approx \eta P_s$. Intuitively the coefficient η tells us how much of the pressure at the servo valve that is applied at the common piston. The assumptions leads to the equations

$$\begin{aligned} A_1 p_1(t) &\approx A_2 \eta P_s + \frac{A_3}{A_4} f_n(t) \\ A_2 p_2(t) &\approx A_2 \eta P_s, \end{aligned} \tag{4.3}$$

which have been shown to work well in practice.

Derivation of Model

The model is derived by combining the flow through the servo valve and the cylinder. Using [Trostmann, 1987] and [Gou, 1991] we find that the flows through the servo valve can be modeled as

Case 1: $x_{vn}(t) \geq 0$

$$\begin{cases} Q_1(t) = k_1 x_{vn}(t) \sqrt{p_1(t)} = \overline{k}_1 x_{vn}(t) \sqrt{\overline{P}_s - f_n(t)} \\ Q_2(t) = k_1 x_{vn}(t) \sqrt{p_2(t)} = 0 \end{cases} \tag{4.4}$$

Case 2: $x_{vn}(t) < 0$

$$\begin{cases} Q_1(t) = k_1 x_{vn}(t) \sqrt{p_1(t)} = \overline{k}_1 x_{vn}(t) \sqrt{\eta \overline{P}_s + f_n(t)} \\ Q_2(t) = k_1 x_{vn}(t) \sqrt{p_2(t)} = \overline{k}_1 x_{vn}(t) \sqrt{\eta \overline{P}_s}, \end{cases} \tag{4.5}$$

where k_1 is a positive constant. The supply pressure $\overline{P}_s$ and $\overline{k}_1$ have been transformed to equivalent constants assuming that $A_1 \approx A_2$. The zero point for the valve glider is at the middle position and the positive direction of movement is from the right to the left. The two sets of equations comes from the different flow paths depending on the position of the valve glider. The equations are derived using Bernoulli's laws for flow through an orifice—which in this case is the variable opening area of the servo valve.

Choosing the zero point for the common piston in the lowermost (to the right) position and the positive direction of movement to be upwards (from the right to the left), the flow through the oil cylinder can be modeled as

$$Q_1(t) + Q_2(t) = -(A_1 + A_2)\dot{z}_n(t) + A_1 k_2 (z_t - z_n(t))\dot{f}_n(t) + k_3 f_n(t), \quad (4.6)$$

where z_t is the top position of the common piston, z_n is the position of the common piston and k_2 and k_3 are positive constants. The first term on the right hand side is the flow due to the movement of the piston. The second term is due to the compressibility of the hydraulic oil which is proportional to the volume. This explains the appearance of $A_1(z_t - z_n)$ which is the volume of the left side as a function of the position z_n. The third term is the leak flow between the common piston and oil cylinder wall, which is assumed proportional to the pressure difference between the two sides which by (4.2) and (4.3) is proportional to the rolling force f_n.

Combining (4.4), (4.5), and (4.6) we obtain the following differential equations for the hydraulic system, where we introduce the variable z_{h_n} as the output of the model

Model for hydraulic system

$$-\dot{z}_{h_n}(t) = a_{hn1}\xi_n(t) - a_{hn2}(z_t - z_{h_n}(t))\dot{f}_n(t) - a_{hn3} f_n(t), \quad (4.7)$$

where

$$\xi_n(t) = \begin{cases} x_{vn}(t)\sqrt{\overline{P}_s - f_n(t)} & x_{vn}(t) \geq 0 \\ x_{vn}(t)(\sqrt{\eta \overline{P}_s} + \sqrt{\eta \overline{P}_s + f_n(t)}) & x_{vn}(t) < 0. \end{cases}$$

Inputs to the model are the valve glider position x_{vn} and the rolling force measurement f_n and the output is the position of the common piston z_{h_n}. For a perfect model match we have that $z_{h_n} = z_n$.

4.2 Rolling Stand

We will now derive models for the rolling stand, which consist of the rolling mill frame, rolls and steel plate. Inputs to this model are the positions of the hydraulic systems and outputs are the plate thicknesses. As explained in Chapter 3 both a model and an observer are needed for the thickness control system. The difference between the model and the observer is that

the rolling force measurements are available to the observer but not to the model.

In the following we will first derive the model with the thickness profile across the plate width as output. The output is then converted to a number of normal coordinates, which are governed by a linear state space equation. We find that the rolling force can also be found from from the normal coordinates. This is used for deriving the observer which has an estimate of the normal coordinates as output.

The author has found no reports in the literature that build a multivariable dynamical model for the rolling stand. For descriptions of simpler models see, for instance, [Fujii and Saito, 1975], [Kokai *et al.*, 1985], [Mizuno, 19], and [Stone, 1969].

Physical Model

The rolling stand with the plate consists of three main parts:

- roll pack—used for reducing the plate thickness;
- mill frame—holds the rolls;
- steel plate.

Since the border of the model for the hydraulic system is the common piston, the model for the rolling stand includes the grease cylinder. This implies that the compressibility and damping of the grease will be implicitly included in the rolling stand model. A schematic diagram is shown in Figure 4.3

The main characteristic of interest in the modeling of the rolling stand is the elastic deflection of the roll pack and the mill frame and the plastic deformation of the steel plate. The model should cover the behavior of both the rolling stand and the steel plate. We first assume that the mill frame only deflects in vertical direction which is supported by the fact that vertical component of the rolling forces are dominating. The next assumption is that the plate is always centered in the rolling mill, this is ensured in practice by centering devices on each side of the rolling mill. Since the work and backup rolls are pressed together with a large force during rolling and the backup rolls work as the only support for the work rolls the work and backup rolls are joined to one roll. As a final part of the preparations for the modeling we set the width of the rolling stand is equal to the plate width, this includes some of the deflection of the rolls in the deflection of the mill frame in the model. This makes it possible to use the mill spring coefficient K from the existing control system for the physical model. Another advantage is that all the parameters will be independent of the spatial variable in the width direction x, which results

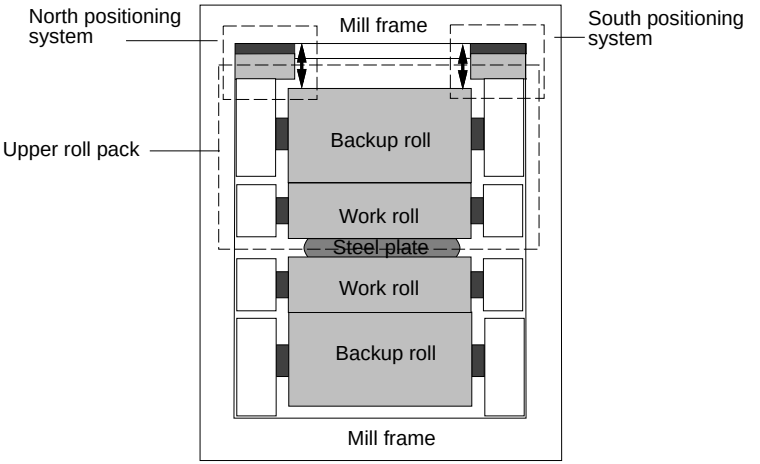

Figure 4.3 Diagram of the main parts of the rolling stand which are the roll pack, the mill frame, rolls, and steel plate. These are the elements we want to include in the model.

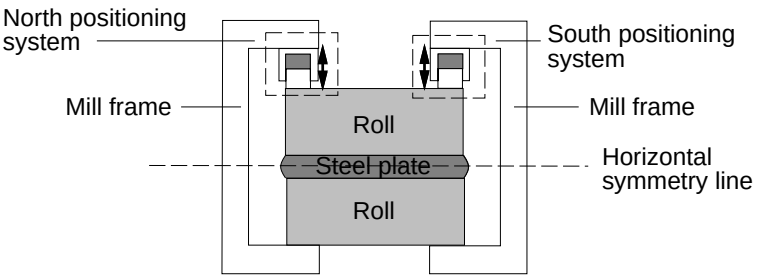

Figure 4.4 Diagram of the main parts of the rolling stand, illustrating the assumptions made in the modeling: the work and backup rolls behave as one roll, the plate is always centered in the plate mill, and that the width of the rolls are equal to the plate width.

in a simpler structure of the mathematical model. The above assumptions make it possible to make the simplified model shown in Figure 4.4.

Considering plate halves above and below the horizontal symmetry line we now assume the forces applied for deforming the two parts are equal. A difference in the two forces will result in an adjustment of the vertical position of the plate and thus reestablish the equality of the forces after a while. Since these forces are small compared to the rolling forces we believe that the effect of the vertical adjustments will be neglectable.

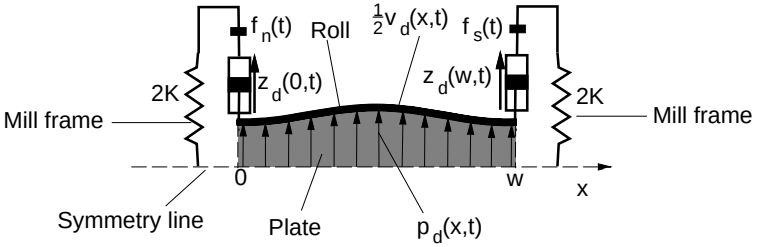

Figure 4.5 Physical model of the rolling stand. This figure is the basis for the energy functions and thus the mathematical model for the rolling stand. In the figure f_n and f_s are the rolling forces, z_d is the roll position, p_d is the pressure distribution between plate and roll, v_d is the plate thickness profile, and K is the mill deflection coefficient.

Assuming that the hardness of the plate is the same for the top and bottom halves gives us the possibility to establish symmetry. This makes it only necessary to model one half of the rolling stand—we here choose to consider the top half.

Using the above assumptions and experience from the system identification the physical model shown on Figure 4.5 is developed. Here the rolling stand is modeled as two springs and the roll pack is modeled as an elastic beam. The mill frame springs and the roll beam are deflected when the roll beam is subjected to the pressure distribution from the material during rolling. Using the positioning systems the thickness of the plate can be adjusted. Ideal plastic behavior is assumed, which implies that the thickness profile of the finished plate is the same as the roll profile. In the model the beam ends are built-in, this implies that the orientation of the beam ends are fixed. This gives two of the boundary conditions for the model derived below.

To obtain a two dimensional model it is assumed that the area of contact between rolls and plate is a line. The thickness profile of the plate is $\frac{1}{2}v_d(x,t)$ and $p_d(x,t)$ is the pressure distribution applied to the work roll by the plate. Note that $z_d(0,t)$ and $z_d(w,t)$ in the figure are not the positions of the hydraulic systems since the width of the rolling stand is set equal to the plate width—this will be taken into consideration when deriving the model.

The available measurements are also shown in Figure 4.5:

- positions of hydraulic systems at the plate edges $z_d(0,t)$ and $z_d(w,t)$;
- rolling forces $f(t) = [\, f_n(t) \quad f_s(t) \,]^T$;
- thickness profile of the plate in the width direction $\frac{1}{2}v_d(x,t)$.

Since we only derive a model for the top half of the plate, we work with half the plate thickness and half the position z_d. The two first measurements are the same as for the hydraulic system while the thickness is measured after the rolling. The output of the model is the thickness profile $\frac{1}{2}v_d(x,t)$.

The Model

Deriving the model is complicated and it is therefore divided into the following steps:

- choice of material model;
- derivation of a partial differential equation (PDE) for the rolling stand;
- construction of an ordinary differential equation (ODE) from the PDE.

The theoretical aspects are described during the derivation.

Material model Since the rolling force is not available in the model we need a model for how the pressure distribution depends on the plate thickness. This is a complex problem, but to preserve simplicity we here assume *plane strain*, which implies that that the material is homogeneous and there consequently is no material flow in the sidewise direction. The result is that the pressure in one point only depends on the plate thickness at that point. It is straight forward to remove the assumption that the material is homogeneous in the sidewise direction and this is done for test purposes in Chapter 7. The important assumption is that there is no material flow in the sidewise direction, since this excludes shear forces when deforming the material. A measure of the sidewise material flow is how much wider the plate gets during rolling. In practice this amount is small compared to the plate width, and this indicates that the sidewise material flow can be neglected in the model.

Generally, the material characteristics include a stiffness and a damping term. The input variables are thickness reduction and roll velocity, see [Roberts, 1983] and [Guo, 1994]. Traditionally the models are nonlinear functions of the reduction

$$r_d(x,t) = \frac{\frac{1}{2}v_{d-1}(x,t) - \frac{1}{2}v_d(x,t)}{\frac{1}{2}v_{d-1}(x,t)},$$

the strain rate (the time derivative of the reduction r_d), and plate temperature. Here $\frac{1}{2}v_{d-1}$ is the thickness profile for the ingoing thickness. Note that the strain rate $\dot{r}_d$ is a function of both $\dot{v}_d$, $\dot{v}_{d-1}$ and the work roll speed v_r.

To prevent waves in the length direction the computer planning system tries to withhold a *constant relative crown*. This means that the shape of the thickness profile is keep constant in the last part of the pass schedule. This implies that we can assume that

$$\tfrac{1}{2}v_d(x,t) \approx \varpi(t)\tfrac{1}{2}v_{d-1}(x,t),$$

where ϖ always is smaller than 1.

Using a nonlinear material model will result in a nonlinear PDE as a model for the rolling stand. This will be hard to handle and assuming that the thickness control works properly we choose to work with a linear material model at a working point, which is valid for small variations of v_d, $\dot{v}_d$, and v_r. Assuming that ϖ varies slowly we postulate that the external transverse force applied to the roll is

$$\begin{aligned} p_d(x,t) = &-a_{m1}(t)(1-\varpi(t))\tfrac{1}{2}v_d(x,t) \\ &- a_{m2}(t)(1-\varpi(t))\frac{d}{dt}\tfrac{1}{2}v_d(x,t) + a_{m3}(t)v_r(t), \end{aligned} \quad (4.8)$$

where v_r is the rotational speed of the work roll and a_{m1}, a_{m2}, and a_{m3} are positive parameters. In the following we will include the variations of ϖ in a_{m1} and a_{m2}. Note that the pressure profile will be a function of the thickness profile obtained in earlier passes, this gives the rolling process repetitive structure, see for instance [Foda and Agathoklis, 1992].

The variation of the material parameters is mainly due to the variations of the plate temperature which normally does not change much during one pass. As seen from (4.8) the material model for the steel plate is time varying. The system identification will be based on data from one pass and the controller design will also be done for one pass at the time. The main demand on the model is therefore that it should be valid for one pass at the time and not for the entire rolling. We therefore assume that the material parameters a_{m1}, a_{m2}, and a_{m3} vary slowly compared to the dynamics of the rolling stand. This will make it possible to assume that the material parameters are constant when doing the modeling, system identification, and controller design and we will therefore be able to use methods for time invariant systems for these tasks.

PDE for the rolling stand Assuming that the roll packs behave as so called slender members we can model them as *Euler-Bernoulli beams*, see [Abildgaard, 1991] and [Crandall *et al.*, 1978]. Slender members behave as they were made of a large number of independent layers and this implies that no shear forces are present when the beam is deflected. The bending

moment of the roll pack is then given by

$$M_b = EI \frac{\partial^2 \frac{1}{2} v_d(x,t)}{\partial x^2},$$

where E is Young's modulus of elasticity and I is the second moment of area of the work roll, see [Pedersen, 1995b]. The roll pack is, however, not exactly a slender member, but since the roll bending is small compared to the roll geometry the shear strain will be small compared to the normal strain when the roll is deformed. This justifies the assumptions.

To represent the effect of a position change on the thickness profile $\frac{1}{2} v_d(x,t)$ for all x we introduce the function

$$z_d(x,t) = \begin{bmatrix} 1 - \frac{x+\frac{1}{2}(l-w)}{l} & \frac{x+\frac{1}{2}(l-w)}{l} \end{bmatrix} \begin{bmatrix} \frac{1}{2} z_n \\ \frac{1}{2} z_s \end{bmatrix} \quad x \in [0,w],$$

where l is the width of the rolling stand. The variable $z_d(x,t)$ describes the roll position across the plate width, see Figure 4.5.

The model for the rolling stand is found by forming the energy function for the mechanical structure shown in Figure 4.5 and then using the Euler-Lagrange equations on the energy functions, see [Meirovitch, 1980]. The method used here is the same as that used in optimal control, here we introduce the performance function

$$\int_{t_1}^{t_2} L_l(t)dt = \int_{t_1}^{t_2} (T_l(t) - V_l(t))dt,$$

where T_l is the total kinetic energy and V_l is the total potential energy for the system. In order to fulfill the physical laws, the system will always be in the state minimizing the performance function L_l, see [Hansen, 1993].

The energy functions for the physical model in Figure 4.5 are found to

$$\begin{aligned} T_l(t) &= \frac{1}{2} \int_0^w \rho A (\tfrac{1}{2} \dot{v}_d(x,t))^2 dx \\ V_l(t) &= \frac{1}{2} \int_0^w \left(EI (\tfrac{1}{2} v_d^{(2)}(x,t))^2 + a_{m1} \left(\tfrac{1}{2} v_d(x,t) \right)^2 \right) dx \\ &\quad + \frac{1}{2} 2K \left((\tfrac{1}{2} v_d(0,t) - z_d(0,t))^2 + (\tfrac{1}{2} v_d(w,t) - z_d(w,t))^2 \right), \end{aligned}$$

where $^{(i)}$ denotes i times partial derivation with respect to x, ρ is the mass density of steel, A is the cross sectional area of the roll pack and $2K$ is the spring constant for half a leg of the mill frame, see [Pedersen, 1995b].

The term in T_l is the kinetic energy due to the velocity of the roll pack, the first term in V_l are the potential energy due to the bending of the roll pack, the second term is the potential energy used for deforming the steel plate and the two last terms is the energy used for deforming the springs of the sides of the rolling stand.

The original *Euler-Lagrange* formulation only covers conservative systems, i.e., systems without losses. To include the losses of the material model these are represented as non-conservative virtual work, see [Meirovitch, 1980]

$$\delta W(t) = \int_0^w \left(-a_{m2}\tfrac{1}{2}\dot{v}_d(x,t) + a_{m3}v_r(t)\right)\tfrac{1}{2}\delta v_d(x,t)dx,$$

and can in this way be included in the Lagrangian formulation.

Using Euler-Lagrange's equations we obtain the PDE, see [Meirovitch, 1980]

$$\begin{aligned} EI\tfrac{1}{2}v_d^{(4)}(x,t) + a_{m1}\tfrac{1}{2}v_d(x,t) + \rho A\tfrac{1}{2}\ddot{v}_d(x,t) = \\ -a_{m2}\tfrac{1}{2}\dot{v}_d(x,t) + a_{m3}v_r(t),\ x \in (0,w) \end{aligned}$$

with the boundary conditions

$$\begin{aligned} \tfrac{1}{2}v_d^{(1)}(0,t) &= 0 \\ \tfrac{1}{2}v_d^{(1)}(w,t) &= 0 \\ (EI/2K)\tfrac{1}{2}v_d^{(3)}(0,t) + \tfrac{1}{2}v_d(0,t) &= z_d(0,t) \\ -(EI/2K)\tfrac{1}{2}v_d^{(3)}(w,t) + \tfrac{1}{2}v_d(w,t) &= z_d(w,t). \end{aligned} \tag{4.9}$$

Note that since we have a 4th order PDE we have four boundary conditions. The first two boundary conditions state that the orientation of the beam ends are fixed while the two last imply that the forces at the beam ends should be equal to the force applied to the springs.

A problem is now that we have non-homogeneous boundary conditions. This can be solved by a state transformation

$$\begin{aligned} u(x,t) &= \tfrac{1}{2}v_d(x,t) - \varepsilon(x)\tfrac{1}{2}z(t),\ x \in [0,w] \\ &= \tfrac{1}{2}v_d(x,t) - \left(\tfrac{1}{2} + \tfrac{w}{2l}\cos(\tfrac{\pi}{w}x)\right)\tfrac{1}{2}z_n(t) - \left(\tfrac{1}{2} - \tfrac{w}{2l}\cos(\tfrac{\pi}{w}x)\right)\tfrac{1}{2}z_s(t) \end{aligned} \tag{4.10}$$

where $z^T = [z_n\ z_s]$, u is the new state variable, and

$$\varepsilon(x) = \begin{bmatrix} (1+\cos(\frac{\pi}{w}x)) & (1-\cos(\frac{\pi}{w}x)) \end{bmatrix} \begin{bmatrix} 1 - \frac{x+\frac{1}{2}(l-w)}{l} & 0 \\ 0 & \frac{x+\frac{1}{2}(l-w)}{l} \end{bmatrix}.$$

The state transformation moves the terms for the roll position $z_d(x,t)$ from the boundary conditions to the PDE and in this way we obtain an extra input.

Applying the state transformation we obtain the PDE

$$\begin{aligned} EIu^{(4)} + a_{m2}\dot{u} + a_{m1}u + \rho A\ddot{u} = a_{m3}v_r - a_{m1}\varepsilon\tfrac{1}{2}z - EI\varepsilon^{(4)}\tfrac{1}{2}z \\ - a_{m2}\varepsilon\tfrac{1}{2}\dot{z} - \rho A\varepsilon\tfrac{1}{2}\ddot{z},\ x \in (0,w), \end{aligned} \quad (4.11)$$

with the (now homogeneous) boundary conditions

$$\begin{aligned} u^{(1)}(0,t) &= 0 \\ u^{(1)}(w,t) &= 0 \\ (EI/2K)u^{(3)}(0,t) + u(0,t) &= 0 \\ -(EI/2K)u^{(3)}(w,t) + u(w,t) &= 0. \end{aligned}$$

We now have the PDE with boundary conditions on standard form and can thus proceed with the solution of the problem.

Obtaining the ODE For the PDE we define the eigenvalue problem

$$\left(EI\frac{\partial^4}{\partial x^4} + a_{m1}\right)\phi_i(x) = \lambda_i \rho A \phi_i(x). \quad (4.12)$$

This equation is, in general, fulfilled for an infinite set of real eigenvalues λ_i and eigenfunctions ϕ_i which furthermore have to fulfill the boundary conditions. Note that the eigenfunctions must belong to the same function space as the solution to the PDE (they both have the same number of continuous derivatives).

It can by partial integration and use of the boundary conditions be shown that the differential operator L is *self adjoint* ($\langle La, b\rangle = \langle a, Lb\rangle$ where $\langle\cdot\rangle$ is the inner product in $L_2[0,w]$). This implies that the eigenfunctions are orthogonal and they furthermore form a complete set. Since the solution to the PDE also belongs to this space it can be expanded as

$$u(x,t) = \sum_{i=1}^{\infty} \phi_i(x) q_i(t),$$

where the q_i's are called *normal coordinates* and are continuous functions of t.

Since it is hard to work with an infinite series it is necessary to use an approximate method when obtaining the ODEs. The method that will be

used here is *Galerkin's method*. This has the advantage that it preserves the symmetry of the system when the approximate solution is calculated. Furthermore, the method is simple to use and it is easy to understand the main idea.

It is first of all assumed that the approximate solution $\hat{u}$ is given by the finite series

$$\hat{u}(x,t) = [\phi_1(x)\ \phi_2(x) \cdots \phi_n(x)][q_1(t)\ q_2(t) \cdots q_n(t)]^T. \tag{4.13}$$

Introducing the approximate solution for u in the PDE, premultiplying with the eigenfunctions $[\phi_1\ \phi_2 \cdots \phi_n]^T$ and integrating with respect to x from 0 to w yields a set of differential equations for the normal coordinates q_i's.

We now proceed with finding the eigenfunctions from (4.12) and the boundary conditions. In order to satisfy (4.12) it is necessary that

$$\phi_i^{(4)}(x) = k\phi_i(x),\ i = 1, \ldots$$

where k is a real constant. The solution for this differential equation is

$$\phi_i(x) = c_{i1}\cos(\beta_i x) + c_{i2}\sin(\beta_i x) + c_{i3}\cosh(\beta_i x) + c_{i4}\sinh(\beta_i x),$$

which also is suggested in [Meirovitch, 1980]. We thus find that $\lambda_i = (EI\beta_i^4 + a_{m1})/\rho A$.

Inserting the solution in the boundary conditions results in the system of equations

$$\begin{bmatrix} 0 & \beta_i & 0 & \beta_i \\ -\beta_i\sin(\beta_i w) & \beta_i\cos(\beta_i w) & \beta_i\sinh(\beta_i w) & \beta_i\cosh(\beta_i w) \\ 1 & -\beta_i^3 EI/2K & 1 & \beta_i^3 EI/2K \\ X_1 & X_2 & X_3 & X_4 \end{bmatrix} \begin{bmatrix} c_{i1} \\ c_{i2} \\ c_{i3} \\ c_{i4} \end{bmatrix} = 0,$$

where

$$\begin{aligned} X_1 &= \beta_i^3(EI/2K)\sin(\beta_i w) - \cos(\beta_i w) \\ X_2 &= -\beta_i^3(EI/2K)\cos(\beta_i w) - \sin(\beta_i w) \\ X_3 &= \beta_i^3(EI/2K)\sinh(\beta_i w) - \cosh(\beta_i w) \\ X_4 &= \beta_i^3(EI/2K)\cosh(\beta_i w) - \sinh(\beta_i w). \end{aligned}$$

The coefficients (up to a scaling constant) lie in the null space of the above matrix. For the null space to have a dimension larger than zero,

the determinant of the system should be zero—this can be utilized to find the β_i's. Setting the determinant equal to zero yields the equation

$$(8\beta_i^3 KEI \sinh(\beta_i w) - 8K^2 \cosh(\beta_i w)) \cos(\beta_i w) + 8\beta_i^3 KEI \cosh(\beta_i w) - 4\beta_i^6 EI^2 \sinh(\beta_i w)) \sin(\beta_i w) + 8K^2 = 0,$$

which is transcendental and therefore has to be solved numerically. To ensure uniqueness of the eigenfunctions the coefficients are normalized such that

$$\int_0^w \rho A \phi_i^2(x) dx = 1, \ i = 1, \ldots .$$

Inserting the values for the physical constants found in in [Pedersen, 1995b] we can find the eigenfunctions for one specific plate width w.

For us the two first eigenfunctions are the most interesting. The reason for this is that they describe the mean value and the wedge of the roll gap, see Figure 4.6. The eigenvalues β_i are used in increasing magnitude when finding the eigenfunctions, this implies that the variations of the eigenfunctions as a function of x increases with i. The terms $\int_0^w \varepsilon \phi_i dx$, $\int_0^w \varepsilon^{(4)} \phi_i dx$, and $\int_0^w \phi_i dx$ therefore decrease with increasing i. This is due to the more and more high frequency nature of the eigenfunctions and the fact that the mean values of all other eigenfunctions than ϕ_1 are zero.

Looking at the differential equation found later in this chapter we conclude that the steady state gains of the differential equations for the normal coordinates q_i decrease with increasing i. Investing these steady state gains from $\frac{1}{2}z$ to q we find that they typically are of a order of magnitude 10^{-1} for the two first eigenfunctions ϕ_1 and ϕ_2, and then decrease by a factor 10^{-3} for the following eigenfunctions. The system identification has been performed using the three first eigenfunctions, but as indicated by the above, it was found that ϕ_3 had little or no importance. We therefore only include the two first eigenfunctions in the model for the rolling stand.

Applying Galerkin's method on (4.11) yields the *polynomial matrix description (PMD)*, see [Kailath, 1980], relating the normal coordinates q to the roll positions z, and the work roll speed v_r

$$\left(Ip^2 + a_{m2}\Gamma_1 p + EI\Gamma_2 + a_{m1}\Gamma_1\right) q(t) = a_{m3}\Gamma_5 v_r(t) - \left(\rho A \Gamma_3 p^2 + a_{m2}\Gamma_3 p + a_{m1}\Gamma_3 + EI\Gamma_4\right) \tfrac{1}{2} z(t),$$

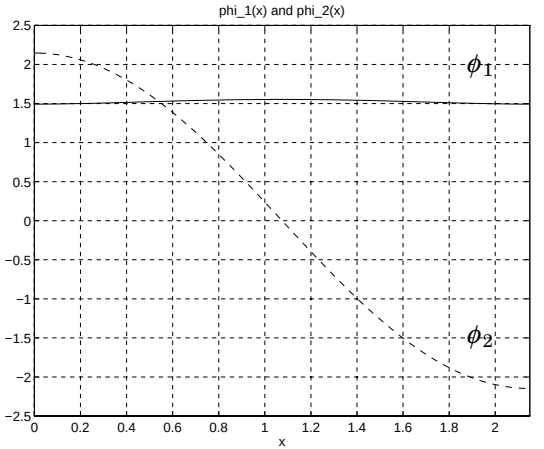

Figure 4.6 The first two eigenfunctions ϕ_1 and ϕ_2 for the rolling stand. They describe the mean value and the wedge of the roll gap and are the ones that will be considered in the following.

where

$$\Gamma_1(i,j) = \int_0^w \phi_i(x)\phi_j(x)dx = \frac{1}{\rho A}\delta_{ij}$$
$$\Gamma_2(i,j) = \int_0^w \phi_i^{(4)}(x)\phi_j(x)dx = \frac{\beta_i^4}{\rho A}\delta_{ij}$$

$$\Gamma_3(i) = \int_0^w \phi_i(x)\varepsilon(x)dx$$
$$\Gamma_4(i) = \int_0^w \phi_i(x)\varepsilon^{(4)}(x)dx$$
$$\Gamma_5(i) = \int_0^w \phi_i(x)dx$$

where (i,j) denotes the position of the i'th row and the j'th column. δ is the Kronecker function

$$\delta_{ij} = \begin{cases} 1, & \text{when } i = j \\ 0, & \text{otherwise} \end{cases}$$

Using the state transformation $y_{c_1} = q_c + \rho A \Gamma_3 \frac{1}{2} z$ to remove the direct term and the methods given in [Kailath, 1980] we obtain the state space equations

The model

$$\left[\begin{array}{c} \dot{y}_{c_1} \\ \dot{y}_{c_2} \\ \hline q_c \end{array}\right] = \left[\begin{array}{c|c} A_c & B_c \\ \hline C_c & D_c \end{array}\right] \left[\begin{array}{c} y_c \\ \hline \frac{1}{2}z \\ v_r \end{array}\right]$$

$$= \left[\begin{array}{cc|cc} -a_{m2}\Gamma_1 & I & 0 & 0 \\ -EI\Gamma_2 - a_{m1}\Gamma_1 & 0 & EI(\rho A\Gamma_2\Gamma_3 - \Gamma_4) & a_{m3}\Gamma_5 \\ \hline I & 0 & -\rho A\Gamma_3 & 0 \end{array}\right] \left[\begin{array}{c} y_{c_1} \\ y_{c_2} \\ \hline \frac{1}{2}z \\ v_r \end{array}\right] \tag{4.14}$$

The inputs are the roll positions z and the roll speed v_r, and the outputs are the normal coordinates q_c. $y_c^T = [\, y_{c_1} \quad y_{c_2} \,]$ are the states of the model. Since several state transformations are involved when finding the above model the state variables can not be given any direct physical interpretation. For a perfect model match we have that $q_c = q$.

The Observer

The purpose of the observer is to estimate the states of the model (4.14) in an appropriate way. The difference is that we here have the rolling force measurements at our disposal.

Using the fact that the shear force is equal to the rolling force at the beam ends we have that

$$-EIu^{(3)}(x,t) = 2Ku(0,t) = f_n(t) \tag{4.15}$$

$$EIu^{(3)}(x,t) = 2Ku(w,t) = f_s(t). \tag{4.16}$$

Note that these are also the two last boundary conditions for (4.11). It is in this way possible to use the rolling forces f for finding the normal coordinates q. Using the approximative relationship

$$u(x,t) \approx \phi_1(x)q_1(t) + \phi_2(x)q_2(t)$$

we can by (4.15) and (4.16) derive the matrix equation

$$\left[\begin{array}{c} f_n(t) \\ f_s(t) \end{array}\right] \approx 2K \left[\begin{array}{cc} \phi_1(0) & \phi_2(0) \\ \phi_1(w) & \phi_2(w) \end{array}\right] \left[\begin{array}{c} q_1(t) \\ q_2(t) \end{array}\right]. \tag{4.17}$$

Using the relationships found from (4.14) we get

$$q_c(t) = y_{c_1}(t) - \rho A\Gamma_3 \tfrac{1}{2}z(t) \tag{4.18}$$

$$\dot{y}_{c_1}(t) = -a_{m2}\Gamma_1 y_{c_1}(t) + y_{c_2}(t) \tag{4.19}$$

introducing the model output q_c for q in (4.17), and using this equation together with (4.18) and (4.19) it is possible to find an estimate for y_c. To simplify the structure of the observer we assume that $\dot{y}_{c_2}$ is small and obtain

The observer

$$y_e(t) = \begin{bmatrix} \Gamma_6 \\ a_{m2}\Gamma_1\Gamma_6 \end{bmatrix} f(t) + \begin{bmatrix} \rho A \Gamma_3 \\ a_{m2}\Gamma_3 \end{bmatrix} \tfrac{1}{2} z(t) \tag{4.20}$$

where

$$\Gamma_6 = \frac{1}{2K} \begin{bmatrix} \phi_1(0) & \phi_2(0) \\ \phi_1(w) & \phi_2(w) \end{bmatrix}^{-1}$$

Inputs are the roll positions z, the rolling forces f. The vector y_e is the estimate of the states of the model y_c. The steady state gains of the model and the observer are the same. For perfect model match we have y_e equal to y_c.

4.3 Total Model

As we have seen in (4.15) and (4.16) it is possible to find the rolling force from the model for the rolling stand. The rolling force and its time derivative are used in the model for the hydraulic systems. This makes it possible to make a total model for simulation by combining the models for the hydraulic systems and the model for the rolling stand. Using (4.17) and inserting the output of the model q_c for the normal coordinates q we have that

$$f_c(t) = \begin{bmatrix} f_{c_n}(t) \\ f_{c_s}(t) \end{bmatrix} = 2KF \begin{bmatrix} q_{c_1}(t) \\ q_{c_2}(t) \end{bmatrix}, \tag{4.21}$$

where

$$F = \begin{bmatrix} \phi_1(0) & \phi_2(0) \\ \phi_1(w) & \phi_2(w) \end{bmatrix}$$

By the above expression we can establish a connection between the *models for the hydraulic positioning systems* and the *model* for the normal

coordinates

$$-\dot{z}_{h_n}(t) = a_{hn1}\xi_n(t) - a_{hn2}(z_t - z_{h_n}(t))\dot{f}_n - a_{hn3}f_n(t)$$
$$-\dot{z}_{h_s}(t) = a_{hs1}\xi_s(t) - a_{hs2}(z_t - z_{h_s}(t))\dot{f}_s - a_{hs3}f_s(t)$$

where

$$\xi_n(t) = \begin{cases} x_{vn}(t)\sqrt{\overline{P}_s - f_n(t)} & x_{vn}(t) \geq 0 \\ x_{vn}(t)(\sqrt{\eta\overline{P}_s} + \sqrt{\eta\overline{P}_s + f_n(t)}) & x_{vn}(t) < 0 \end{cases}$$
$$\xi_s(t) = \begin{cases} x_{vs}(t)\sqrt{\overline{P}_s - f_s(t)} & x_{vs}(t) \geq 0 \\ x_{vs}(t)(\sqrt{\eta\overline{P}_s} + \sqrt{\eta\overline{P}_s + f_s(t)}) & x_{vs}(t) < 0 \end{cases}$$

where x_{vs} is the valve glider position for the south hydraulic system, and z_{h_s} is the output from the model of the south hydraulic system.

$$\left[\begin{array}{c} \dot{y}_c \\ \hline q_c \end{array}\right] = \left[\begin{array}{cc|cc} -a_{m2}\Gamma_1 & I & 0 & 0 \\ -EI\Gamma_2 - a_{m1}\Gamma_1 & 0 & EI(\rho A\Gamma_2\Gamma_3 - \Gamma_4) & a_{m3}\Gamma_5 \\ \hline I & 0 & -\rho A\Gamma_3 & 0 \end{array}\right] \left[\begin{array}{c} y_c \\ \hline \frac{1}{2}z_h \\ v_r \end{array}\right].$$

We can now substitute f and $\frac{d}{dt}f$ with the rolling force model output

$$f_c(t) = 2KFq_c(t)$$
$$\tfrac{d}{dt}f_c(t) = 2KF\tfrac{d}{dt}q_c(t).$$

Note that $\frac{d}{dt}q_c$ can be calculated using $\frac{d}{dt}y_c$ and the models for the hydraulic systems. A principal diagram of the model structure is shown in Figure 4.7. By joining the two models we have a system with the valve glider positions for the hydraulic systems x_v and the roll speed v_r as inputs and the normal coordinates q_c as outputs. The complete model will in the following be used for the simulations.

The controlled outputs, which are the thicknesses at a distance μ from the plate edges, see Chapter 7, can in the simulations be calculated from

$$\begin{aligned} v_c(t) = \begin{bmatrix} v_{c_n}(t) \\ v_{c_s}(t) \end{bmatrix} &= 2\begin{bmatrix} \hat{u}(\mu,t) \\ \hat{u}(w-\mu,t) \end{bmatrix} + \begin{bmatrix} \varepsilon(\mu)z_h(t) \\ \varepsilon(w-\mu)z_h(t) \end{bmatrix} \\ &= 2\Phi\begin{bmatrix} q_{c_1}(t) \\ q_{c_2}(t) \end{bmatrix} + \begin{bmatrix} \varepsilon(\mu)z_h(t) \\ \varepsilon(w-\mu)z_h(t) \end{bmatrix} \end{aligned} \tag{4.22}$$

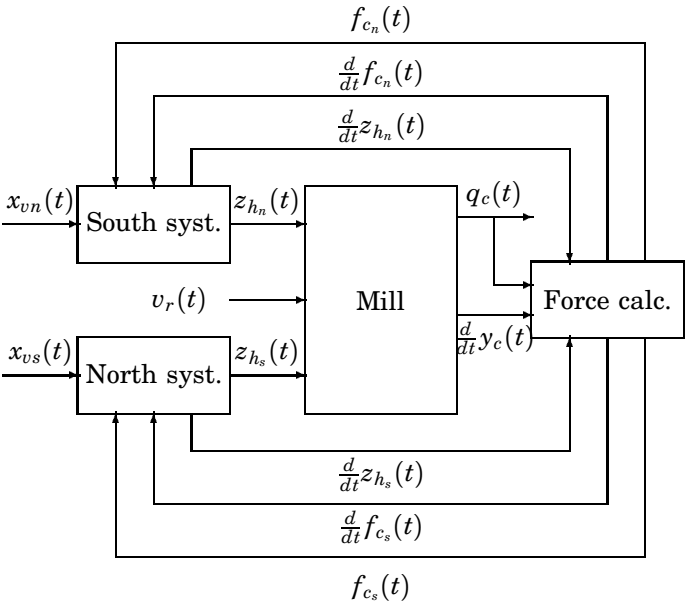

Figure 4.7 The total model for the rolling mill made by combining the models for the hydraulic systems and the model for the rolling stand. The rolling forces and their derivatives are calculated using two of the boundary conditions for the PDE.

where

$$\Phi = \begin{bmatrix} \phi_1(\mu) & \phi_2(\mu) \\ \phi_1(w-\mu) & \phi_2(w-\mu) \end{bmatrix}.$$

In this way the plate thicknesses at the edges v_c can be found using the normal coordinates q_c and the output from the model for the hydraulic systems z_h.

The *observer*

$$y_e(t) = \begin{bmatrix} \Gamma_6 \\ a_{m2}\Gamma_1\Gamma_6 \end{bmatrix} f_c(t) + \begin{bmatrix} \rho A\Gamma_3 \\ a_{m2}\Gamma_3 \end{bmatrix} \tfrac{1}{2} z_h(t)$$

will be used for estimating the states y_c of the model for the rolling stand when implementing the controller in the simulations. Here the additional force measurements are available for a better estimate of the plate thickness. The estimate for the normal coordinates q_c can be calculated from

$$q_e(t) = [\, I \quad 0 \,]\, y_e(t) - \rho A\Gamma_3 \tfrac{1}{2} z_h(t).$$

Again the thickness at the north and south edge v_{e_n} and v_{e_s} can be calculated using q_e and (4.22).

4.4 Conclusions

We have now derived models for the hydraulic systems and the rolling stand. The model for the hydraulic systems is nonlinear with the rolling force and servo valve glider position as inputs and the roll position as output. The model for the rolling stand is linear and multivariable with roll positions and rolling speed as inputs and normal coordinates for the eigenfunctions of the rolling stand as outputs. A static observer with roll positions and the rolling forces as inputs and the states of the model for the rolling stand as outputs is also found.

Using the boundary conditions for the rolling stand, the rolling forces can be calculated. This makes it possible to combine the model for the hydraulic systems and the model for the rolling stand into a total model for the whole rolling mill. The total model will be used for computer simulations.

The load of the hydraulic systems is included in the model for the rolling stand. Since we in this model have a linear model for the damping friction between the roll pack and the mill frame is indirectly modeled as viscous friction. That this and the other assumptions in the modeling are reasonable will be investigated in the system identification.

To find the unknown parameters of the models for the hydraulic systems and the rolling stand it is necessary to perform a system identification. The collection and preparation of the data for the system identification is described in Chapter 5.

5

Thickness Control—Data Collection

This chapter describes the data collection and the preprocessing of the data necessary before the system identification can be performed. The data have been collected during normal production without any extra excitation.

It will later be seen that the excitation is not ideal—this could be improved by injecting an external input signal. Two things can be said against this. First of all, the bandwidths of the hydraulic systems are small in comparison to the interesting modes of the rolling stand, and secondly the rolling process is quite sensitive and there is a risk of destroying expensive equipment. Because of this it has been chosen to collect the data during normal operation. This also has the advantage that they are collected under realistic conditions.

Ten plates were measured. The data shown in this chapter will all be from the same plate, which has a nominal thickness of 10 mm, a width of 2.15 m and a length of 10.5 m. The data from this plate will also be used for all the examples in the rest of this report. The measurements are quite unique since much effort has been made to get all the important signals for the rolling mill in one synchronized time series.

5.1 Measurement Equipment

From Chapter 4 we know that the relevant input and output signals for the models are:

- The positions of the servo valve gliders x_{vn} and x_{vs}.
- The positions of the common pistons z_n and z_s.
- The rolling forces f_n and f_s.

Name	Variable
North valve glider position	x_{vn}
North hydraulic position	z_n
North rolling force	f_n
Roll speed	v_r
South valve glider position	x_{vs}
South hydraulic position	z_s
South rolling force	f_s

Table 5.1 The variables of the models which are possible to measure as electrical signals. See also Figure 4.1.

- The rotational speed of the upper work roll v_r.
- The plate thickness at the north edge, the center and the south edge $v_d(x_1, t)$, $v_d(x_2, t)$, and $v_d(x_3, t)$.

The plate thickness is measured at the edges and the center since these three measurements give us the possibility to determine the plate crown. All variables in Table 5.1 exist as electrically measurable signals in the rolling mill control systems, while the thickness has to be measured after the rolling when the plate is cold.

Electrically Measurable Signals

The signals measured electrically are shown in Table 5.1. The measurements are done during the last pass. The last pass is the one that the effects the plate thickness. An example of the signals is shown in Figure 5.1. Since the measurement of the valve glider positions is quite noisy we measure the reference signal for the valve glider position instead. The thickness control is in *absolute mode* which yields the best excitation since this gives that largest variations in force and position. Note the low frequency excitation of z_n and z_s, furthermore, note that it is only possible to collect data for approximately 4 s for the plate before the pass ends.

It is not possible to measure the thickness of the plate during rolling, see Chapter 2. Furthermore, the accuracy of the existing thickness measurement device, which is placed after the rolling mill, is not sufficient. It is therefore necessary to measure the plates after the rolling when the plate is cold. Using the data for material density for steel ρ presented in Chapter 10 the thermal expansion from 20°C to 1000°C is computed to 1.4% this is considered neglectable and is therefore not considered in the following.

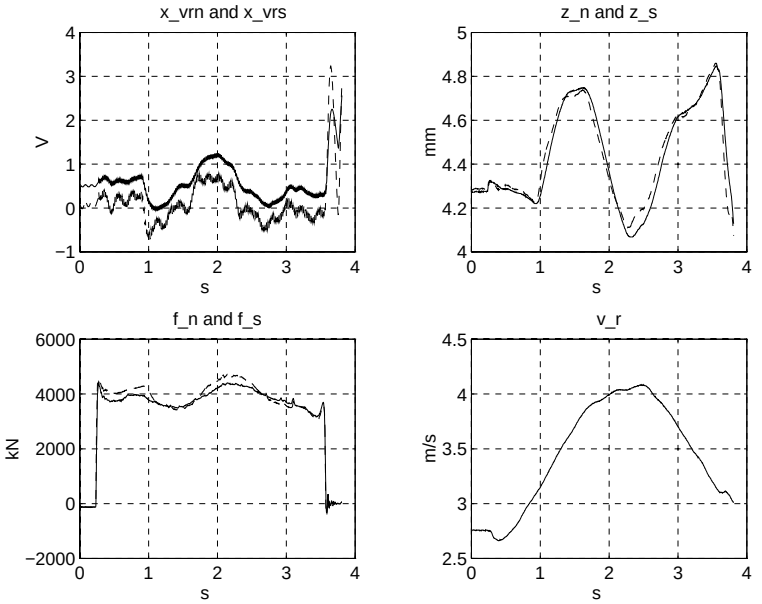

Figure 5.1 An example of the variables that are collected during one pass. Upper left: the references for the north servo valve x_{vrn} (full) and south servo valve x_{vrs} (dashed). Upper right: north position z_n (full) and south position z_s (dashed). Lower left: north rolling force f_n (full) and south rolling force f_s (dashed). Lower right: peripheral speed of the upper work roll v_r.

It was first tried to measure the plate thickness manually with a distance of 10 cm using a micrometer screw gauge. These measurements showed large variations and it was believed that this was due to poor precision of the screw gauge. A measurement device with an electronic screw gauge with serial communication interface was then constructed, a pulse encoder for length measurement was also mounted. A constant orientation to the plate when performing the measurements in a more continuous way yielded a higher accuracy. The thickness measurements were collected using a digital controller with the feature that the sampling frequency could be controlled using the pulse encoder, see [Bengtsson, 1994].

A fundamental problem when using the data is that the electrically measurable signals are obtained using *time sampling* and the thickness measurements are obtained using *spatial sampling*. This problem is solved by using the gaugemeter equation (3.2) for calculating a thickness estimate from the time sampled signals and then finding the times of the

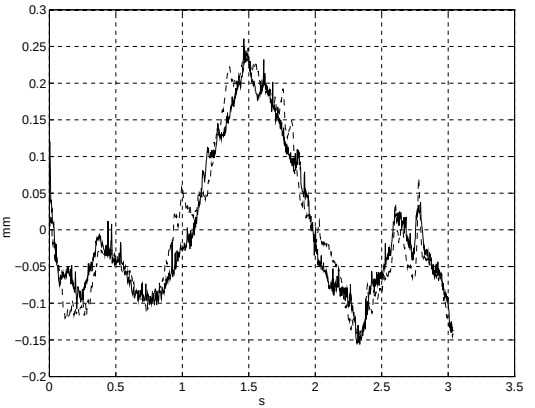

Figure 5.2 Measured thickness $\overline{v}$ (full) and estimated thickness $\overline{v}_e$ (dashed) thickness, when they are not low-pass filtered. The spatial resolution of the thickness measurements is 5 mm.

thickness measurements by minimizing the distance to the estimated thickness, for more details please refer to [Pedersen, 1995b]. The resulting thickness measurement and the thickness estimate are shown in Figure 5.2. Notice the nice fit. This illustrates that the gaugemeter principle gives a good estimate of the mean value of the plate thickness at the two edges.

5.2 Measurements for Identification

To obtain representative results for the identification it is chosen to measure 10 plates with 5 different nominal thicknesses and 2 different widths, the dimensions are shown in Table 5.2.

The widths of 2 and 3 m are chosen since they are close to the minimum and maximum of the plates rolled. The chosen thickness interval is representative for the plate production since the thickness of 95 % of the produced plates are in this interval. The data were collected during normal production and additional information about plate temperature, roll position and calculated thickness was thus available from the reports from the control system planning the rolling, see Chapter 2.

Thickness [mm]	Small width [m]	Large width [m]
6	2	3
10	2	3
20	2	3
30	2	3
40	2	3

Table 5.2 Nominal dimensions of the measured plates. The data from these ten plates will the basis for the system identification.

5.3 Conclusions

The inputs and outputs for the model for the rolling mill have now been collected. The data consist of the key variables for the last pass for 10 plates covering relevant thickness and width intervals.

Since the thickness measurements are found using spatial sampling and the other variables are found using time sampling it is necessary to align the data in some way. This is done estimating the time scale of the thickness measurements using the gaugemeter equation.

We now have the model and the input and output data represented as a time series. We are thus ready for the system identification which will be carried out Chapter 6.

6

Thickness Control—System Identification

In this chapter the parameters of the models for the hydraulic systems, the model for the rolling stand, and the observer for the rolling stand will be identified. The purposes of the models are controller design and simulation. Simplicity will be preferred to advanced structure. It will, in general, be possible to improve the results by adding more degrees of freedom, but this will imply lack of physical understanding and will therefore be avoided.

Due to the lack of excitation, nonparametric methods will not be used. Instead we will use restrictive parameterizations. This implies that all constants known in advance will be inserted in the models before the system identification is performed. The main advantage of this is that one is quite sure that the model is correct if only a couple of parameters of a physically derived structure are identified.

Much effort and time has been put into finding appropriate parametrizations and the problem of identifying the mill dynamics have been reduced to finding two parameters. Furthermore, the parameter variations are correlated with key variables. In this way we find parametric model variations which will be useful in the controller design.

The author has found no work on identification of rolling mills and the system identification is therefore described in detail. The model for the hydraulic systems is transformed to discrete time and a parameterization of the model is chosen. After this, the identification method is chosen, and the results of the identification are presented. The procedure for the identification of the rolling stand is similar, with the exception that we here have to find the parameters of both the model and the observer.

6.1 Hydraulic Systems

The model for the hydraulic systems was derived in Chapter 4. Here it will be rewritten to a form appropriate for the system identification. This implies a transformation to a suitable discrete time form. Since the model is nonlinear we will be working with nonlinear system identification. Only results for the model for the north hydraulic system will be shown here, since the model for the south system is similar.

Rewriting Equations

To be able to perform the system identification it is necessary to transform the differential equation to discrete time form. Exploiting an idea given in [Johansson, 1993] we simply integrate the nonlinear differential equations for the north hydraulic system, see (4.7)

$$-\dot{z}_{h_n}(t) = a_{hn1}\xi_n(t) - a_{hn2}(z_t - z_{h_n}(t))\dot{f}_n - a_{hn3}f_n(t), \tag{6.1}$$

where

$$\xi_n(t) = \begin{cases} x_{vn}(t)\sqrt{\overline{P}_s - f_n(t)} & x_{vn}(t) \geq 0 \\ x_{vn}(t)(\sqrt{\eta\overline{P}_s} + \sqrt{\eta\overline{P}_s + f_n(t)}) & x_{vn}(t) < 0. \end{cases}$$

If we furthermore divide by $z_t - z_{h_n}$ (which is always nonzero) before integrating we save a numerical differentiation because the integrand $(z_t - z_{h_n})\frac{d}{dt}f_n$ then can be evaluated analytically. The result is

$$y_n(t_1, t_2) = a_{hn1}\xi_{n_1}(t_1, t_2) + a_{hn2}\xi_{n_2}(t_1, t_2) + a_{hn3}\xi_{n_3}(t_1, t_2), \tag{6.2}$$

where

$$\begin{aligned} y_n(t_1, t_2) &= \ln\frac{z_t - z_{h_n}(t_2)}{z_t - z_{h_n}(t_1)} \\ \xi_{n_1}(t_1, t_2) &= \begin{cases} \displaystyle\int_{t_1}^{t_2} \frac{\sqrt{\overline{P}_s - f_n(t)}}{z_t - z_{h_n}(t)}dt & x_{vn}(t) \geq 0 \\ \displaystyle\int_{t_1}^{t_2} \frac{(\sqrt{\eta\overline{P}_s + f_n(t)} + \sqrt{\eta\overline{P}_s})}{z_t - z_{h_n}(t)}dt & x_{vn}(t) < 0 \end{cases} \\ \xi_{n_2}(t_1, t_2) &= f_n(t_2) - f_n(t_1) \\ \xi_{n_3}(t_1, t_2) &= \int_{t_1}^{t_2} \frac{f_n(t)}{z_t - z_{h_n}(t)}dt. \end{aligned}$$

Note that the parameters are unaffected by the discretization and that the system is still linear in the parameters. The integrals, which are not possible to evaluate analytically, can be calculated numerically.

Parameterization

Different parameterizations of the hydraulic model have been investigated and it is found that the parameterization of (6.2) works well. We thus have the three parameters a_{hn1}, a_{hn2}, and a_{hn3} to estimate. An analysis of the identifiability of the model for the hydraulic systems is found in [Pedersen, 1995b].

Identification

The performance index used in the identification is

$$V_n = \sum_{k=1}^{N} \theta_n^2(k),$$

where $\theta_n(k)$ is the prediction error of the model. The model for the north system is

$$y_{h_n}(k) = a_{hn1}\xi_1(k) + a_{hn2}\xi_2(k) + a_{hn3}\xi_3(k), \tag{6.3}$$

where

$$\xi_1(k) = \begin{cases} \displaystyle\int_{k-h}^{k} \frac{\sqrt{\overline{P}_s - f_n(t)}}{z_t - z_n(t)} dt & x_{vn}(t) \geq 0 \\ \displaystyle\int_{k-h}^{k} \frac{(\sqrt{\eta\overline{P}_s + f_n(t)} + \sqrt{\eta\overline{P}_s})}{z_t - z_n(t)} dt & x_{vn}(t) < 0 \end{cases}$$

$$\xi_2(k) = f_n(k) - f_n(k-h)$$

$$\xi_3(k) = \int_{k-h}^{k} \frac{f_n(t)}{z_t - z_n(t)} dt.$$

The model for the south system is analogous and is therefore not shown. For the identification it has been found that a sampling interval of $h = 0.025$ s is a good choice. Using this value of h some of the noise is averaged out while the dynamics of the system is still captured. $\eta = 0.15$ is found to give the best results.

To prevent extensive nonlinear noise transformations and to weight the data in an appropriate frequency interval the data is filtered using a fourth order Butterworth filter with a cut-off frequency of 100 Hz. The

relatively high cut off frequency is necessary due to the high frequency nature of ξ_2. The filtering is done using the MATLAB-function `idfilt`. Assuming that the noise can be described as additive filtered white noise implies that the model used for the identification is

$$y_{h_n}(k) = a_{hn1}\xi_1(k) + a_{hn2}\xi_2(k) + a_{hn3}\xi_3(k) + C(q^{-1})e(k),$$

where

$$C(q^{-1}) = 1 + c_1 q^{-1} + \cdots + c_n q^{-n}$$

and e is a white noise sequence and q is the forward shift operator. Note that the model has the same structure as an ARMAX-model with $A(q^{-1}) = 1$.

Since we have a non-standard problem we formulate the system identification as an optimization problem. Recalling that the model has ARMAX structure we simply compute the prediction error as

$$\theta_n(k) = \frac{1}{C(q^{-1})}\left(y_n(k) - (a_{hn1}\xi_1(k) + a_{hn2}\xi_2(k) + a_{hn3}\xi_3(k))\right),$$

where

$$y_n(k) = \ln \frac{z_t - z_n(k)}{z_t - z_n(k-1)}.$$

This implies that we use the *Maximum Likelihood method*, see [Åström and Eykhoff, 1971]. It is found that a third order noise polynomial is appropriate in the system identification. The minimum of the performance function is found using the nonlinear least squares function `leastsq` in MATLAB. The integrals in the regressors are computed using the MATLAB-function `trapz`.

Results

The identification is performed on the discrete time model (6.3) using the ten data sets described in Chapter 5. Since the signal for the position of the valve glider is very noisy the reference has been used instead. Using spectral analysis it has been found that the dynamics of the servo valve is neglectable compared with the dynamics of the process. The change of variables is therefore not expected to affect the system identification.

A plot of a typical result is shown in Figure 6.1. The agreement is quite good considering the assumptions made when deriving the model. Furthermore, the prediction error is close to white noise which indicates

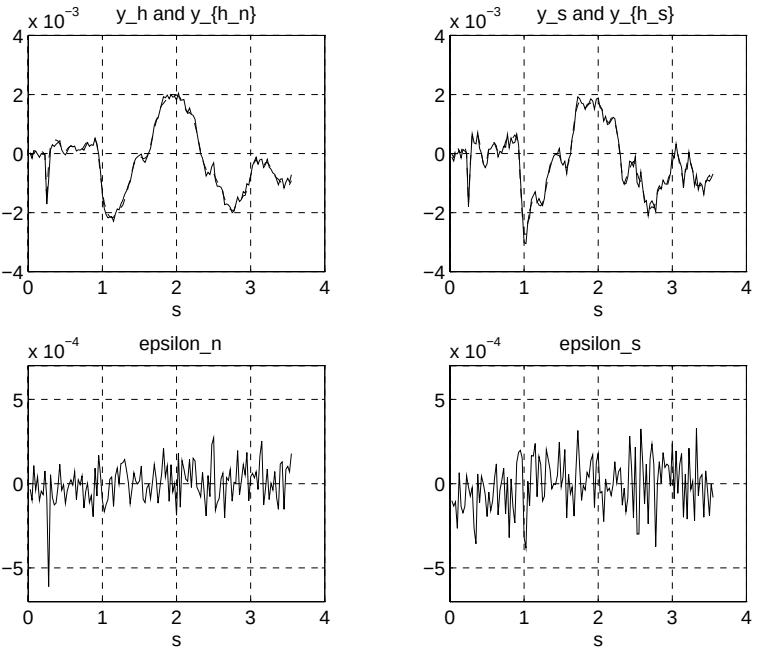

Figure 6.1 Results of the system identification of the hydraulic systems. Left side top: fit of the measured output y_n (full) and the predicted output y_{h_n} (dashed) and bottom: the prediction error θ_n. Right side top: fit of the measured output y_s (full) and and predicted output y_{h_s} (dashed) and bottom: the prediction error θ_s.

that we have an unbiased estimate of the parameters. Note that the beginning and end of the passes are included in the data—the peak in the prediction error for the north system arises when the plate enters the mill.

An example of a simulation using the original differential equation and the measured system response is shown in Figure 6.2. The implementation of the time derivatives when calculating $\frac{d}{dt}f$ is done using the backward difference approximation. The simulations are performed using the MATLAB-function `ode45` with the reference for the valve glider positions x_{vr} and the rolling forces f as input signals. The parameters used in the model are the ones identified from the data set shown. It is seen that there is good correspondence between the two responses. This shows that the assumption that the supply pressure P_s is constant and the assumptions regarding the pressures at the right and left sides of the common piston at the oil side work well in practice.

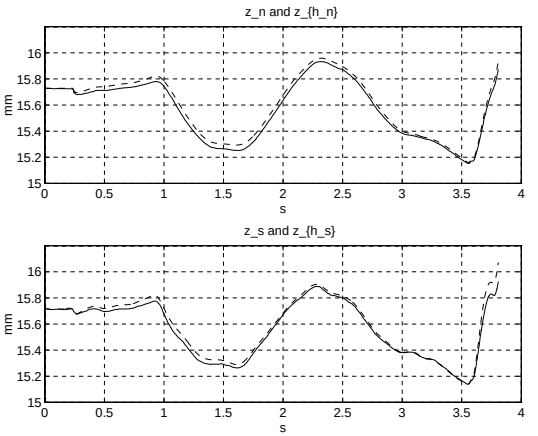

Figure 6.2 Simulation of the positions of the hydraulic systems using the parameters obtained from identification in simulation. Upper plot, full: measured response for north system z_n and dashed: simulated response for north system z_{h_n}. Lower plot, full: measured response for south system z_s and dashed: simulated response for north system z_{h_s}.

	North		**South**
a_{hn1}	$8.9 \cdot 10^{-1} \pm 5 \cdot 10^{-2}$	a_{hs1}	$8.1 \cdot 10^{-1} \pm 5 \cdot 10^{-2}$
a_{hn2}	$-7.6 \cdot 10^{-4} \pm 2 \cdot 10^{-4}$	a_{hs2}	$-9.2 \cdot 10^{-4} \pm 4 \cdot 10^{-4}$
a_{hn3}	$-2.6 \cdot 10^{-2} \pm 2 \cdot 10^{-2}$	a_{hs3}	$-2.7 \cdot 10^{-2} \pm 2 \cdot 10^{-2}$

Table 6.1 Table for nominal values of parameters with deviations for the hydraulic systems. The parameters are found using the 10 available data sets.

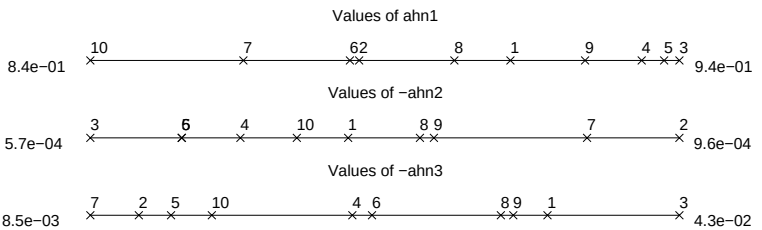

Figure 6.3 The distribution of the parameters for the north hydraulic system. The numbers refer to the ten data sets.

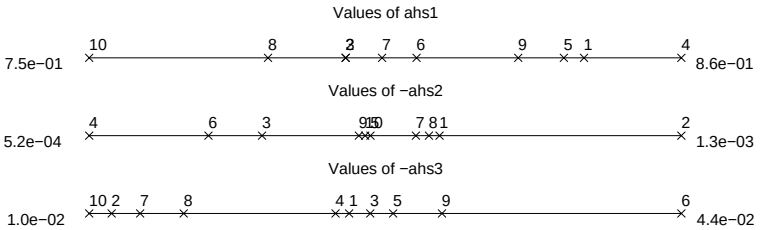

Figure 6.4 The distribution of the parameters for the south hydraulic system. The numbers refer to the ten data sets.

The parameters obtained from the identification of all the data sets are shown in Table 6.1. The distribution of the parameters for the two systems are shown in Figures 6.3 and 6.4. For the design in Chapter 7 we want to define a set of nominal parameters. The nominal parameters are chosen to be the center of the interval of the parameter estimates.

When identifying the above parameters the regressors were scaled to be of the same magnitude as the output—this was done to prevent numerical problems. Generally, all the regressors are of the same order of magnitude and we thus conclude that it is the parameters a_{hn1}, and a_{hs1} that have major influence. This implies that the model for the hydraulic systems will be close to an integrator if it is linearized. It is seen that these parameters vary less than 10% while the other parameters all vary within the same order of magnitude.

One could expect that the leak flows vary with the positions z_n and z_s due to differences in the wear of the oil cylinders. The variations of the parameters a_{hn3} and a_{hs3} are therefore not surprising. The compressibility of the oil covers many phenomena and it is therefore difficult to say much about the variations of the parameters a_{hn2} and a_{hs2}. The zero point for the servo valve for the southern system varies quite much and it has therefore been necessary to compensate for this. Comparing with the north side the accuracy of the parameter estimates seems to be unaffected by this.

Due to the small variations of the dominating parameters it is expected that parameter variations are of little importance. To confirm this we simulate the differential equation using the nominal parameter values. The result is shown in Figure 6.5. It is seen that the mean value of the simulated output drifts away, this is because the system is close to an integrator. This implies that the model will be sensitive to offsets in the input and since the zero point of the valve glider varies a bit this introduces the above effect. We solve the above problem by simply including an integrator when designing the controller.

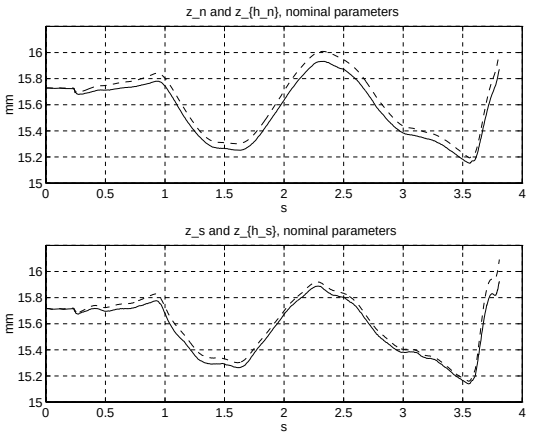

Figure 6.5 Simulation of the positions of the hydraulic systems using the nominal parameters from Table 6.1, the data set is the same as in Figure 6.2. Upper plot, full: measured response for north system z_n and dashed: simulated response for north system z_{h_n}. Lower plot, full: measured response for south system z_s and dashed: simulated response for north system z_{h_s}. This figure should be compared to Figure 6.2.

6.2 Rolling Stand

The two models for the rolling stand derived in Chapter 4 are linear and we thus have a more or less standard problem. To preserve the structure the parameters of the model and the observer will be identified using the original continuous time state space form. This can be done using the *System identification toolbox* in MATLAB, see [Ljung, 1991].

Not considering estimation of the roll eccentricity, the only reference on identifying rolling mill dynamics found is [Cumming, 1972]. In this reference the parameters of scalar equations are estimated using a correlator, and it is therefore a bit out of date.

Parameterization

Since we use the continuous time state space models (4.14) and (4.20) for the system identification no model transformations are necessary here. We thus proceed with the parameterization of the models.

The Model In the system identification it is found that the peripheral speed of the work roll $v_r(t)$ has little or no influence on the plate thickness and this input is therefore removed from the model. This is probably due to the fact the the friction inside the material can be modeled well as

static friction, which is independent of the magnitude of the deformation speed. We thus have the model structure

$$\begin{bmatrix} \dot{y}_c(t) \\ \hline q_c(t) \end{bmatrix} = \left[\begin{array}{c|c} A_c & B_c \\ \hline C_c & D_c \end{array}\right] \begin{bmatrix} y_c(t) \\ \hline \frac{1}{2}z(t) \end{bmatrix}$$
$$= \left[\begin{array}{cc|c} -a_{m2}\Gamma_1 & I & 0 \\ -EI\Gamma_2 - a_{m1}\Gamma_1 & 0 & EI(\rho A\Gamma_2\Gamma_3 - \Gamma_4) \\ \hline I & 0 & -\rho A\Gamma_3 \end{array}\right] \begin{bmatrix} y_c(t) \\ \hline \frac{1}{2}z(t) \end{bmatrix}, \tag{6.4}$$

where a_{m1}, a_{m2} are unknown scalar parameters. The state space equations are of fourth order. For an analysis of the identifiability of the model for the rolling mill see [Pedersen, 1995b].

The Observer Since changes in roll position $\frac{1}{2}z$ has a direct impact on the plate thickness, it is only necessary to scale the coefficients of the rolling force f and we thus introduce the matrix O_{fe}. The model structure then is

$$q_e(t) = O_{fe}\Gamma_6 f(t), \tag{6.5}$$

where

$$O_{fe} = \begin{bmatrix} o_{fe_1} & 0 \\ 0 & o_{fe_2} \end{bmatrix}.$$

The two unknown parameters in the observer are o_{fe_1}, and o_{fe_2}.

Identification

Since we have a multivariable problem we use the performance function

$$V = \det\left(\sum_{k=1}^{N} \theta(k)\theta(k)^T\right),$$

where θ is the prediction error. This implies that we are using multivariable maximum likelihood identification, see [Åström and Eykhoff, 1971]. To keep the models simple we choose not to introduce noise models and we therefore work with the state space structure

$$\begin{aligned} \dot{y}_c(t) &= A_c y_c(t) + B_c \tfrac{1}{2}z(t) + e(t) \\ q(t) &= C_c y_c(t) + D_c \tfrac{1}{2}z(t) + e(t), \end{aligned}$$

where e is white noise and q are the normal coordinates used in the series expansion of the solution. The normal coordinates can be determined using the thickness measurements at the three different positions across the plate width and the equation

$$\tfrac{1}{2}v_d(x,t) = \varepsilon(x)\tfrac{1}{2}z(t) + \sum_{i=1}^{2}\phi_i(x)q_i(t), \tag{6.6}$$

which is found by combining (4.10) and (4.13). Inserting the thicknesses of the three measurement tracks at the north edge, center, and south edge with positions x_1, x_2, and x_3 yields

$$\begin{bmatrix} \frac{1}{2}v_d(x_1,t) \\ \frac{1}{2}v_d(x_2,t) \\ \frac{1}{2}v_d(x_3,t) \end{bmatrix} = \begin{bmatrix} \varepsilon(x_1) \\ \varepsilon(x_2) \\ \varepsilon(x_3) \end{bmatrix} \tfrac{1}{2}z(t) + \begin{bmatrix} \phi_1(x_1) & \phi_2(x_1) \\ \phi_1(x_2) & \phi_2(x_2) \\ \phi_1(x_3) & \phi_2(x_3) \end{bmatrix} \begin{bmatrix} q_1(t) \\ q_2(t) \end{bmatrix}. \tag{6.7}$$

The above equation system is over-determined and is therefore solved in a least squares sense in MATLAB.

To obtain a well conditioned problem, all the signals are scaled to have amplitudes of the same order of magnitude. In the identification a fourth order Butterworth filter with a cut-off frequency of 10 Hz is used for filtering the position $\frac{1}{2}z$, the rolling force f, and the normal coordinates q. To obtain agreement between the mean thickness calculated by the model and the measurements, the mean value of the thickness at the plate edges is set to the value calculated using the gaugemeter equation, see Chapter 3. The procedure for the observer is similar to the above and is therefore not repeated here.

Results

The identification has been performed directly on the state space structure using `pem` in MATLAB. Since the sampling interval is small we can assume that the input signals are constant between the sampling instants when transforming the model to discrete time. Using the values found in [Pedersen, 1995b] for the mill spring coefficient $2K$, the stiffness of the roll pack EI, the mass of the roll pack ρA, and the value for the plate width w, we calculate the eigenvalues β_1 and β_2, and the two first eigenfunctions ϕ_1 and ϕ_2. The eigenfunctions are therefore computed in advance and are not estimated in the system identification, where they enter through the Γ_i-matrices.

Results for the Model The identification is based on the model with the parameterization shown in (6.4), the position of the hydraulic system

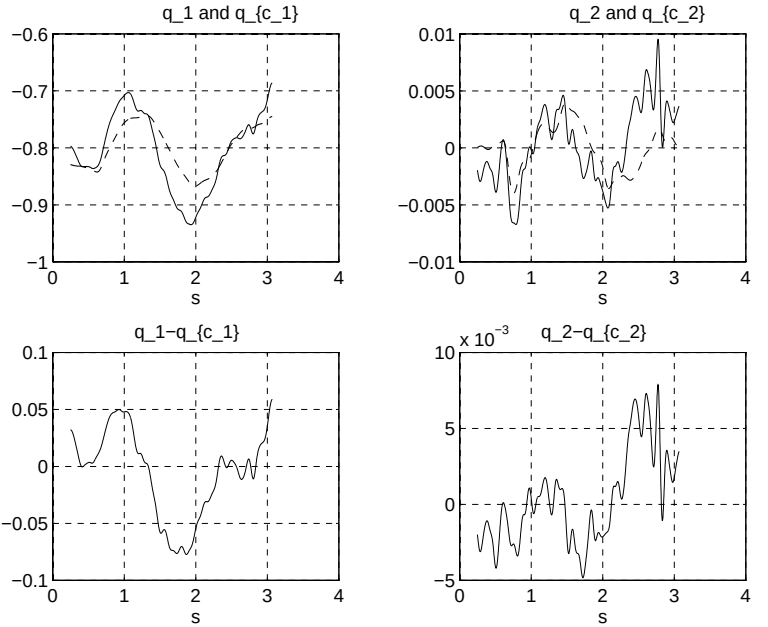

Figure 6.6 Identification results for the model. Left side, top: measured value of the normal coordinate q_1 (full) and estimated value of the normal coordinate q_{c_1} (dashed), bottom: prediction error for q_{c_1}. Right side, top: measured value of the normal coordinate q_2 (full) and estimated value for the normal coordinate q_{c_2} (dashed), bottom: prediction error for q_{c_2}. The results are not very good due to a time varying parameter a_{m1}.

$\frac{1}{2}z$ and the normal coordinates q found using (6.7). We obtain the results shown in Figure 6.6. The results are representative for all 10 data sets.

As seen from the figure, the agreement is not very good, this is because the parameter a_{m1} is time varying. The mean values of the normal coordinates are, however, estimated quite well. The variations of a_{m1} are investigated in more detail in [Pedersen, 1995b]. Note that the difference between the thickness at the two sides is predicted quite well considering the time varying parameter. This indicates that the plane strain assumption works well in our case.

Trial and error tests show that the precise value of the damping a_{m2} is not critical for the result of the identification. This is probably because of the low frequency excitation of the roll positions z. We thus fix it at the value $a_{m2} = 200$, which is the mean value found in the identification. The parameter a_{m1} is considered to be the most important parameter since it,

a_{m1}	$1.55 \cdot 10^4 \ -1.62 \cdot 10^5$
a_{m2}	$2.00 \cdot 10^3$

Table 6.2 Parameters for the model found using all 10 data sets.

together with β_1, determines both the undamped natural frequency and the stationary gain of the system. When identifying the parameter for the 10 data sets, we find that a_{m1} varies one order of magnitude. Trying to correlate it with key parameters for the rolling process we find that a_{m1} varies systematically with the plate hardness k_p, for more details please refer to [Pedersen, 1995b].

Performing the identification on all 10 data sets we find the parameters shown in Table 6.2. Due to variations of a_{m1}, which are well correlated with k_p, we introduce no nominal data set for the model but use the values specified by Table 6.2 instead.

A relevant question in connection with the variation of the parameter a_{m1} is: *How does this influence the dynamics of the rolling stand?* To investigate this we have seen that the dynamics of the model for the rolling stand can be divided into two SISO transfer functions. When transforming from normal coordinates q_c to plate thickness v_c the direct term almost disappears. Neglecting this gives the relationships

$$\begin{aligned}
\overline{v}_c(t) &= \overline{G}_{v_c}(p)\overline{z}(t) \\
&= \frac{\phi_1(\mu)\rho A\gamma_{3_1} EI\beta_1^4}{\rho Ap^2 + a_{m2}p + EI\beta_1^4 + a_{m1}}\overline{z}(t) \\
\grave{v}_c(t) &= \grave{G}_{v_c}(p)\grave{z}(t) \\
&= \frac{\phi_2(\mu)\rho A\gamma_{3_2} EI\beta_2^4}{\rho Ap^2 + a_{m2}p + EI\beta_2^4 + a_{m1}}\grave{z}(t)
\end{aligned}$$

where $\overline{v}_c$, $\grave{v}_c$ is half the difference between the north and south plate thickness v_{c_n} and v_{c_s}, $\overline{z}$ is the mean value of the north and south roll positions z_n and z_s, and $\grave{z}$ is half the difference between z_n and z_s. We see that $\overline{G}_{v_c}$ and $\grave{G}_{v_c}$ have no zeros and it therefore only is necessary to investigate the locations of the poles of the transfer functions. Inserting the values of a_{m1} and a_{m2} found in the system identification yields the pole locations shown in Figures 6.7 and 6.8.

We see that the poles tend to become faster and less damped when the plate hardness a_{m1} increases. Unfortunately the steady state gain of $\overline{G}_{v_c}$ and $\grave{G}_{v_c}$ also decreases with increasing plate hardness a_{m1} and it can therefore not be concluded that is becomes easier to control the plate

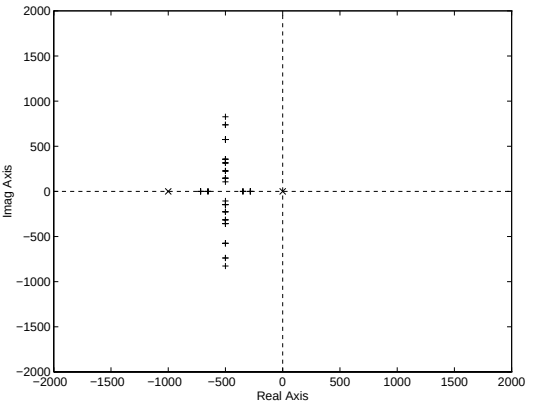

Figure 6.7 The pole locations for $\overline{G}_{v_c}$ as a function of a_{m1}. The crosses corresponds to $a_{m1} = 0$ and the poles with the largest imaginary part corresponds to the maximal value of a_{m1}. It is seen that the poles are real when a_{m1} is small and becomes faster and less damped when the value of a_{m1} increases.

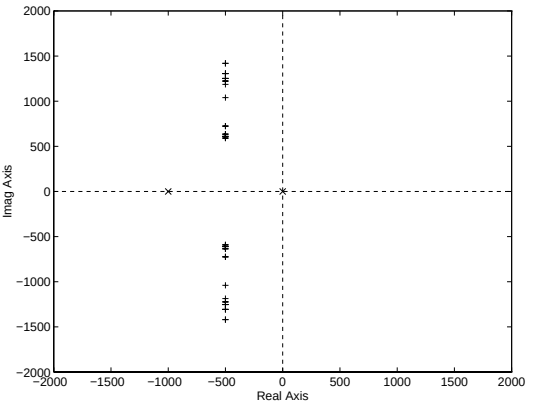

Figure 6.8 The pole locations for $\grave{G}_{v_c}$ as a function of a_{m1}. The crosses corresponds to $a_{m1} = 0$ and the poles with the largest imaginary part corresponds to the maximal value of a_{m1}. It is seen that the poles becomes faster and less damped when the value of a_{m1} increases.

thickness for the hard plates. For results of the system identification of a time varying model please refer to [Pedersen, 1995b].

Results for the Observer Using the observer given by (6.5), the rolling force f, and q found from (6.7) we perform the system identification for

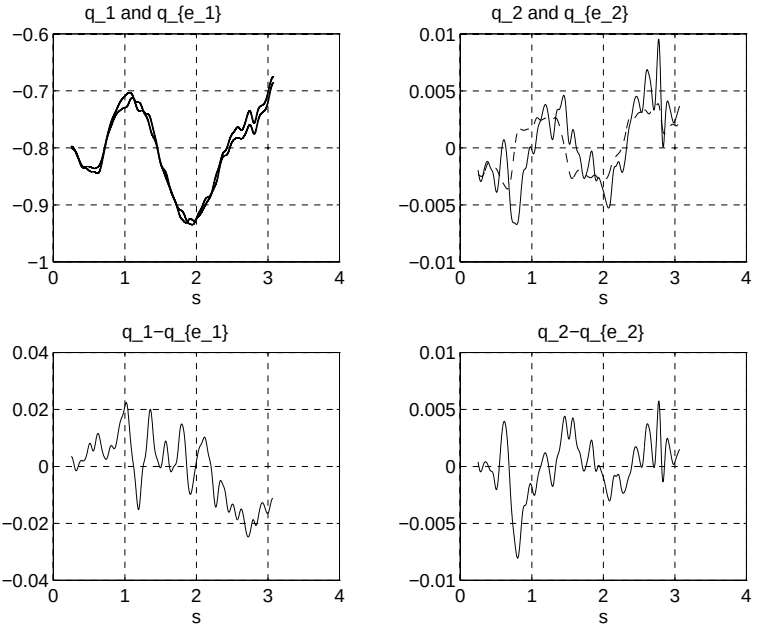

Figure 6.9 Identification results for the observer. Left side, top: measured value for the normal coordinate q_1 (full) and estimated value for the normal coordinate q_{e_1} (dashed), bottom: prediction error for q_{e_1}. Right side, top: measured value for the normal coordinate q_2 (full) and estimated value for the normal coordinate q_{e_2} (dashed), bottom: prediction error for q_{e_2}.

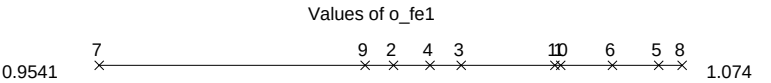

Figure 6.10 Distribution of the parameter o_{fe_1} for the observer. The nominal value of the parameter is 1.

the observer. A typical result is shown in Figure 6.9. Note that we now are able to predict the normal coordinates q quite well since we have knowledge of the variations of the plate hardness a_{m1} through the rolling force measurement. The results shown are representative for all 10 data sets.

The values of the parameter o_{fe_1} are shown in Figure 6.10. It is seen here that $o_{fe_1} \approx 1$, as expected. Ideally the parameters o_{fe_2} should also have the value 1, but from the system identification we find that $o_{fe2} \approx 0.2$

for the plate width $w = 2.15$ and $o_{fe2} \approx 0.4$ for $w = 3.15$. The reason that we only have data for two values of the plate width w is that the ten data sets are from plates with only two different widths. The reason for the plate widths being larger than specified in Chapter 5 is that the plates are rolled a bit wider than specified and then cut to the nominal measures after rolling.

Inspecting the force measurements we find that the boundary conditions

$$
\begin{aligned}
& f_n(t) = 2Ku(0,t) \approx 2K(q_1(t)\phi_1(0) + q_2(t)\phi_2(0)) \\
& f_s(t) = 2Ku(w,t) \approx 2K(q_1(t)\phi_1(w) + q_2(t)\phi_2(w)) \\
& \Downarrow \\
& \overline{f}(t) \approx 2K\phi_1(0)q_1(t) \qquad (6.8) \\
& \hat{f}(t) \approx 2K\phi_2(0)q_2(t), \qquad (6.9)
\end{aligned}
$$

where $\overline{f}$ is the mean value of the rolling forces and, $\hat{f}(t)$ is the difference between the forces, are not fulfilled. The plots of the left and right sides of (6.8) and (6.9) are shown in Figure 6.11. Here we see that the left and right side of (6.8) agrees quite well but that there is a significant deviation between the left and right side of (6.9). The amplitude of the difference of the rolling forces $\hat{f}$ is too large—this explains why o_{fe_2} becomes smaller than 1.

One explanation to the above could be that the connection between the two legs of the rolling stand is not included in the physical model. It is quite possible that the above difficulty could be avoided by inserting a spring between the two sides of the physical model. Another possibility is that the force measurement is inaccurate. If this is found to be the case, an improvement of the force measurements is necessary to obtain a better agreement between model and data.

Using the results from the identification we arrive at the values for the nominal parameters shown in Table 6.3. Since the identification is based on a fixed value of the parameter o_{fe_2} and the variation of o_{fe_1} is small, no simulations of the nominal model is shown, since they will be similar to the results of Figure 6.9.

Using (6.6) the thickness predicted by the observer at the measurement points can be calculated. The results are shown in Figure 6.12. We note that now the predicted and measured thicknesses agree quite well due to the rolling force measurement. Also for the observer the calculated plate crown is close to its measured value.

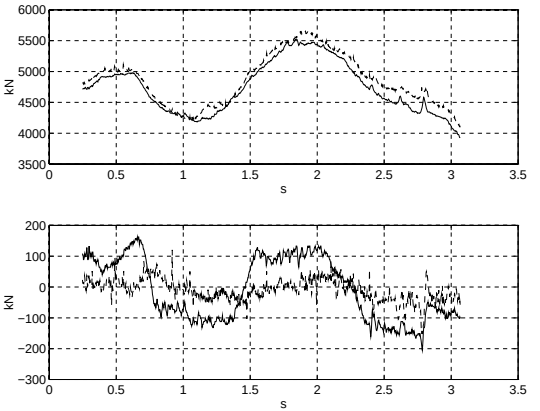

Figure 6.11 Illustration of that the rolling force measurements do not fulfill the boundary conditions. Upper plot: mean value of the rolling forces $\overline{f}$ full and $2K\phi_1(0)q_1$ (dashed). Lower plot: difference between the rolling forces $\tilde{f}$ full and $2K\phi_2(0)q_2$ (dashed).

	$w = 2.15$	$w = 3.15$
o_{fe_1}	1	1
o_{fe_2}	0.2	0.4

Table 6.3 Parameters of the observer as functions of the plate width w. The parameters are found using all the 10 data sets

6.3 Total Model

In Chapter 4 we derived a total model including both the hydraulic systems and the rolling stand. The models for the hydraulic systems, the model for the rolling stand, and the observer for the rolling stand are implemented in OMSIM using (6.1) and (6.4), see [Andersson, 1994]. This simulation environment is well equipped for handling discrete event systems, such as the hydraulic positioning systems where the structure of the differential equations changes at $x_{vn} = 0$ and $x_{vs} = 0$.

The parameters used for the simulations are the ones found from the system identification. An exception is that the parameter of the observer o_{fe_2} is set back to 1, for the model and the observer to match. Note that this only affects the estimation of the states of the model.

The results of a simulation of the total model are shown in Figure 6.13.

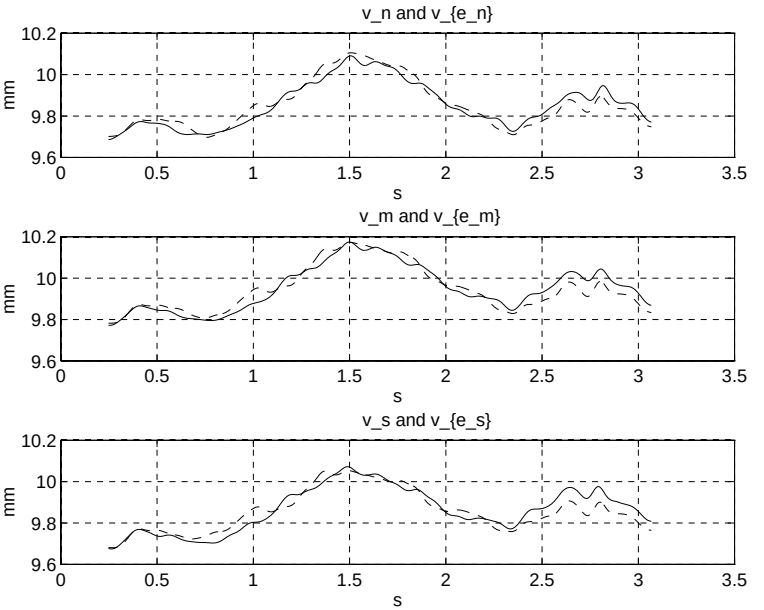

Figure 6.12 The thickness at the plate edges and center calculated using the observer. Upper plot: the measured value $v_d(x_1)$ (full) and the calculated value v_{e_n} (dashed) of the thickness at the northern edge. Center plot: the measured value $v_d(x_2)$ (full) and the calculated value v_{e_m} (dashed) of the thickness at the center. Lower plot: the measured value $v_d(x_3)$ (full) and the calculated value v_{e_s} (dashed) of the thickness at the southern edge v_s.

The input signals are chosen as

$$x_{vrn}(t) = \begin{cases} 10 & 0 \leq t < 0.1 \\ 0 & t > 0.1 \end{cases}$$
$$x_{vrs}(t) = \begin{cases} 10 & 0 \leq t < 0.2 \\ 0 & t > 0.2. \end{cases}$$

where x_{vrn} is the reference signal for the north servo valve and x_{vrs} is the reference signal for the south servo valve. At $t = 0$ the outgoing thickness is equal to the ingoing thickness of the plate, which is 11.64 mm and the rolling force is zero. Then the hydraulic positioning systems moves downwards, the rolling force increases and the outgoing thickness decreases. At $t = 0.1$ the north system stops, but it is seen that the rolling force and the thickness at the north side continue to change due

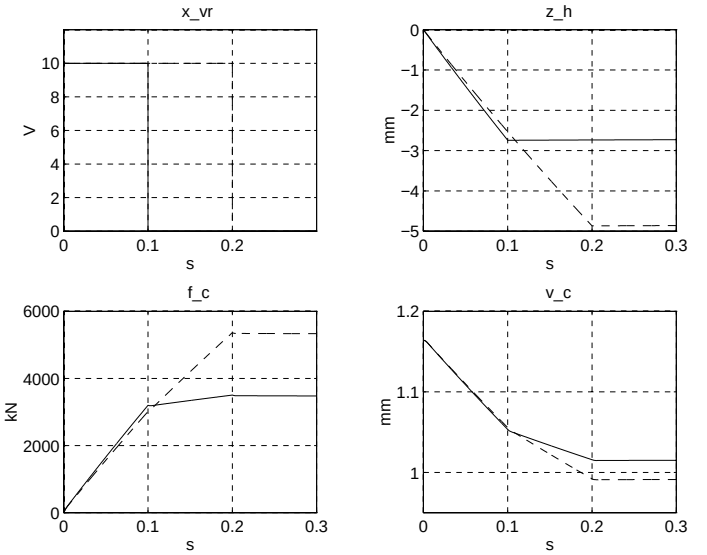

Figure 6.13 Simulations of total model for rolling mill. Upper left: control signal for valve glider positions for north x_{vrn} (full) and south x_{vrs} (dashed) hydraulic system. Upper right: Positions of north hydraulic system z_{h_n} (full) and south hydraulic system z_{h_s} (dashed). Lower left: north rolling force f_{c_n} (full) and south rolling force f_{c_s} (dashed). Lower right, plate thickness north edge v_{c_n} (full) and plate thickness south edge v_{c_s} (dashed).

to the movement of the position of the south system. This illustrates the multivariable structure of the system.

It is seen that the hydraulic systems act as integrators. They move with a slightly different speed for the same input due to the different values of the parameters a_{hn1} and a_{hs1}. The states of the model y_c and the states of the observer y_e are shown in Figure 6.14. The simulation here is the same as the one shown in Figure 6.13. It is seen that the states of the model and the states of the observer agrees well.

6.4 Conclusions

In this chapter we have found the parameters of the model for the rolling mill. For the hydraulic systems we have found a set of nominal parameters and for the model for the rolling stand we have found one constant and one time varying parameter. For the observer we have found two parameters, one constant and one which varies with the plate width. The agreement

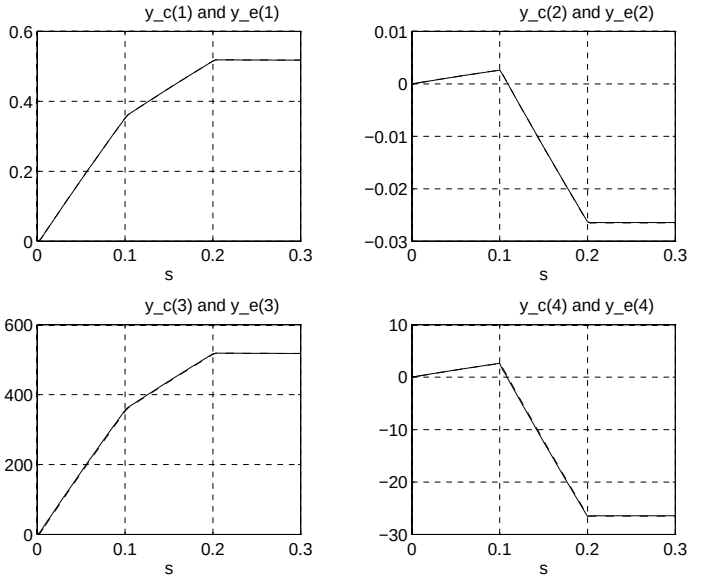

Figure 6.14 Comparison of the four states of the model y_c (full) and the state estimate found by the observer y_e (dashed). It is seen that the agreement between the real and estimated value is good.

between model and data are all satisfactory, it was, however, necessary to introduce extra parameters in the observer since two of the four boundary conditions used for calculating the plate thickness were not fulfilled.

The models have been implemented in a suitable simulation environment and we are now ready for the controller design. This will be done in Chapter 7.

7

Thickness Control—Design

The purpose of this chapter is to design a thickness controller for the rolling mill, which consists of the hydraulic positioning systems and the rolling stand. The purpose of the controller is to ensure that the desired plate thickness is obtained with as small deviations as possible, despite the process disturbances.

The performance specifications of the control systems are first given, this includes description of typical disturbances and the multivariable nature of the system. Then the controlled outputs are chosen, the multivariable structure, the dynamics of the system, and the steady state gains are analyzed.

The above forms the basis for the choice of methods for controlling the rolling mill. The controllers are then designed using the models and parameters found in the previous chapters. In general, time invariant methods will be used for the controller design and we therefore assume that the material parameters are constant during the pass in the following. The effects of the variations of the material parameters will be investigated in the simulations.

In the last section of this chapter the performance of the control system is investigated using computer simulations. Here the effects of reference changes and typical disturbances are found and commented.

No work on multivariable thickness control of hot rolling mills has been found. Several descriptions of the single-input single-output case are given in [Kokai *et al.*, 1985], [Saito *et al.*, 1981], [Teoh *et al.*, 1984], [Ferguson *et al.*, 1986] and many more. Furthermore, advanced control and estimation methods have been used in connection with the elimination of the effects of roll eccentricity, see [Yeh *et al.*, 1991], [Teoh *et al.*, 1984], and [Asada *et al.*, 1986]. For further details see Chapter 3.

7.1 Performance Specifications

As described in Chapters 2 and 3 the purpose of the thickness control is to obtain a specified constant thickness, despite disturbances such as

- variations of the plate hardness;
- variations of the ingoing thickness.

The thickness control problem is thus a regulator problem, see [Åström and Wittenmark, 1997]. A central goal of the control is to minimize the thickness variations of the rolled plates. The quality level possible to obtain depends on saturation of the control signal and the amplitude of the variations. It might therefore be necessary to minimize the variations by other means to obtain the desired value of the thickness variations.

The rolling process is a multivariable system, this has to be taken into consideration when controlling the process. A natural demand is to be able to control the thickness at the north and south edge independently of each other. This will make it possible to handle reference changes and control errors at one edge with minimal effect on the thickness at the other edge. Furthermore, the controller has to be able to compensate for asymmetric material conditions. This is not possible with the existing control, see Chapter 3.

A third important issue is the stability of the thickness control system. The stability is disturbed by two effects:

- variations of the material characteristics;
- the controlled variable (the thickness) has to be estimated.

This has lead to a detuning of the compensation for mill deflection in traditional thickness control systems, see Chapter 3. An analysis of the stability of the thickness control system is given in [Pedersen, 1995b].

In the system identification of the hydraulic systems in Chapter 6 we found that the models of the hydraulic systems were sensitive to offsets in the control variable. It was concluded that including an integrator in the controller would solve this problem when controlling the roll position. We therefore include an integrator in the controller design. It will bee seen later that using an integrator is also a good idea in connection with the control of the plate thickness.

The handling of the start and the end of the pass will not be discussed in the following. Since the plate ends usually are non rectangular, the physical model for the rolling stand does not cover this case, since the plate will not have full width when entering the roll gap. The plate ends furthermore tend to be colder than the rest of the plate. To ensure a proper start up and shut down of the control it is likely that a special control strategy is necessary to handle the beginning and end of the passes.

7.2 Analysis of Model

The first natural question that arises is, at how many points in the width direction is it possible to control the thickness of the plate using the two hydraulic actuators. We study this to choose the number of outputs we want to control. Looking at the state equations of the model we see that in steady state we have that

$$\begin{aligned} \dot{y}_c(t) = 0 &= A_c y_c(t) + B_c \tfrac{1}{2} z(t) \\ &\Downarrow \\ y_c(t) &= -A_c^{-1} B_c \tfrac{1}{2} z(t), \end{aligned}$$

where the system matrix A_c is invertible. The above implies that we are only able to control the state vector in stationarity within a two dimensional plane. We can therefore not control more than two outputs in stationarity with the thickness control. The thickness of a plate are normally measured at a distance μ from the plate edges. Our outputs are thus chosen as

$$\begin{aligned} \begin{bmatrix} v_n(t) \\ v_s(t) \end{bmatrix} &= \begin{bmatrix} v_d(\mu, t) \\ v_d(w-\mu, t) \end{bmatrix} \\ &= 2 \begin{bmatrix} \phi_1(\mu) & \phi_2(\mu) \\ \phi_1(w-\mu) & \phi_2(w-\mu) \end{bmatrix} \begin{bmatrix} q_1(t) \\ q_2(t) \end{bmatrix} + \begin{bmatrix} \varepsilon(\mu) \\ \varepsilon(w-\mu) \end{bmatrix} z(t). \end{aligned}$$

Using our physical insight we choose the north position z_n for controlling the north thickness v_n and the south position z_s for controlling the south thickness v_s.

Investigating the multivariable structure of the system we apply a step of 1 mm at the north position z_n. The open-loop step response is shown in Figure 7.1. We see that the thickness at both edges is affected by the position change at one of the sides. Furthermore, it can be seen from the step responses that two systems with different dynamics are involved. This is due to the fact that the dynamics for the normal coordinates q_{c_1} and q_{c_2} are different. Note the direct term, which is the result of inaccuracies in connection with the state transforms used in the modeling. The direct term is small compared to the steady state gain of the system and it will be neglected in the controller design. It will though be included in the simulations.

The multivariable effect illustrated in Figure 7.1 causes trouble when controlling the thickness at the two sides independently. If the thickness at the north side deviates from the specified value while the south thickness does not, it is not possible to obtain the correct thickness by just

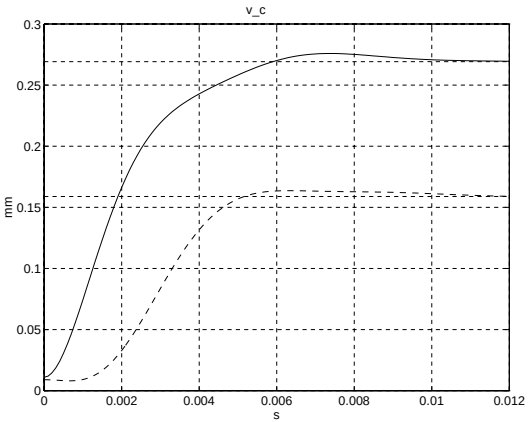

Figure 7.1 Simulation using the total model in Section 6.3. Open-loop result of a step change of 1 mm in the north position z_n. The step is applied at $t = 0$. Full: thickness at north edge v_{c_n} and dashed: thickness at south edge v_{c_s}. It is seen that the position change at one side affects the thickness at both sides of the rolling stand

adjusting the hydraulic position at the north side. It is thus necessary to consider the multivariable nature of the system when designing the controller. Ideally it should be possible to control the thickness at the two sides independently of each other.

Looking at the mean values for position $\overline{z}$ and thickness $\overline{v}$, and neglecting the direct term, the relationship is given by the second order linear system

$$\overline{v}(t) = \overline{G}_{v_c}(p)\overline{z}(t) = \frac{\phi_1(\mu)\rho A\gamma_{3_1} EI\beta_1^4}{\rho Ap^2 + a_{m2}p + EI\beta_1^4 + a_{m1}}\overline{z}(t).$$

The dynamics of this transfer function varies due to the variations of a_{m1}. A similar transfer function $\grave{G}_{v_c}$ can be derived for the wedge of the position $\grave{z}$ and the wedge of the thickness $\grave{v} = \frac{1}{2}(v_n - v_s)$. Using the values obtained from the system identification the undamped natural frequencies of the two transfer functions $\overline{\omega}_n$ and $\grave{\omega}_n$ are in the intervals

$$\overline{\omega}_n \in [200,\ 432] \text{ rad/s}$$
$$\grave{\omega}_n \in [342,\ 658] \text{ rad/s}.$$

The steady state gains of the rolling stand $\overline{k}_g$ and $\grave{k}_g$ are in the intervals

$$\overline{k}_g \in [0.136,\ 0.404]$$
$$\grave{k}_g \in [-0.0142,\ 0.287],$$

that is, they vary a factor 3. Generally, $\overline{k}_g$ will lie in the interval between zero and one. If the plate hardness is close to zero, $\overline{k}_g$ will be close to one and when the plate becomes very hard $\overline{k}_g$ will be close to zero. This illustrates why an important part of the optimization of the rolling mill is to do the rolling in minimal time to keep the plate as hot as possible.

Since the hydraulic positioning systems are the actuators of the thickness control system, they set the limits of achievable performance. The variables that mainly affect the limitations of the positioning systems are:

- the supply pressure $\overline{P}_s$;
- the valve glider positions x_v.

This introduces limits on the values of the rolling forces f, the roll positions z and the reduction r_d. The maximal mill deflection is determined by the maximal rolling force and thus by $\overline{P}_s$. Since this limit is smaller than the maximal position z_t it is the above limitations and not the structure of the hydraulic systems that set the limits for the positions z.

The hydraulic systems operate under very different conditions. The rolling force, which determines the gain of the system, varies from zero to the value of the supply pressure $\overline{P}_s$ and this should be taken into consideration, when designing the controller for the hydraulic systems.

Experiments show that using small closed loop step responses for the existing hydraulic systems including PI-controllers we find that they have a damping factor of $\zeta = 0.7$ and a peak time $t_p = 0.07$. This yields a undamped natural frequency of the hydraulic systems of

$$\omega_{nh} = 24.6 \text{ rad/s}.$$

We see that the dynamics of the hydraulic systems are considerably slower than the dynamics of the mill stand. This is one of the reasons why it is difficult to eliminate the high frequency variations of the plate thickness. Making the hydraulic system faster is of course a question about saturation of the control signal, but according to the constructor of the existing control system it is possible to make it considerably faster when implementing a digital controller.

7.3 Choice of Control Methods

The controller design will be done in continuous time. This makes it possible to utilize the structure of the physical models we have derived and identified in the previous chapters. It will be necessary to implement the control strategies using digital equipment and the control strategy therefore has to be transformed to discrete time. This can be done using the approximate methods described in [Åström and Wittenmark, 1997]. The price to be paid for this procedure is that it is necessary to implement the controller using a higher sampling frequency than if the design was done in discrete time.

To make the hydraulic systems work well at all operating points, it is necessary to use a non-linear control strategy. Since we only have a first order system and all states and inputs can be measured or estimated, it is chosen to use feedback linearization for controlling the hydraulic systems, see [Slotine and Li, 1991].

The responses of the two sides of the rolling mill are separated using eigenspace design described in [Harvey and Stein, 1978]. This makes it possible to assign specified values to the eigenvectors of the closed loop system. The additional eigenvectors and eigenvalues for which we have no specifications are furthermore placed in a “nice" way.

The variation of the material hardness a_{m1} changes the steady state gain of the system and it is necessary to compensate for this in some way. The plate thickness can, despite the parameter variations, be estimated using the observer. Using an integrator it is possible to ensure that the closed loop steady state gain is not affected by the parameter variations. The variations of the plate hardness a_{m1} will still affect the dynamics and the stability of the system.

The parameter variations raise the question if adaptive control is needed. It will therefore in simulations be investigated if the performance of the chosen design strategy is satisfactory or if a truly adaptive controller is needed.

7.4 Design of Controllers

In the following sections the controllers for the hydraulic systems and the rolling stand will be designed. The hydraulic systems will be controlled using feedback linearization and the rolling stand will be controlled by a state feedback, found using eigenspace design.

Hydraulic Systems

Since we have a first order system it is quite easy to derive a control law that linearizes the system. Even if some of the usual assumptions on the input function such as independence of the control variable x_{v_n} and smoothness are not fulfilled it is still possible to do the feedback linearization. As usual we only show the results for the north system since the procedure of the south system is the same. To increase the number of the degrees of freedom in the eigenspace design we give the hydraulic systems a time constant κ when doing the feedback linearization. κ is then used as a design parameter in the eigenspace design.

We choose the control signal as

$$x_{vrn}(t) = \frac{1}{-a_{hn1}\xi_{n_1}(t)} \left(-a_{hn2}\xi_{n_2}(t) - a_{hn3}\xi_{n_3}(t) + r_{l_n}(t) - \kappa z_{h_n}(t)\right), \quad (7.1)$$

where

$$\xi_{n_1}(t) = \begin{cases} \sqrt{\bar{P}_s - f_n(t)} & x_{vn}(t) \geq 0 \\ \sqrt{\eta \overline{P}_s} + \sqrt{\eta \overline{P}_s + f_n(t)} & x_{vn}(t) < 0 \end{cases}$$

$$\xi_{n_2}(t) = (z_t - z_{h_n}(t)) \frac{d}{dt} f_{c_n}(t)$$

$$\xi_{n_3}(t) = f_n(t).$$

Here r_{l_n} is the control signal from the thickness controller. The north position z_n, the position of the valve glider x_{vn}, and the north rolling force f_n can be measured directly and $\frac{d}{dt} f_{c_n}$ can be estimated using the relationship

$$\frac{d}{dt} f_{c_n}(t) = 2KF \frac{d}{dt} q_c(t),$$

found in Section 4.3. To determine the derivative of the normal coordinates $\frac{d}{dt} q_c$ we can use the model for the rolling stand and the differential equations for the hydraulic systems. This is not trivial since a good estimate of the plate hardness a_{m1} is necessary to do this. An alternative is to use approximative numerical differentiation of the rolling force f to find $\frac{d}{dt} f$.

We note that the control strategy demands that $f_n < \overline{P}_s$. When the pressure due to the rolling force f_n gets close to the supply pressure $\overline{P}_s$ the thickness control will in any case be switched off to prevent overload of the hydraulic system. It is therefore not necessary to worry about the case $f_n = \overline{P}_s$.

Using the above strategy the model for the hydraulic system reduces to

$$\dot{z}_{h_n}(t) = -\kappa z_{h_n}(t) + r_{l_n}(t)$$

and can thus be inserted as an extra state in the state space equations for the rolling stand.

Thickness Controller for the Rolling Stand

We now proceed with the design of the controller for the rolling stand. The main idea is to design a well tuned controller which can handle asymmetric disturbances. The design will be performed on the model for the rolling stand combined with the now linear hydraulic systems and two additional integrator states. The main idea in the eigenspace principle is that, in addition to the desired closed loop poles, a set of desired closed loop eigenvectors is also specified—this is possible since we are working with a multivariable system, see [Kailath, 1980] and [Moore, 1976].

The response of the closed loop system due to the initial conditions q_{c_o} can be written as

$$v_c(t) = \sum_{j=1}^{n} C_c \nu_j (\psi_j^T q_{c_o}) e^{\lambda_j t}, \tag{7.2}$$

where the λ_j's are the closed loop eigenvalues and ν_j are the right closed loop eigenvectors defined by

$$(I\lambda_j - (A_c - B_c L))\nu_j = 0 \tag{7.3}$$

and ψ_j are the left closed loop eigenvectors fulfilling $\psi_j^T \nu_j = 1$, see [Kailath, 1980] for details.

It is possible to affect the eigenvectors by the choice of the feedback matrix L. It is here assumed that the closed loop eigenvalues are simple, this implies that the closed loop eigenvectors all are linearly independent. Assuming that the closed loop eigenvalues $\lambda_j \neq \mathrm{sp}(A_c)$ we can rewrite (7.3) as

$$\begin{aligned} \nu_j &= (I\lambda_j - A_c)^{-1} B_c \mu_j \\ \mu_j &= -L\nu_j. \end{aligned} \tag{7.4}$$

The idea of the eigenspace design is then to choose the feedback matrix L to obtain the desired eigenvectors, if possible.

The desired closed loop eigenvalues for the new thickness controller are chosen to give the same magnitudes of the control signals as used by the existing control system. There are two reasons for this:

- It is hard to say when the hydraulic positioning systems saturate since this depends on the nature of the disturbances and the characteristics of the supply equipment. It is therefore more natural to adjust the response speed of the controller when it is implemented.
- It will be possible to compare the performance of our control system to the performance of the existing control system.

Using the control law found in the previous section the hydraulic systems can be included as a part of the state space model. Since it is half of the position $\frac{1}{2}z$ that is used in the model for the rolling stand it is most convenient to use half of the position as a state. As seen in the previous section the steady state gain of the open loop system varies due to the variations of the plate hardness a_{m1}. The simplest way of avoiding this for the closed loop system is to calculate the plate thickness

$$v_c(t) = \begin{bmatrix} \Phi & 0 \end{bmatrix} y_c(t)$$

and introduce two integral states i

$$\frac{d}{dt} i = \tfrac{1}{2} r(t) - v_c(t)$$

where $r^T = \begin{bmatrix} r_n & r_s \end{bmatrix}$ are the references for the plate thickness. The state space representation including the hydraulic positions and the integral states is

$$\left[\begin{array}{c} \dot{y}_c(t) \\ \frac{1}{2}\dot{z}_h(t) \\ \hline i(t) \\ \hline v_c(t) \end{array}\right] = \left[\begin{array}{c|c} A_{ch} & B_{ch} \\ \hline C_{ch} & D_{ch} \end{array}\right] \left[\begin{array}{c} y_c(t) \\ \frac{1}{2}z_h(t) \\ \hline i(t) \\ \hline r_l(t) \\ \frac{1}{2}r(t) \end{array}\right]$$

$$= \left[\begin{array}{ccccc|cc} -a_{m2}\Gamma_1 & I & 0 & 0 & 0 & 0 \\ -EI\Gamma_2 - a_{m1}\Gamma_1 & 0 & EI(\rho A\Gamma_2\Gamma_3 - \Gamma_4) & 0 & 0 & 0 \\ 0 & 0 & -\kappa I & 0 & I & 0 \\ -\Phi & 0 & 0 & 0 & 0 & I \\ \hline \Phi & 0 & 0 & 0 & 0 & 0 \end{array}\right] \left[\begin{array}{c} y_c(t) \\ \frac{1}{2}z_h(t) \\ \hline i(t) \\ \hline r_l(t) \\ \frac{1}{2}r(t) \end{array}\right] \tag{7.5}$$

Using the eigenspace design approach first described in [Harvey and Stein, 1978] and later generalized in [Stein, 1979] we find that by choosing the weighting matrices for a LQG controller in a special way it is possible to obtain a set of specified closed loop eigenvalues and eigenvectors. The eigenvalues and eigenvectors are obtained asymptotically as the control

weight σ tends to zero. The number of design parameters are thus reduced to one when the eigenvalues and eigenvectors are chosen. The result is the algebraic Riccati equation with σ as design parameter

$$0 = PA_{ch} + A_{ch}^T P + Q + PB_{ch_1} R^{-1} B_{ch_1}^T P/\sigma \tag{7.6}$$

can be used for finding the feedback matrix

$$L = R^{-1} B_{ch_1}^T P/\sigma. \tag{7.7}$$

The derivation of the matrices A_{ch}, B_{ch_1}, B_{ch_2}, Q, R is described in [Pedersen, 1995b].

Unfortunately, it is difficult to solve the Riccati equation algebraically and we therefore have to use numerical tools for finding L. An example of the results of the design with closed loop eigenvalues $\lambda_f = 125$, a time constant for the linearized hydraulic systems $\kappa = 50$, and a control weight $\sigma = 1{\cdot}10^{-4}$ are shown in Figure 7.2. Note that the two sides are practically decoupled. Full decoupling requires large gains of the feedback matrix. This is not a good idea considering saturation and stability aspects.

When computing the steady state gain of the closed loop system we find that

$$C_{ch}(-A_{ch} + B_{ch_1} L)^{-1} B_{ch_2} \approx I.$$

This indicates that the separation of the two sides has been successful since a reference change for one of the sides does not affect the other side in stationarity.

As stated earlier it is not possible to measure the process output, and we can therefore not use a traditional observer. Instead we use the static relationships found in Section 4.2 and extend it with the position measurement $\frac{1}{2}z$ and the integral states i

$$\begin{bmatrix} y_e(t) \\ \frac{1}{2}z(t) \\ i(t) \end{bmatrix} = D_{eh} \begin{bmatrix} \frac{1}{2}z(t) \\ f(t) \\ i(t) \end{bmatrix} = \begin{bmatrix} \rho A \Gamma_3 & \Gamma_6 & 0 \\ a_{m2}\Gamma_3 & a_{m2}\Gamma_1\Gamma_6 & 0 \\ I & 0 & 0 \\ 0 & 0 & I \end{bmatrix} \begin{bmatrix} \frac{1}{2}z(t) \\ f(t) \\ i(t) \end{bmatrix}. \tag{7.8}$$

The advantage of this approach is that we capture the variations of a_{m1} using the rolling force measurement.

The controller structure is shown in Figure 7.3. Note that the principal structure is the same as the traditional one described in Chapter 3. An investigation of the robustness shows that the system is stable for the parameter variations found in the system identification, for details please refer to [Pedersen, 1995b].

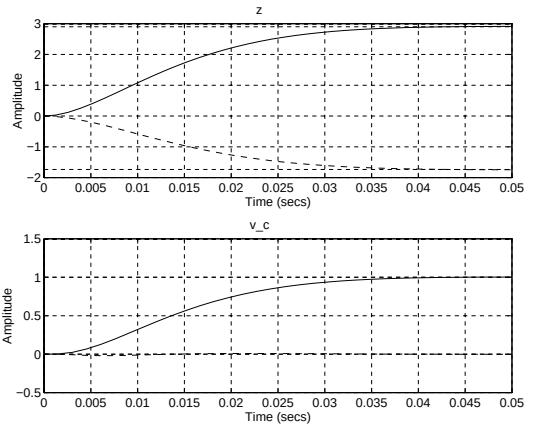

Figure 7.2 Result of eigenspace design, response for step reference change of the thickness at the north edge. Upper plot, full: north position z_{h_n} and dashed: south position z_{h_s}. Lower plot, full: thickness at north edge v_{c_n} and dashed: thickness at south edge v_{c_s}. Note that the south thickness is almost unaffected by the change of the thickness at the north edge.

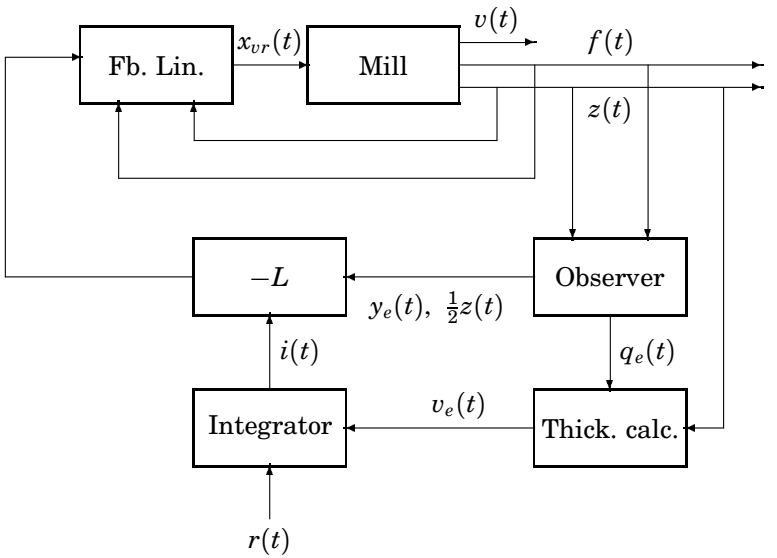

Figure 7.3 The structure of the total controller, including feedback linearization, state feedback and integrator.

Final Form of Controller

The final form of the controller can be found from the feedback linearization (7.1) and the state feedback (7.7).

$$\begin{bmatrix} x_{vrn}(t) \\ x_{vrs}(t) \end{bmatrix} = \Delta_1 \left(\Delta_2 - L \begin{bmatrix} \tilde{y}_e(t) \\ \frac{1}{2}\tilde{z}(t) \\ i(t) \end{bmatrix} \right) \tag{7.9}$$

where

$$\Delta_1 = \begin{bmatrix} -\frac{1}{a_{hn1}\xi_{hn1}(t)} & 0 \\ 0 & -\frac{1}{a_{hs1}\xi_{hs1}(t)} \end{bmatrix}$$
$$\Delta_2 = \begin{bmatrix} -a_{hn2}\xi_{n2}(t) - a_{hn3}\xi_{n3}(t) - \kappa z_n(t) \\ -a_{hs2}\xi_{s2}(t) - a_{hs3}\xi_{s3}(t) - \kappa z_s(t) \end{bmatrix}$$

where $\xi_{s_1}, \ldots, \xi_{s_3}$ are defined as $\xi_{n_1}, \ldots, \xi_{n_3}$ with the variables for the north side replaced with the variables for the south side. $\tilde{y}_e$, and $\tilde{z}$ are the deviations from the working points for the two vectors found using the observer.

The input vector for the controller can be found from (7.8). Note that this is a pretty simple second order nonlinear controller which will be straight-forward to implement. We therefore conclude that despite the tedious design the controller structure is quite simple.

7.5 Evaluation of Performance

Several questions can be asked in connection with the performance of the thickness control. The two usual main concerns are

- response to reference changes;
- effects of typical disturbances.

Both subjects will be investigated in the following. The performance of the new control system will be compared to the performance of the existing control system, when possible. A central question is whether it is necessary to redesign the controller and how often this should be done. This will also be investigated below. Again we simulate the whole system in continuous time, that is we assume that the control law is implemented using a high sampling frequency.

The linear transfer functions for the existing controllers for the hydraulic systems and the thickness controller used in the computer simulations have been provided by the constructor of the control system on

the rolling mill at The Danish Steel Works Ltd. To be able to compare the new and existing controllers the existing control is adjusted to compensate fully for the mill spring. This implies that the system is not detuned, see Section 3.3.

The feedback linearization is implemented using the mean values of the parameters for the north and south sides. To keep the implementation simple $\frac{d}{dt}f$ is found using $\frac{d}{dt}q_c$ from the model used for simulating the rolling stand.

Simulations

To investigate the response to reference changes and the effect of typical disturbances we will perform a number of simulations using the simulation model described in Chapter 6. The dynamics, static gain, and the decoupling of the two sides can be investigated using a step change of the reference at one and both sides. Even if the integrator ensures that the static gain is unity despite the variations of the plate hardness a_{m1}, the dynamics of the system varies with this parameter. From the system identification it is found that $a_{m1} \in [2 \cdot 10^4,\ 2 \cdot 10^5]$. The controller is designed for $a_{m1} = 5 \cdot 10^4$. It is therefore chosen to simulate the responses for mean values of the plate hardness $\overline{a}_{m1} = \{2 \cdot 10^4,\ 5 \cdot 10^4,\ 2 \cdot 10^5\}$ to investigate the effects of the parameter variations on the dynamics of the closed loop system and the decoupling of the two sides. The above values of $\overline{a}_{m1}$ can be considered representative for the values where it is important that the thickness control operates well.

The simulations of changes of the thickness reference at both sides and at one side subsequently are shown in Figures 7.4 and 7.5. Shown are the control signals for the servo valves x_{vrn} and x_{vrs}, and the plate thickness at the edges v_c. The reference at both sides r is changed from 11.64 mm to 10.5 mm at $t = 0$ s and the reference at the north side r_n is changed from 10.5 to 10.25 at $t = 0.5$ s. Since it is not possible to control the two sides independently with the existing control system, r_n is not changed at $t = 0.5$ in the simulations of the existing controller shown in Figure 7.4.

From the simulations of the reference changes it is seen that the magnitudes of the control signals are similar. The existing control system is less damped and has a considerably longer settling time than the new one. Furthermore, the integrator of the existing control is considerably slower, which is not desirable. It should be noted here that the existing control system is tuned on line and it might turn out that the less damped dynamics are desirable when eliminating the force disturbances.

From Figure 7.5 it is seen that the time constant of the new control system also varies quite much with the plate hardness a_{m1}. But in all three cases the separation of the two sides works well when the value for

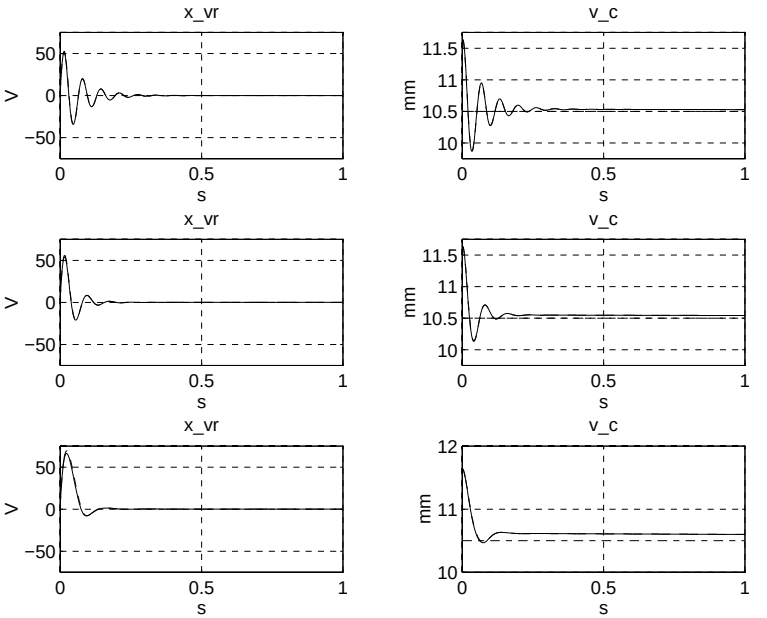

Figure 7.4 Simulation of the existing control system. A step change of the thickness references for both sides to 10.5 mm is done at $t = 0$. Left plots, full: control signal for north servo valve x_{vrn} and dash-dotted: control signal for south servo valve x_{vrs}. Right plots, full: the thickness at the north edge v_{c_n} and dash-dotted: the thickness at the south edge v_{c_s}. The top plots show a simulation for a soft plate and the lower plot a simulation for a hard plate. The plots in the middle are for the parameter value used for the design of the eigenspace controller. Since we are not able to change the thickness at only one side the two responses are similar and can therefore not be distinguished. It is seen that the thickness does not reach the desired value of 10.5 mm in the time interval shown in the figure. Since the rolling speed is between two and four meters per second, the plots show the plate thickness for a plate length in this interval.

$\overline{a}_{m1}$ is used for the design. In the other cases the thickness at the south side varies a couple of hundredths of a mm when the thickness at the north sides is changed. The damping of the control system is satisfactory for all three values of $\overline{a}_{m1}$. Since the size of the control signal is the same for all values of a_{m1}, not much will be gained from redesigning the controller.

From the above simulations we conclude that it is not necessary to redesign the controller because of the variations of a_{m1} unless very hard demands on damping and separation of the two sides are present. Note that, because of the variation of the model parameters with the plate

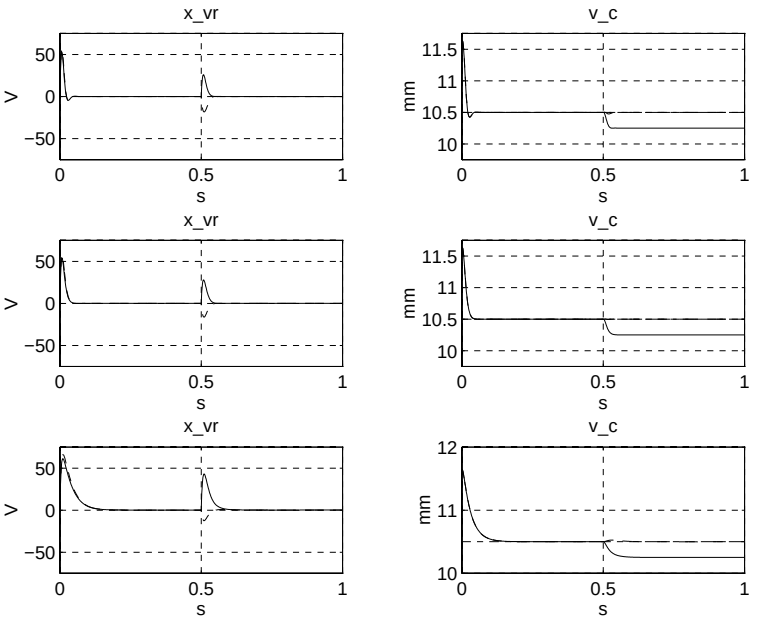

Figure 7.5 Simulation of the new control system. A step change of the thickness references for both sides to 10.5 mm is done at $t = 0$, and a step change of the thickness reference for the north side is done at $t = 0.5$. Left plots, full: control signal for north servo valve x_{vrn} and dash-dotted: control signal for south servo valve x_{vrs}. Right plots, full: the thickness at the north edge v_{c_n} and dash-dotted: the thickness at the south edge v_{c_s}. The top plots show a simulation for a soft plate and the lower plot a simulation for a hard plate. The plots in the middle are for the parameter value used for the design of the eigenspace controller. Since the rolling speed is between two and four meters per second, the plots show the plate thickness for a plate length in this interval.

width w, it will only be necessary to change the controller when w changes. Since the plate width does not change significantly during the rolling of one plate, it will only be necessary to redesign the controller once for each plate.

We now proceed with investigating the effects of the variations of a_{m1} during the pass. As mentioned before these variations mainly consist of slow variations due to cold zones from the reheat furnaces and fast variations from the cooling by the roller tables. It is here chosen to use step changes of the plate hardness to investigate the dynamics and the steady state characteristics of the response to the variations of the plate hardness a_{m1}. The variations of a_{m1} are divided into

- changes in the mean value;
- changes in the value across the plate width.

In the first type of variations the symmetry of the rolling process is preserved, this is not the case for the second type of variations.

In the modeling in Chapter 5 it is assumed that material characteristics are symmetric, but it is quite easy to introduce asymmetric material conditions in the model for the rolling stand. This can be done assuming that that the plate hardness across the plate width is

$$a_{m1}(x,t) = a_{m1}(t)\left(1 + \tau(t)\frac{2x-w}{w}\right),\ x \in [0,\ w].$$

The last term represents a linear variation of the plate hardness across the plate width and τ is a unit step. Neglecting the influence on the eigenvalues β_i and the eigenfunctions ϕ_i we choose to implement the changes in Γ_1 which becomes

$$\Gamma_1(t) = \begin{bmatrix} \frac{1}{\rho A} & \tau(t)\int_0^w \phi_2(x)\frac{2x-w}{w}dx \\ \tau(t)\int_0^w \phi_2(x)\frac{2x-w}{w}dx & \frac{1}{\rho A} \end{bmatrix}.$$

Inserting the above in the simulation program we are able to, approximately, investigate the effects of asymmetric material conditions.

The simulations of the variations of the plate hardness a_{m1} during the pass are shown in Figures 7.6 and 7.7. Again the simulations are done for mean values $\overline{a}_{m1} = \{2\cdot 10^4,\ 5\cdot 10^4, 2\cdot 10^5\}$ to investigate the responses for different plate hardnesses. The reference is changed from 11.64 mm to 10.5 mm at $t = 0$, a_{m1} is changed to $0.8a_{m1}$ at $t = 0.5$ and τ is changed from 0 to 0.2 at $t = 1$. The variations of mean value and the wedge of a_{m1} are both set to 20%, this is inspired by the system identification where we found that a_{m1} varies $\pm 20\%$ in the length direction.In the traditional controller the start value of the plate thickness differs from 10.5, this is due to the rather slow integrator.

From the simulations we see that the impact of the hardness variations is most significant for large plate hardnesses a_{m1}. For $\overline{a}_{m1} = 2\cdot 10^4$ the effect of the variations are hardly noticeable, for $\overline{a}_{m1} = 5\cdot 10^4$ they have some effects on the plate thickness, and for $\overline{a}_{m1} = 2\cdot 10^5$ they have a major impact on the plate thickness. The settling time and damping of new control is better than for the traditional control. Again similar values of the control signal are used for the new and the existing control.

Note that the new control is able to handle the asymmetric material conditions while the traditional controller is not. Generally, it is for the thin, and therefore hard, plates that the most strict demands on the plate

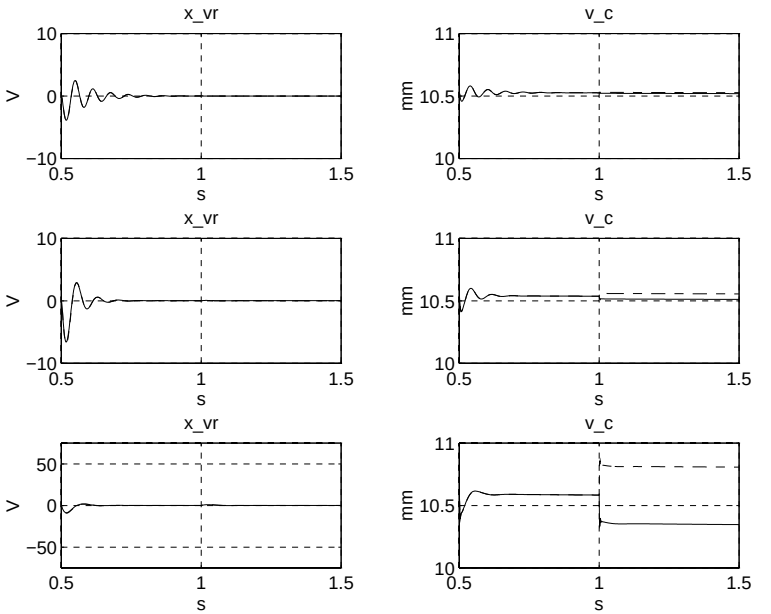

Figure 7.6 Simulation of the existing control system with a desired thickness of 10.5 mm. A step change of the mean value of the plate hardness a_{m1} is done at $t = 0.5$ and asymmetric hardness conditions are introduced by a step change of τ at $t = 1$. Left plots, full: control signal for north servo valve x_{vrn} and dashed: control signal for south servo valve x_{vrs}. Right plots, full: the thickness at the north edge v_{c_n} and dashed: the thickness at the south edge v_{c_s}. The top plots show a simulation for a soft plate and the lower plot a simulation for a hard plate. The plots in the middle are for the plate hardness used for the design of the eigenspace controller.

thickness are present. The deviations shown for the traditional controller will result in a rejection of the plate. Additional problems with different length of the plate edges and the following problems with the plate top view shape can also be expected.

More simulations to investigate the effects of variations of the mill spring coefficient $2K$ and the roll stiffness EI could be done. The variations of these parameters do not affect the symmetry of the rolling process. Furthermore, the variations mostly affect the estimation of the plate thickness and the responses of the new and existing control systems will therefore be similar. It is therefore chosen not to show the simulations of these cases.

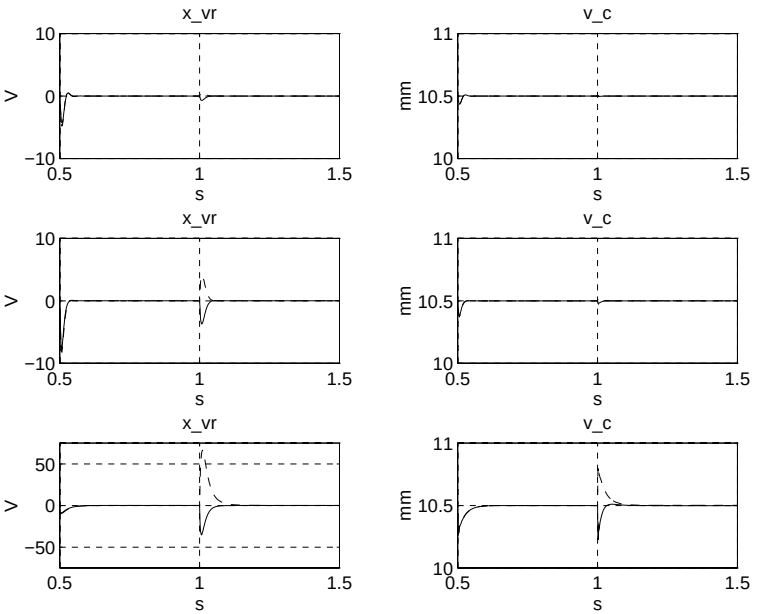

Figure 7.7 Simulation of the new control system with a desired thickness of 10.5 mm. A step change of the mean value of the plate hardness a_{m1} is done at $t = 0.5$ and asymmetric hardness conditions are introduced by a step change of τ at $t = 1$. Left plots, full: control signal for north servo valve x_{vrn} and dashed: control signal for south servo valve x_{vrs}. Right plots, full: the thickness at the north edge v_{c_n} and dashed: the thickness at the south edge v_{c_s}. The top plots show a simulation for a soft plate and the lower plot a simulation for a hard plate. The plots in the middle are for the plate hardness used for the design of the eigenspace controller.

7.6 Conclusions

We have designed new controllers for the hydraulic positioning systems and the rolling stand. The hydraulic systems are linearized using feedback linearization and included in the model for the rolling stand. A state feedback for the now linear system is designed using eigenspace control. The main objective in connection with the eigenspace design is to separate the response of the thickness at the two sides. The dynamics of the new control system are chosen to obtain the same magnitude of the control signals as used by the existing controller. To ensure that the steady state gain of the system will be unity despite the variations of the material parameters two integral states are introduced in the controller.

The stability of the linear control system is investigated in [Pedersen,

1995b] and it is found that it will be stable for the expected parameter variations. The performance of the new and existing control systems are compared using simulations. It is found that the dynamic performance of the new control system is better than the one of the traditional control system. The new control system is, furthermore, able to handle asymmetric material conditions and differences in the thickness references for the two sides, this is not the case with the existing control system.

8

The Slab Temperature Control Problem

The purpose of this chapter is to give an introduction to the slab temperature control problem. This is done by first giving a brief description of the reheat furnace and then defining the slab temperature control problem. The chapter is finished by an analysis of the main characteristics of the heating problem.

8.1 Reheat Furnaces

The main purpose of a reheat furnace is to heat *slabs* (steel blocks which are raw material for the plate mill) from a temperature around 20°C to a temperature of approximately 1120°C before they are processed in the rolling mill. The reheating furnaces are typically large box shaped structures which are heated by a large number of oil or gas *burners* placed in the furnace floor, roof, or walls. The interior of the furnace is build using special made ceramic bricks.

The fuel is mixed with a suitable amount of air in the burners before it is combusted in the furnace, and the exhaust gases leave the furnace through the *stack*. The stack is most commonly placed in the charge side of the furnace to ensure a maximal utilization of the hot air from the burners. Before the exhaust air is released it is passed through a *recuperator* where it is used to heat the incoming air to the burners. To prevent cold air from entering the furnace the *furnace pressure* is kept a small amount over the atmospheric pressure. This is obtained by controlling the flow through the stack. Due to formation of *scale*, which is a result of an oxidation of the slab surface, it is sometimes attempted to control the *oxygen content* of the furnace atmosphere. The scale formation usually consumes several percent of the steel volume heated by the furnace.

The slabs enter the furnace at the *charge end* and leave the furnace at the *discharge end*. In most furnaces the slabs are transported through the furnace by water cooled walking beams, if it is a *walking beam furnace*, or pushed through the furnace on water cooled skids, if it is a *pusher furnace*. The transport systems cools the slabs locally and the result is *skid marks*, which are cold zones at the bottoms side of the slabs. Some furnaces do not have a slab transport system, instead the slabs are charged and discharged using a crane, these furnaces are called *batch furnaces*.

When operating the furnace temperature three things are given much attention

- **Slab temperature**. This includes slab *mean temperature*, *temperature gradient* in the thickness direction, and skid marks.
- **Furnace throughput**. This covers the number of tons per hour heated by the furnace.
- **Fuel consumption**. As can be imagined the furnaces use large amounts of energy for heating the slabs. Therefore, it is important that the slabs are heated using as little energy as possible.

The most important thing in furnace control is to heat the slabs to the specified temperature profile with a minimal energy consumption. The furnace capacity is more or less given by the furnace design, but can of course also be affected by the control system. An analysis and discussion of the furnace characteristics with respect to capacity, slab mean temperature, and energy consumption will be given in Section 8.4, while the control systems for the slab heating are described in Section 8.2.

The example used throughout this thesis is the no. 2 reheat furnace at The Danish Steel Works Ltd. This is a 46 m long walking hearth furnace, which implies that the slabs are transported using walking beams protected by ceramic bricks. The furnace is heated by 33 gas burners placed in the furnace wall and roof. Under normal operation the furnace contains approximately 60 slabs. The slabs are moved approximately 600 mm in each step which has a duration of 20 s. This implies that the slabs are moved approximately 10% of the time. The furnace has three parallel tracks, but in the following we will only consider one track. A schematic diagram of the furnace is shown in Figure 8.1.

The furnace is divided into 5 control zones as indicated in the figure. Zone 0 is a uncontrolled zone, while Zone 1 is side fired. The burners are indicated by the six circles. Zones 2, 3, and 4 are top fired and the burners are shown by the arrow heads in the roof. The open arrows show the main direction of the air flow through the furnace. The furnace temperature is measured in nine points by thermocouples placed in the furnace roof with one thermocouple placed over each track. This implies that there are three thermocouples in the width direction at each measurement point. Normally, the mean values of these three thermocouples are used as the furnace temperature measurement values. The thermocouples are the rectangles placed in the furnace roof. The four thermocouples marked with a "$*$" are used for controlling the zone temperature while the four thermocouples in the furnace roof with light frames are only used for measurement for the slab temperature control system. For control purposes the furnace temperature is assumed to be uniform throughout each zone.
The furnace temperatures are controlled by an ABB FICS system. The slab temperatures are controlled by an ABB FOCS[a] system, which calculates the slab temperatures from material data, temperature readings from the thermocouples, and the air and gas flows to the burners.

[a] Fuel Optimization Control System

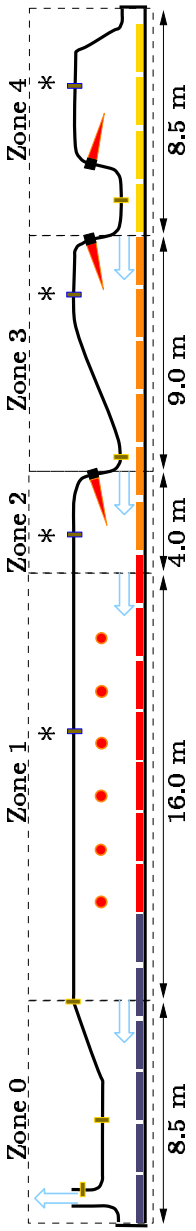

Figure 8.1 A schematic diagram of the reheat furnace no. 2 at The Danish Steel Works Ltd.

8.2 Present Control Algorithms

The reheat furnace control systems are normally divided into a *furnace temperature control system* and a *slab temperature control system*. These systems are referred to as *level I* and *level II* systems, respectively. The main task of the level I control system is to control the furnace temperature. The furnace temperature control is handled by dividing the burners into a number of groups. The air and fuel flows to all burners in one group are then controlled using the temperature measurement from one or more thermocouples placed in the zone. The control problem is multivariable due to the flow between the zones, but the zone temperatures are normally controlled independently of each other.

The main task of the level II systems is the control of the slab temperature to ensure proper heating quality and minimal energy consumption. The slab temperatures are controlled by varying the furnace temperatures. The minimal energy consumption is achieved by heating the slabs as late as possible to the specified temperature. The desired slab temperature reference is called the *heating curve* and is normally dependent on the slab position in the furnace, slab dimensions, etc. The furnace temperatures are controlled to obtain the maximal heat input as far away from the stack as possible. In this way the heat absorption of the slabs is maximized, see [Fontana *et al.*, 1983].

A general problem in slab temperature control is that it is not possible to obtain a proper measurement of the slab temperature. The surface temperature of the slabs can, however, be measured using radiation pyrometers. A disadvantage of this measurement method is that if the slab has a large temperature gradient the surface temperature will not be a true measure of the mean slab temperature. It is also possible to measure the surface temperature in the rolling mill where the steel temperature usually is more homogeneous, in this case there will be a considerable time delay between heating and temperature measurement, see [Schurko *et al.*, 1987]. Given an accurate model for the temperature drop during rolling the pyrometer measurement can be used for adapting the parameters of the slab temperature model.

For more details about the present furnace control algorithms, see [Pedersen, 1998]. In that literature review it is concluded that the importance of the prediction of the slab temperature is seen from the fact that the models normally are used only for temperature prediction. Very few examples of controller designs based on the slab temperature models have been found in the literature. The most common solution for determining the furnace temperature set points are optimization algorithms using the prediction models or PI-controllers. It is also remarkable that only two references on system identification have been found. No other reports on

parameter estimation of the rather complex PDE models are given than the one in this thesis.

8.3 The Slab Temperature Control Problem

Only a few model based controller designs have been found in the literature. This indicates that the slab temperature control problem could be a good topic of research. The fact that only a few cases of system identification have been found confirms this choice. The remarks are relevant for both the level I and the level II furnace control systems, but we choose to work with the level II systems since they are the part of the control systems working closest with the main variable of interest in the furnace control—the slab temperature.

The central variable in the design will be the mean temperature of the slabs, but also the temperature gradient and the furnace energy consumption will be considered. Given the level I control systems described in Section 8.2, the furnace is subdivided into a number of furnace temperature control zones. In the control of the slab temperature each zone will be considered separately, along the same lines as the arguments for deriving the principle of optimality it can be seen that a good control of the furnace can be accomplished by a good control of the temperature of the slabs in each furnace control zone.

The design problem is therefore a furnace zone containing n_j slabs, see Figure 8.2. The slabs are moved through the furnace with velocity v_s by the slab transport system, and the slab temperatures of zone j, $T_1^j, \ldots, T_{n_j}^j$ are controlled by varying the furnace temperature T_m^j of the j'th zone which influences the furnace temperature profile T_t.

8.4 Analysis of the Slab Heating

In the following we will have a look at the furnace throughput, slab temperature profile, and furnace energy consumption. We start with a model for the slab temperature profile in its most general form.

In the literature the slab temperature distribution is often described by a one dimensional partial differential equation in the thickness direction of the slab, where it is assumed that the heating is mainly due to radiation and convection from gas, furnace walls, and roof. Using the one dimensional model implies that it is assumed that the temperature of the individual slab does not vary in the length or in the width direction. If there is no heat transport through the slab sides this is a valid assumption.

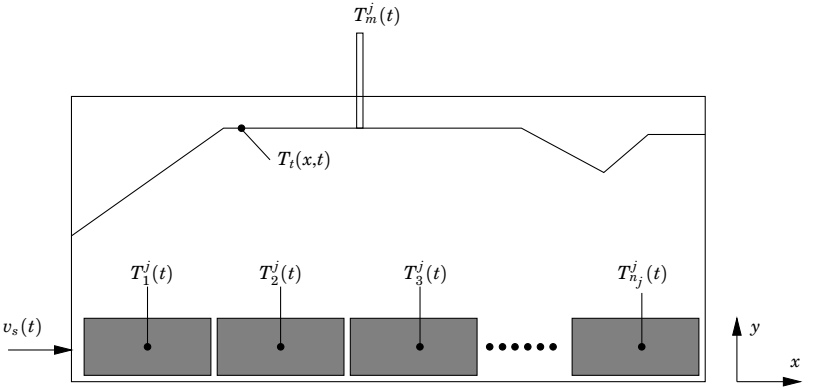

Figure 8.2 Illustration of the slab temperature control problem. The temperatures of the n_j slabs passing through the j'th zone with velocity v_s are controlled by varying the furnace temperature profile T_t in the zone. The coordinates x and y are also shown in the figure.

The model can be described by the one dimensional heat equation, see [Siegel and Howell, 1992]

$$\begin{aligned} h\rho(T)c_p(T)\frac{\partial T}{\partial t}(y,t) &= \frac{\partial}{\partial y}\left(\lambda(T)\frac{\partial T}{\partial y}(y,t)\right) \\ \lambda(T)\frac{\partial T}{\partial y}(0,t) &= q_b(t) = \lambda_b(T(0,t) - T_b(t)) \\ \lambda(T)\frac{\partial T}{\partial y}(h,t) &= q_t(t) = \sigma\varepsilon_t(T_t^4(t) - T^4(h,t)) + \lambda_t(T_t(t) - T(h,t)) \\ T(y,0) &= T_o(y) \end{aligned} \tag{8.1}$$

where T is the temperature distribution of the slab dependent of height y and time t. The slab thickness is denoted by h, ρ is the specific mass of steel, c_p is the specific heat capacity of steel, λ is the heat conductivity of steel, all depend on the slab temperature T. Furthermore, σ is Boltzmann's constant, and ε_t is an emission factor of the slab top side. The variable T_o is the initial temperature distribution dependent of y, T_b is the temperature below the slab and T_t is the temperature over the slab. Finally, λ_t and λ_b are the heat transfer coefficients for the slab top and bottom, respectively. A simpler version of (8.1) is often used for modeling slab temperature, see [Rixin and Baolin, 1992] and [Hollander and Zuurbier, 1982]. Since the slab is mainly heated from the top in furnace no. 2 the radiation term at the slab bottom is left out in the model. This is in good agreement with the identification results presented in Chapter 10.

In the following analysis of the slab heating process, the slab thickness h is chosen to 260 mm which is the maximal value for the reheat furnace no. 2. Slab with a nominal thickness of 260 mm have the longest heating times and the largest temperature gradients and can therefore be seen as the worst case with respect to these characteristics.

Unfortunately, (8.1) is a nonlinear partial differential equation (PDE) and it is difficult to solve analytically, therefore a simplified analysis has to be performed. To do this we assume that the temperature of the slab is constant in the thickness direction, i.e. that it is independent of y and that we only have heat conduction due to radiation which implies that λ_t and λ_b are zero. This implies that we are only studying the mean temperature. In this case (8.1) reduces to

$$\begin{aligned} h\rho c_p \frac{d\overline{T}}{dt}(t) &= \sigma \varepsilon_t (T_t^4 - \overline{T}^4(t)) \\ \overline{T}(0) &= T_o \end{aligned} \tag{8.2}$$

where $\overline{T}$ is the mean temperature of the slab in the thickness direction. Equation (8.2) is a nonlinear ordinary differential equation (ODE) and can be solved if it is rewritten as a differential equation in the mean slab temperature $\overline{T}$

$$\begin{aligned} \frac{dt(\overline{T})}{d\overline{T}} &= \frac{h\rho c_p}{\sigma \varepsilon_t} \frac{1}{(T_t^4(t) - \overline{T}^4)} \\ t(\overline{T}_o) &= 0. \end{aligned}$$

Assuming that the furnace temperature T_t is constant this equation has the solution

$$\begin{aligned} t(\widehat{T}) &= \frac{h\rho c_p}{2T_t^3 \sigma \varepsilon_t} \left(\tan^{-1}\left(\widehat{T}\right) + \tanh^{-1}\left(\widehat{T}\right) \right) \\ t(\widehat{T}_o) &= 0 \end{aligned} \tag{8.3}$$

where $\widehat{T} = \overline{T}/T_t$. Equation (8.3) is a transcendental equation and $\widehat{T}$ can not be isolated, but it still gives interesting qualitative information about the heating process. Defining $t_{0.99}$ as the time where the slab has reached 99% of the furnace temperature T_t we have the equation

$$\frac{h}{t_{0.99}} \propto 0.58 \frac{\sigma \varepsilon_t}{\rho c_p} T_t^3 \tag{8.4}$$

where $\propto$ means *proportional to*. Since the furnace throughput can be approximated by $h/t_{0.99}$ and we see from (8.4) that the furnace capacity is

proportional to T_t^3 if the shape of the furnace temperature as a function of time t is kept constant. This implies that the furnace capacity increases dramatically with increased furnace temperature. Note that an increase of the furnace temperature T_t will result in both shorter heating times $t_{0.99}$ *and* higher slab temperatures. A 10% increase in temperature yields a reduction in heating time by 33%. Note that beside the reduction in heating time the slab is also heated to a 10% higher temperature. It should be noted that we are only considering the mean temperatures of the slab. To have proper material quality it is necessary that the slab temperature is reasonable uniform.

The energy used for heating slabs to the specified temperature is given by the heat capacity of the steel block and can therefore not be affected by the furnace control system. It is on the other hand possible to affect the heat losses from the furnace. The energy losses may be divided into losses from the furnace structure and losses through the exhaust gases.

The heat losses will increase with increasing gas temperature everywhere in the furnace. Assuming steady state the conduction and convection losses through the furnace structure q_c are proportional to

$$q_c \propto \int_0^l (T_t(x) - T_s)\, dx$$

where T_s is the temperature of the surroundings and l is the furnace length. Since $T_t \gg T_s$ the argument of the integral will always be positive. To save energy we therefore want the furnace temperature to be as low as possible.

The heat losses through the exhaust gases are proportional to

$$q_s \propto \dot{m}_s(0) T_t(0)$$

where the mass flow of the gas through the stack, $\dot{m}_s$, depends on position x. We see that higher temperatures and flows in the stack increases the energy losses of the furnace. Most reheat furnaces are *counter flow furnaces* which means that the stack is placed at the charge end of the furnace. The energy consumption can then be minimized by ensuring that the furnace temperature in the charge end is as low as possible.

8.5 Conclusions

In this chapter we have described the reheat furnaces used in the steel industry for heating the raw material for the rolling mills. The furnace control systems are normally divided into level I systems for controlling

the furnace temperature and level II systems for controlling the slab temperatures. After a short presentation of the state of the art of furnace control systems it is chosen to go on with the work of designing a controller for the slab temperature.

After the definition of the control problem the slab heating is analyzed. The main characteristics of the control problem with respect to furnace capacity, temperature gradients, and energy consumption are derived and it is concluded that furnace temperature and slab thickness are important parameters of the heating process. To minimize energy consumption it is necessary to heat the slabs as late as possible when operating the furnace.

9

Temperature Control—Data Collection

The purpose of this chapter is to describe the data collection of the slab and furnace temperatures. The measurements will be used in the system identification in Chapter 10, where the structure and parameters of the mathematical models for the furnace and slab temperature are determined. We will start with a short description of the measurement device and then have a closer look at a measurement series.

9.1 The Data Collection Device—The Pig

The data collection device is a Thermophil STOR^{TM} which is a portable data collection unit made especially for measuring slab temperatures when transported through the reheat furnace. When measuring the slab temperature the Thermophil is put into a metal box filled with water. The box is mounted in a special made test slab, see Figure 9.1, and transported through the furnace in the usual way. The only constraint is that the test slab maximally can stay in the furnace until the water is evaporated, which is about 7 hours. When the test slab is discharged from the furnace, the data collection device is removed and the data are transferred to a PC using a serial link.

The slab temperatures are measured using steel coated thermocouples mounted in holes that go 10%, 50%, and 90% into the slab in the thickness direction. A fourth thermocouple is used for measuring the temperature of the furnace atmosphere on the top side of the slab.

Figure 9.1 The data collection device mounted on a test slab. The wires going into the slab are the steel coated thermocouples. The water box is covered heat protective material to minimize the exposure to heat radiation.

9.2 A Measurement Series

The measurements of the slab top, center, and bottom temperatures and the furnace atmosphere temperature are taken directly from the data record of the pig[1] run is shown in Figure 9.3.

During the pig run the FOCS system calculates the slab position in the furnace and measures the gas, and air flows and the temperatures from the thermocouples mounted in the roof. An example of these data is shown in Figure 9.2. The data collection is carried out for all zones during the pig run. All in all 9 different data sets will be used in this thesis.

The furnace temperature from the FOCS system is used as input for the slab temperature calculation and is generated by linear interpolation of the temperature reading from the thermocouples mounted in the roof,

[1]Originally the name is used for a self moving device for cleaning pipelines in both Danish and English. Of some reason this name is also used for the slab temperature measurement device at The Danish Steel Works Ltd. and the author has therefore taken the liberty to translate this term to English.

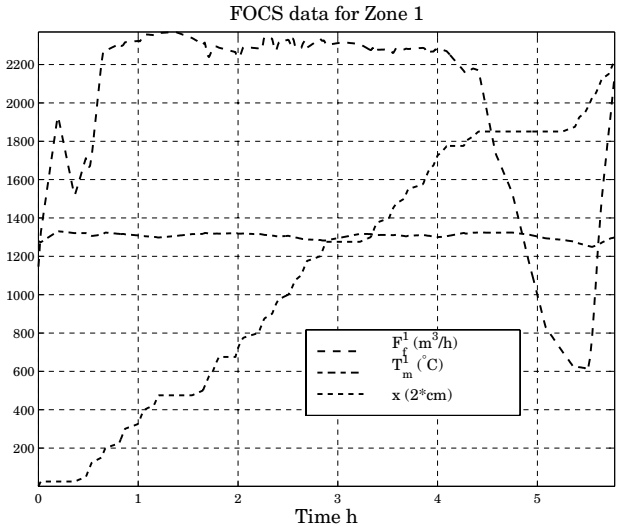

Figure 9.2 Example of FOCS data for zone 1 during a pig run. Among other things, the FOCS system records the fuel flow F_f^1, zone temperature T_m^1, and slab position x.

see Figure 8.1, using the slab and thermocouple positions. The roof temperature is used as input to the slab temperature models. It is seen from Figure 9.3 that there is a reasonable agreement between the roof and atmosphere temperature measurements, it is, however, sometimes necessary to adjust the slab position to obtain proper agreement between the two temperature measurements, the reason for this probably being inaccurate data from the FOCS system. In a few of the measurements no good agreement can be obtained between the atmosphere temperature T_a and the roof temperature T_t. One reason for this can be flame radiation from the burners and cold air leaking into the furnace from the outside.

Two uncertainties of the furnace measurements are known to the author. The first is that, even if the pig measures the slab temperatures with a fairly good accuracy within ± 5°C, the top slab temperature measurement $T_{10\%}$ can be disturbed by heat conduction along the coating of the thermocouple. The top slab temperature should therefore be handled with a bit more caution than the other temperature measurements. The other uncertainty is that the slab position x obtained from the FOCS system are not always correct, the main reason is a to early or to late detection of the time when the pig enters the furnace.

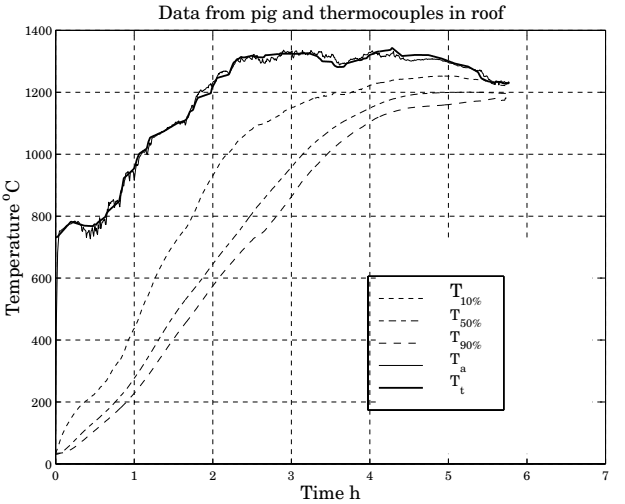

Figure 9.3 Measurement series from a pig run. The slab top temperature $T_{10\%}$, center temperature $T_{50\%}$, bottom temperature $T_{90\%}$, and the atmosphere temperatures T_a are taken directly from the data record from the pig. The roof temperatures are generated by a linear interpolation of the roof thermocouple measurements T_t using the slab position

9.3 Conclusions

This chapter contains a short description of the slab and furnace temperature measurements. The main message is that we measure the top, center, and bottom temperatures of the slab, the temperature of the furnace roof and the atmosphere temperature on the top side of the slab. All measurements are considered reliable, except possibly the slab top temperature measurement and the slab position during the pig run.

10

Temperature Control—System Identification

The purpose of this chapter is to construct models for the furnace and slab temperatures and identify the parameters of these models. The models will later be used for analysis, controller design, and computer simulations of the reheat furnace operation. We will, in general, focus on making advanced and accurate models for the slab temperatures and try to make the models for the furnace temperatures as simple as possible. For the slab temperature two models will be used, a simple model for design and analysis and an advanced model for evaluation of the design.

We will first derive a model for the furnace temperatures, which consist of a differential equation for the zone temperature control thermocouples and a static relation between these temperatures and the temperatures of the other thermocouples in the zone. We will then build two models for the slab temperatures, an ODE model for analysis and controller design, and a PDE model for simulation and verification of the control laws designed later. The connection of the furnace model and the ODE model for the slab temperature is illustrated in Figure 10.1, the structure for the PDE model for the slab temperature is similar and therefore not shown here. Throughout this chapter j is used as zone number and i is used as the slab number in a zone.

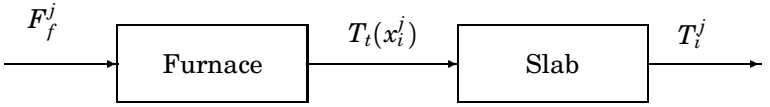

Figure 10.1 Illustration of the models build in this chapter. The furnace model for zone j has fuel flow F_f^j as input and a furnace temperature profile T_t for the i'th slab in zone j with position x_i^j as output. The slab model has the furnace temperature profile as input and the slab temperature T_i^j as output.

10.1 Model for Furnace Temperature

In the following we will derive models for the furnace temperatures. We will first derive a model for the temperatures measured by the thermocouples used for the zone temperature control. When this is done a simple model relating the temperatures of all thermocouples in the zone to the measurements for zone temperature control is constructed.

Zone Temperatures

The model for the zone temperatures will be used for simulation of the zone temperature control. Since the main purpose is the control of the slab temperatures the model for the zone temperatures will be kept as simple as possible, neglecting the fact that the furnace is a considerably more complex structure than the slabs. Our goal with the modeling is therefore to gain insight in the zone temperature dynamics and the interaction between the furnace temperature control zones.

Inspired by [Kusters and van Ditzhuijzen, 1994] we use the physical model shown in Figure 10.2 when constructing the model for the furnace temperatures. As seen from the figure the slab movement also contributes to the transport of thermal energy and we therefore add this term to the model described in [Kusters and van Ditzhuijzen, 1994].

When deriving the model we adopt the standard assumption that the zone temperature profile T_t is uniform throughout the zone in the length direction, which implies that we are able to assume that it is equal to the temperature measurement used for the zone temperature control T_m^j. Furthermore, we assume that the air is incompressible and that the furnace characteristics do not vary with the zone temperature. The zone temperatures T_m^j are the mean value of the thermocouple readings over the three tracks and v_s is computed by differentiating the slab position recordings.

The energy balance for the zone implies that the total heat flow input

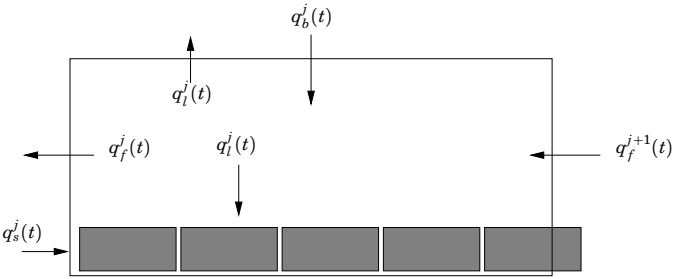

Figure 10.2 Simplified model for furnace zone j. In the figure q_f^{j+1} is the heat flow received in the form of gas from the proceeding zone, q_f^j is the heat flow delivered in the form of gas to the preceding zone, q_b^j is the heat flow input from the burners in the zone, q_l^j represents the heat loss to the surroundings and slabs, and q_s^j is the heat loss due to the movement of the slabs.

balance is

$$\frac{dE_z^j}{dt} = q_f^{j+1}(t) - q_f^j(t) + q_b^j(t) - q_l^j(t) - q_s^j(t) \tag{10.1}$$

where E_z^j is the zone energy content of zone j, q_f^{j+1} represents the heat flow received from the next zone due to the air flow, q_f^j represents the heat flow sent to the previous zone, q_b^j represents the heat flow input from the burners and q_l^j represents the heat flow to the surroundings and heat transferred to the slabs and q_s^j is the heat loss due to the movement of the slabs.

The terms in (10.1) can be represented by

$$q_f^j(t) \propto T_m^j(t) v_z^j(t)$$
$$q_b^j(t) \propto F_f^j(t)$$
$$q_l^j(t) \propto (T_m^j(t) - T_s(t)) + \alpha(T_m^j(t) - \frac{1}{n_j}\sum_{i=1}^{n_j} T_i^j(t)) \approx (1+\alpha)T_m^j(t) - \beta(t)$$
$$q_s^j(t) \propto v_s(t)(T_1^j(t) - T_{n_j}^j(t))$$

where T_m^j is the temperature for zone j, v_z^j is the total air flow from zone j (and into zone $j-1$), F_f^j is the fuel flow to the burners of zone j, and v_s is the velocity of the slabs. n_j is the number of slabs in the zone, T_i^j is the i'th the slab temperature of zone j, and T_s is the temperature outside the

furnace, Note that we have implicitly assumed that the slabs are heated by convection in q_l^j, this is necessary to obtain a linear model.

A reasonable assumption is that the total air flow to and from the zones originates from the burners in all the zones, this implies that

$$v_z^j(t) \propto \sum_{i=j}^{4} F_f^i(t). \tag{10.2}$$

Since the air/fuel rate of the burners is constant this implies that the flow of hot air from a zone is proportional to the gas flow to the burners. The fuel flow is therefore chosen as inputs to the model.

The zone energy content is given by

$$\frac{dE_z^j}{dt} \propto \frac{d}{dt} T_m^j(t)$$

and this together with the above results (10.1) can be represented as

$$\dot{T}_m^j(t) = a_1^j(v_z^{j+1}(t)T_m^{j+1}(t) - v_z^j(t)T_m^j(t)) + a_2^j F_f^j(t) + a_3^j T_m^j(t) + a_4^j v_s(t) - a_5^j \tag{10.3}$$

where a_1^j, a_2^j, a_3^j, a_4^j, and a_5^j now are unknown parameters of the furnace model. For the representation of q_l^j and q_s^j to be correct it is necessary that the average slab temperature, and the initial and final slab temperatures T_1^j and $T_{n_j}^j$ are constant over time. This is not always true, one example is stops, where the slab temperatures tends to increase until the slabs start moving again. This is especially true for zones 1 and 2, since the variations in slab temperatures are largest here. Note that (10.3) is a bilinear equation.

From (10.3) we construct the state space equations

$$\begin{bmatrix} \dot{T}_m^1 \\ \dot{T}_m^2 \\ \dot{T}_m^3 \\ \dot{T}_m^4 \end{bmatrix} = \begin{bmatrix} a_3^1 - a_1^1 v_z^1 & a_1^1 v_z^2 & 0 & 0 \\ 0 & a_3^2 - a_1^2 v_z^2 & a_1^2 v_z^3 & 0 \\ 0 & 0 & a_3^3 - a_1^3 v_z^3 & a_1^3 v_z^4 \\ 0 & 0 & 0 & a_3^4 - a_1^4 v_z^4 \end{bmatrix} \begin{bmatrix} T_m^1 \\ T_m^2 \\ T_m^3 \\ T_m^4 \end{bmatrix} + \begin{bmatrix} a_2^1 & 0 & 0 & 0 \\ 0 & a_2^2 & 0 & 0 \\ 0 & 0 & a_2^3 & 0 \\ 0 & 0 & 0 & a_2^4 \end{bmatrix} \begin{bmatrix} F_f^1 \\ F_f^2 \\ F_f^3 \\ F_f^4 \end{bmatrix} + \begin{bmatrix} a_4^1 \\ a_4^2 \\ a_4^3 \\ a_4^4 \end{bmatrix} v_s - \begin{bmatrix} a_5^1 \\ a_5^2 \\ a_5^3 \\ a_5^4 \end{bmatrix} \tag{10.4}$$

In this equation T_m^j, and v_s are measurable and v_z^j can be obtained from (10.2) where a factor proportional to q_z^j can be computed from F_f^j. The measurements for the system identification are taken from the FOCS system, see Section 9.2.

Before the identification the mean values of the variables are subtracted from the regressors, this implies that the identification is carried out at a working point. Surprisingly the result is that the best model is obtained by only using the coefficients a_2^j and a_3^j. This corresponds to representing each zone with a first order linear system. One reason for this is probably that the quality of the data is not very good due to rare and irregular sampling which makes it hard to find a good estimate for the slab speed for this purpose. Another reason is that we do not know the slab temperatures which are necessary for determining the energy transport due to the slab movement which is one of the major heat transports of the system since approximately 50% of the energy from the natural gas is absorbed by the slabs. Most of the heat input takes place in zones 1 and 2, were the temperature difference between furnace and slabs is large. The temperatures of the two zones are therefore affected significantly by the temperatures of the slabs, which again are affected by the slab speed.

The lack of influence of the heat transport due to the hot gas can be explained by the fact that zone 1 has far larger capacity compared to the other zones, while zone 2 has the second largest capacity. The capacities of zones 3 and 4 are small compared to the two first zones. This makes the influence of the incoming flow to the zones small compared to the flow from the zone itself. A typical result of simulating (10.4) on a validation data set is shown in Figure 10.3.

In general system identification using closed loop data can give problems with the controller being identified instead of the system. Since we are doing closed loop identification here the result of the system identification leads to the question if the identification has given the right result. We investigate this by inspecting the data, by looking at the causality we first notice that it is pretty clear that it is the variations in the flows F_f^i that causes the variations in temperature T_m^j. The identified model follows this pattern and we therefore conclude that we have identified the transfer function of the furnace and not the transfer function of the controller.

The result of the identification is the state space equations

$$\begin{bmatrix} \dot{T}_m^1 \\ \dot{T}_m^2 \\ \dot{T}_m^3 \\ \dot{T}_m^4 \end{bmatrix} = \begin{bmatrix} a_3^1 & 0 & 0 & 0 \\ 0 & a_3^2 & 0 & 0 \\ 0 & 0 & a_3^3 & 0 \\ 0 & 0 & 0 & a_3^4 \end{bmatrix} \begin{bmatrix} T_m^1 \\ T_m^2 \\ T_m^3 \\ T_m^4 \end{bmatrix} + \begin{bmatrix} a_2^1 & 0 & 0 & 0 \\ 0 & a_2^2 & 0 & 0 \\ 0 & 0 & a_2^3 & 0 \\ 0 & 0 & 0 & a_2^4 \end{bmatrix} \begin{bmatrix} F_f^1 \\ F_f^2 \\ F_f^3 \\ F_f^4 \end{bmatrix} \quad (10.5)$$

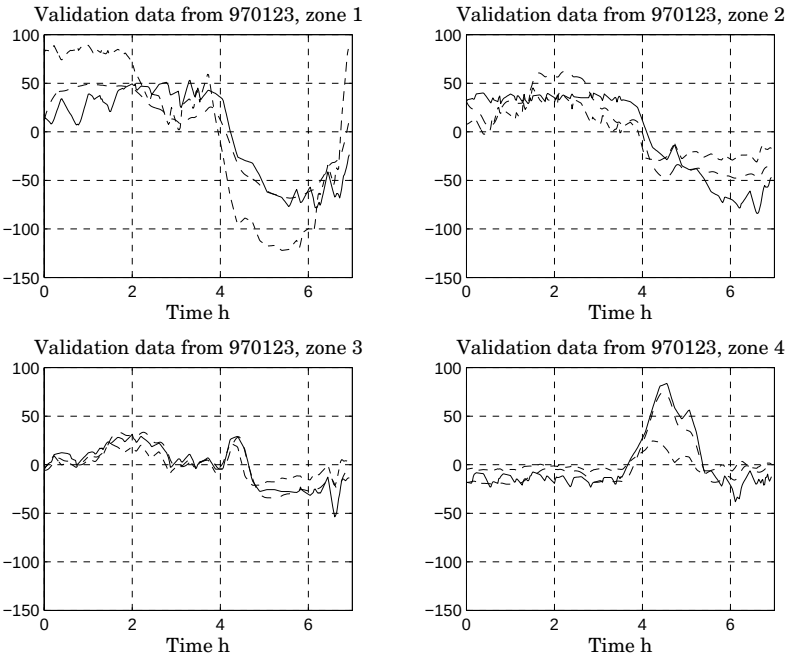

Figure 10.3 Validation of the model for the furnace temperatures (10.4). Input to the model are the fuel flows F_f^j (full) and output are the simulated zone temperatures T_m^j (dashed), which should be compared to the measured zone temperatures (dash-dot). Note the good agreement for zones 3 and 4 and the not so good agreement for zones 1 and 2. The deviation between measurement and output for zones 1 and 2 are believed to be caused by the influence from the energy transport due to the slab movements. Unfortunately we do not have sufficient information to include the slab temperatures in the model.

with the coefficients

$$\begin{bmatrix} a_2^1, & a_3^1 \\ a_2^2, & a_3^2 \\ a_2^3, & a_3^3 \\ a_2^4, & a_3^4 \end{bmatrix} = \begin{bmatrix} 8.1 \cdot 10^{-5}, & -1.4 \cdot 10^{-3} \\ 2.7 \cdot 10^{-4}, & -1.6 \cdot 10^{-3} \\ 2.8 \cdot 10^{-4}, & -1.4 \cdot 10^{-3} \\ 1.3 \cdot 10^{-3}, & -1.1 \cdot 10^{-3} \end{bmatrix}$$

we see that the gains a_2^j and time constants a_3^j are of the same magnitude for the four zones. The gains of the zones are proportional to the burner capacity and inversely proportional to the heat capacity. This can explain why zone 1 has a small gain despite its large capacity (contains many

cold slabs) and zone 4 has a large gain despite its relatively small capacity (contains a few hot slabs). The time constants are proportional to the heat capacity and inversely proportional to the heat losses and they seem to balance each other since all time constants are of the same magnitude.

The working points for the linear model are

$$[F_f^1 \quad F_f^2 \quad F_f^3 \quad F_f^4]_{nom} = [1690 \quad 419 \quad 277 \quad 50.4]$$
$$[T_m^1 \quad T_m^2 \quad T_m^3 \quad T_m^4]_{nom} = [1550 \quad 1570 \quad 1570 \quad 1500]$$

Note that the limitations in fuel flows F_f^j also yield an upper and lower limit for the furnace temperatures T_m^j. The reason for the lower limit is energy stored in slabs and furnace construction which prevents the temperature from falling below a certain limit.

Temperature Profiles

With (10.4) we now have a reasonable representation of the temperature measurement used for the zone temperature control. The next question then is how the temperatures of the rest of the thermocouples shown in Figure 8.1 depend on the values of the zone control temperatures.

In this model we assume that the temperature profile in entire furnace is given by

$$T_t(x_i^j, t) = p(x_i^j) T_m^j(t) \tag{10.6}$$

where x_i^j is the position of the i'th slab in the j'th zone and p is a piecewise linear temperature profile and T_m^j is the value measured by the thermocouple used for the zone temperature control. This representation is also used by [H. E. Pike and Citron, 1970]. If the zone is equipped with more than one thermocouple these temperature measurements can be used for finding p. Typical results of the application of (10.6) are shown in Figure 10.4. The relatively good agreement in Figure 9.3 between the atmosphere temperature measurement and the temperature found by linear interpolation of the thermocouple measurements shows that the linear interpolation of (10.6) works well in practice.

10.2 Models for Slab Temperature

As mentioned in Section 8.4 the slabs are heated by radiation and convection from the gas and furnace walls. To construct a good model it is necessary to look further into these phenomena which are illustrated by Figure 10.5.

The heat transport to and from the slab is due to

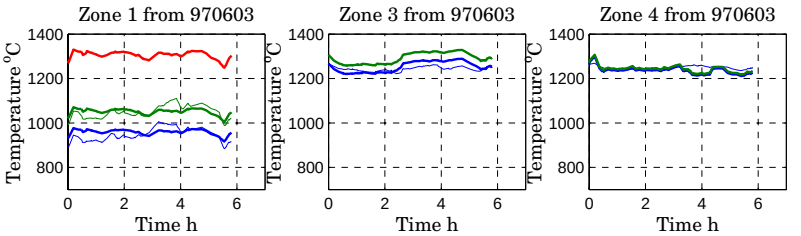

Figure 10.4 Validation of equation (10.6) where the temperature of the four thermocouples used for temperature control is used for predicting the temperatures of the other four other thermocouples in the furnace. In the figures the thin lines are the measurements and the thick lines are the predictions. The temperatures used are the mean values of the three thermocouples over each furnace track. The temperatures for zone 2 is not shown in the plot since it only contains the thermocouple for control.

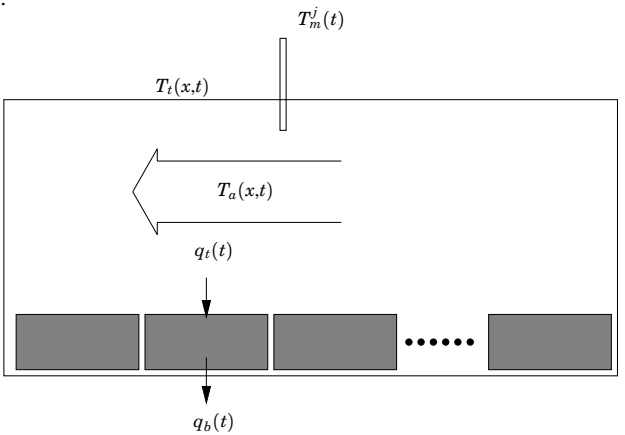

Figure 10.5 Illustration of the slab heating. The slab is heated by radiation and convection from the gas from the burners and radiation from the furnace walls. In the figure T_t is the wall temperature profile, T_a is the atmosphere temperature, T_m^j is the temperature measurement. The variable q_t is the heat flux through the slab top side and q_b is the heat flux through the slab bottom.

- Radiation from furnace walls
- Radiation from gas
- Convection from gas
- Heat conduction to slab transport system

Throughout this work we assume that there is no heat transport between the slabs. None of the results contradict this assumption.

The heat transfer due to radiation is a complex equilibrium of reflections between wall and slab and the absorption and emission of radiation of the gas, for more details see [Baehr and Stephan, 1996]. We will not go into this discussion here, but pragmatically wait until the results of the system identification appears. One thing to bear in mind is that the radiation absorption and emission characteristics of the gas vary quite much with the fuel and we can therefore not expect the coefficients obtained in the system identification to be valid for furnaces not heated by natural gas. The heat transfer due to heat conduction and convection is also hard to predict due to the complex gas flow patterns in the furnace and we will again await the results from the system identification.

The next natural question that arises is what the T_m^j we measure with the thermocouple in the furnace roof represents—is it the roof temperature T_t or is it the atmosphere temperature T_a? Again this can develop to quite a complicated discussion, but looking at Figure 9.3 wee see that the temperatures measured with the thermocouples in the roof and the thermocouple on the pig are pretty much the same, this leads to the obvious assumption that $T_a = T_t$. The results shown later in this chapter shows that this works well in practice.

The system identification of the models for the slab temperature will be a lot easier if we know the coefficients for the heat conduction λ, heat capacity c_p, and density ρ of (8.1). These material data are found in [Leden, 1999], which again cites [Griffiths, 1953] and [Richter, 1973]. Plots of the coefficients are shown in Figure 10.6. Knowing the material data for the slab reduces the identification problem to determining the coefficients of the boundary conditions.

The slab temperatures are controlled by the FOCS system and therefore there is a risk of feedback in the data used for the system identification. Since the feedback is based on the furnace temperature measurement, which is the input to the slab temperature estimator, it is not likely that this will cause problems in the identification. Since the identification will be validated by measurements from a number of pig runs there should be little risk of wrong parameter estimates. The identification is carried out for a limited slab thickness interval, the thinnest slab is 235 mm and the thickest slab is 260 mm. We conclude that the model in any case will be valid for 260 mm slabs, which will be the case treated in the controller design in Chapter 11.

ODE for Slab Temperature

The purpose of the ODE model is analysis of and controller design for the slab heating process. We therefore choose to make this model as simple as possible, given that it is able to predict the output with a reasonable accuracy.

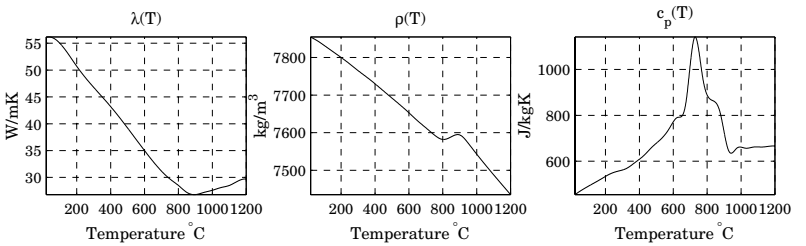

Figure 10.6 Material parameters for the steel type used at The Danish Steel Works Ltd. The peak in the heat capacity c_p represents the energy release/consumption in connection with a phase change of the steel.

In Section 8.3 we choose to control the slab center temperature and we therefore use the slab center temperature measurement as output for our model. Inspired by [Pichler and Langer, 1989], [Hollander and Zuurbier, 1982], and [Leden, 1986] we first identify the parameters of a model where the slab temperature is considered homogeneous. This is obtained by considering a steel block with uniform temperature, unit area, and thickness h. The result is

$$\frac{dT_i^j}{dt} = \frac{1}{h\rho(T_i^j)c_p(T_i^j)} \Big(\sigma\varepsilon_t \left(T_t^4(x_i^j,t) - \left(T_i^j(t)\right)^4 \right) + \lambda_t \left(T_t(x_i^j,t) - T_i^j(t) \right) + \lambda_b \left(T_i^j(t) - T_b \right) \Big) \quad (10.7)$$

where h is the slab thickness, and ρ and c_p are the material parameters described in Section 10.2. σ is Boltzmann's constant. The variables T_t and T_b are the ambient temperatures of the slab top and bottom sides, respectively. The first two terms on the right hand side of (10.7) represent the energy flows to the slab by radiation and convection, respectively, while the third term represents the energy losses to the slab transport system. This term is new in the model compared to the models in the references above.

The parameters ε_t, λ_t, and λ_b are found by simulating (10.7) using `ode45` in MATLAB and minimizing the error between the slab center temperature measurement$T_{50\%}$ and model output T_i^j using the MATLAB optimization routines `leastsq` and `fmins`. During the identification it turns out that we can use the interpolated temperatures from the roof thermocouples from the FOCS system as T_t, see Section 9.2, and that T_b can be considered constant. The result of the identification is shown in Figure 10.7.

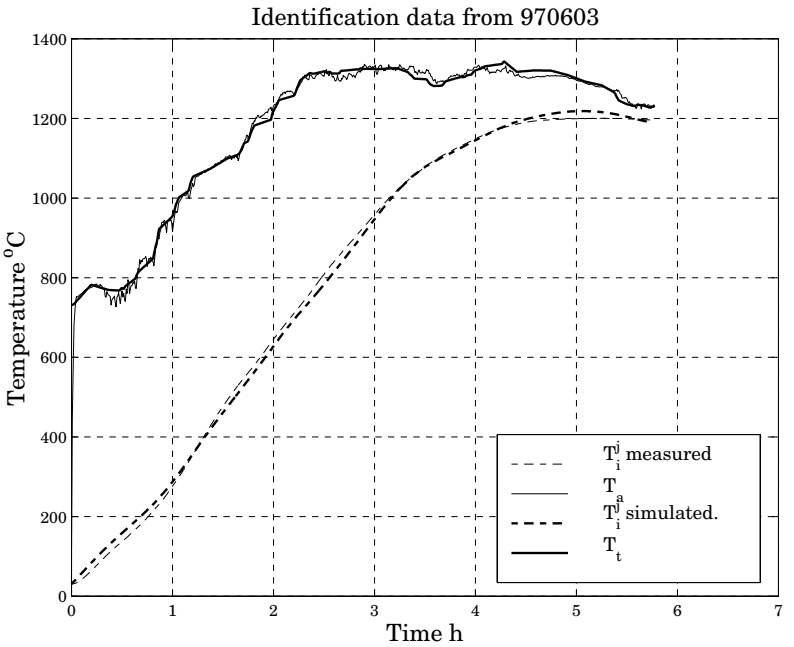

Figure 10.7 Results of the system identification of the ODE for the slab center temperature $T_i^j = T_{50\%}$ (10.7). The plot shows the furnace roof temperature T_t, the measured pig center temperature T_i^j, and the simulated temperature T_i^j found using (10.7).

Eight other data sets have been used for validating the results shown in Figure 10.7. The results of the validation are shown in Figures 10.8 and 10.9. The conclusion of the validation is that (10.7) with the identified parameters is a good model for the slab center temperature. Note that there is a close connection between deviations between the atmosphere temperature measurement T_a and the thermocouple measurement T_t and the bad estimates of the model. This indicates that the model will give valid predictions given the correct inputs. The most likely reason for the large deviations between the atmosphere and the thermocouple temperatures is an inaccurate position calculation of the pig, a wrong position will lead to an error to the interpolation of the thermocouple temperatures and therefore to a wrong input to the model.

The parameter values found in the system identification are

$$[\varepsilon_t, \quad \lambda_t, \quad T_b, \quad \lambda_b] = [0.52 \quad 52 \quad 305 \quad -31] \tag{10.8}$$

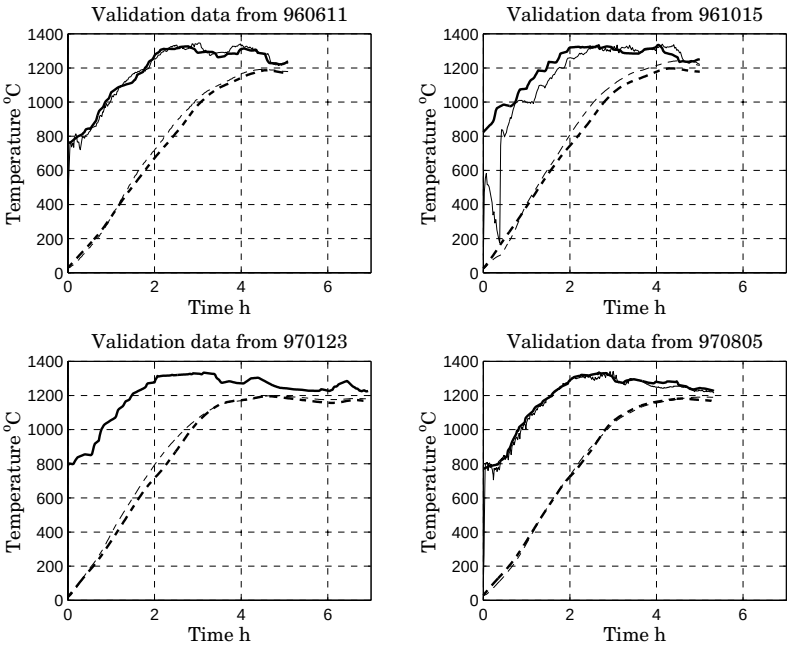

Figure 10.8 Validation of the system identification of Figure 10.7. The line styles used are the same as the ones in Figure 10.7. Note that the atmosphere temperature T_a is the thin full line. The deviations of "961015" seems to be due to errors in the measurement of the input temperature T_t due to a wrong estimate of the slab position x_t^j. Note that we have a good agreement for "970123" despite its residence time of 7 hours. Note that the atmosphere temperature T_a is missing for this pig run.

Assuming that $T_t = T_a$ the resulting emission coefficient between the wall temperature T_t and the slab can be reduced to

$$\varepsilon_t = \left(\varepsilon_{sw} + 0.5 \frac{\varepsilon_s(\varepsilon_g + A_{gs})}{1 - (1 - \varepsilon_s)(1 - A_{gs})} \right)$$

see [Leden, 1985], where ε_s is the emission factor for steel which normally is around 0.8, $\varepsilon_{sw} \approx 0.4$ is the exchange factor for radiation between slab and wall, $\varepsilon_g \approx 0.4$ is the emission factor of the gas, and $A_{gs} \approx 0.5$ is the absorption coefficient of the gas. The result is $\varepsilon_t \approx 0.8$ which is pretty far from the value 0.52 found in the system identification. It should here be mentioned that the model for the furnace no. 2 at The Danish Steel Works Ltd. implemented in the steel temperature simulation program STEELTEMP© heat transfer due to convection is only included in zone 0

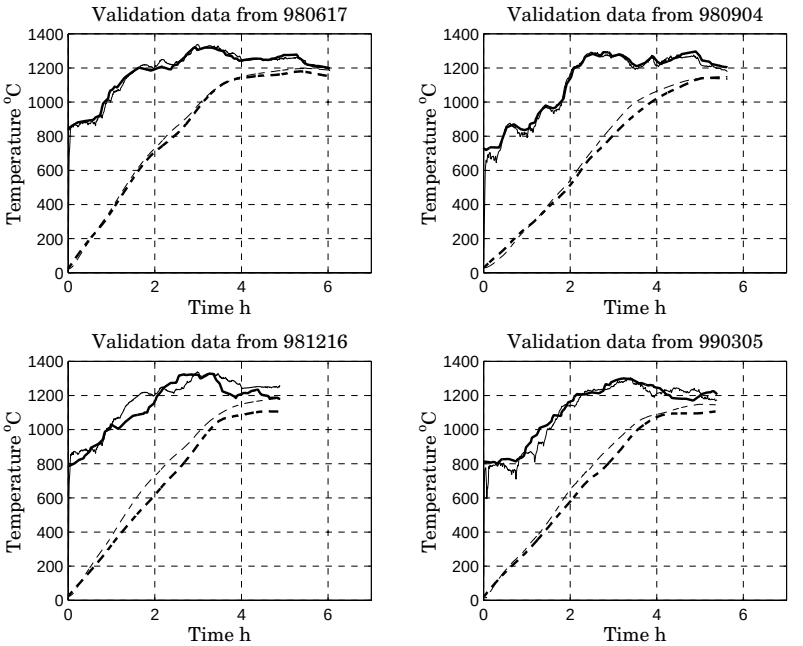

Figure 10.9 Validation of the system identification of Figure 10.7. The line styles used are the same as the ones in Figure 10.7. Note again that the deviations of "981216" and "990305" are due to a inaccurate furnace temperature T_t.

and therefore the heat input due to radiation has to be made larger in this case compared to the model developed here.

The value of T_b is close to the temperature outside the furnace (in Kelvin) and is therefore considered reasonable. It is hard to evaluate the coefficients λ_b and λ_t, but the signs are right and they are both of the same order of magnitude.

Computing the heat fluxes of the regressors of (10.7) shows that 80% of the heat input is due to radiation and 20% is due to convection. The losses to the transport is around 20% of the heat input. Note that this shows that the analysis of the ODE in Section 8.4, where radiation was considered the only heat source, relies on a realistic assumption.

PDE for Slab Temperature

The purpose of the PDE model is to evaluate the slab temperature control and we can therefore allow this model to be more complex than the ODE model described in the previous section. This time we take the model from

Chapter 8

$$
\begin{aligned}
h\rho(T)c_p(T)\frac{\partial T}{\partial t}(y,t) &= \frac{\partial}{\partial y}\left(\lambda(T)\frac{\partial T}{\partial y}(y,t)\right)\\
\lambda(T)\frac{\partial T}{\partial y}(0,t) &= q_b(t) = \lambda_b(x)(T(0,t)-T_b(t))\\
\lambda(T)\frac{\partial T}{\partial y}(h,t) &= q_t(t) = \sigma\varepsilon_t(T_t^4(t)-T^4(h,t)) + \lambda_t(T_t(t)-T(h,t))\\
T(y,0) &= T_o(y)
\end{aligned}
\tag{10.9}
$$

where

$$
\lambda_b(x) = \begin{cases} 0 & \text{for } x \le 37 \text{ m} \\ \lambda_b & \text{for } x > 37 \text{ m} \end{cases}
$$

and use it for the system identification without modifications. The identification is carried out by implementing (10.9), including the nonlinear material data, directly in FEMLAB, which is a FEM simulation tool for MATLAB, and use the optimization routines `leastsq` and `fmins` for determining the parameters of (10.9).

It is no surprise that it is a more difficult task to identify the coefficients of the PDE than the ODE. Several extensions such as introducing heat transfer coefficients λ_t, and λ_b dependent on the fuel flow and slab position has been tried, but the identification results did not improve significantly. We basically end up with the same parameterization as in the identification of the ODE, with the minor change that λ_b now depends on the slab position.

The 37 meters marks the limit between zones 3 and 4 where the slab enters a zone with considerably lower air flow, this leads to a lower furnace pressure and hereby to an increased leak flow of cold air.

In the identification the center temperature $T_{50\%}$ and bottom temperature $T_{90\%}$ are used since they turn out to be the most reliable measurements. The results of the identification are shown in Figure 10.10. Note that the top temperature measurement $T_{10\%}$ deviates from the simulation, a likely cause is heat conduction along the metal coat of the thermocouple as discussed in Section 9.2. Note, furthermore, that the boundary condition for heat conduction to the furnace construction seems to be simplified, since only the mean value of the variations of the slab bottom temperature $T_{90\%}$ are captured by the model. Despite this the overall accuracy of the system identification is good.

From the validation results in Figures 10.8 to 10.12 it is seen that the FEM simulations are more sensitive than the ODE simulations, but note

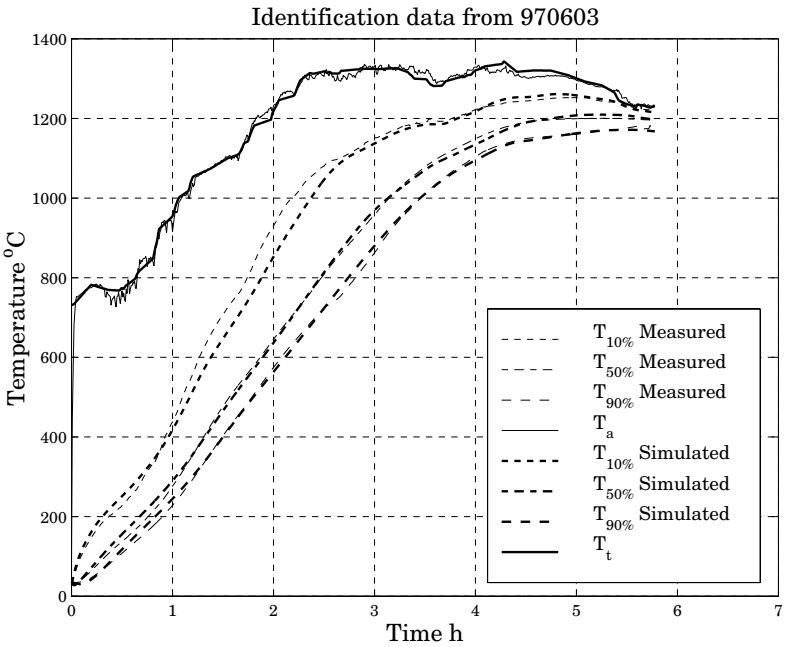

Figure 10.10 Identification results for the PDE (10.9) where we now identify all three pig temperatures $T_{10\%}$, $T_{50\%}$, and $T_{90\%}$. Note that the agreement for $T_{50\%}$, and $T_{90\%}$ is quite good despite the simple boundary conditions, the deviations in $T_{10\%}$ is believed to be caused by inaccurate measurements.

that the accuracy is good whenever the wall temperatures T_t correspond well with the atmosphere temperature T_a.

The parameter values found in the system identification of the PDE are

$$[\,\varepsilon_t, \quad \lambda_t, \quad T_b, \quad \lambda_b\,] = [\,0.43 \quad 77 \quad 358 \quad -8.7\,] \tag{10.10}$$

Comparing to (10.8) we see that the emission factor ε_t is reduced by 20% while the top heat conduction coefficient λ_t is increased by 50%. One explanation for this could be that in the ODE model it is assumed that the entire slab is heated simultaneously, while only the top half of the slab has to be heated in the PDE case. This means that a more powerful heating therefore is needed in the ODE case to obtain the same dynamics as in the PDE case. In the system identification this is done by giving the heating by radiation larger effect in the ODE case than in the PDE case.

In the PDE case both magnitude and exposure of the cooling by the

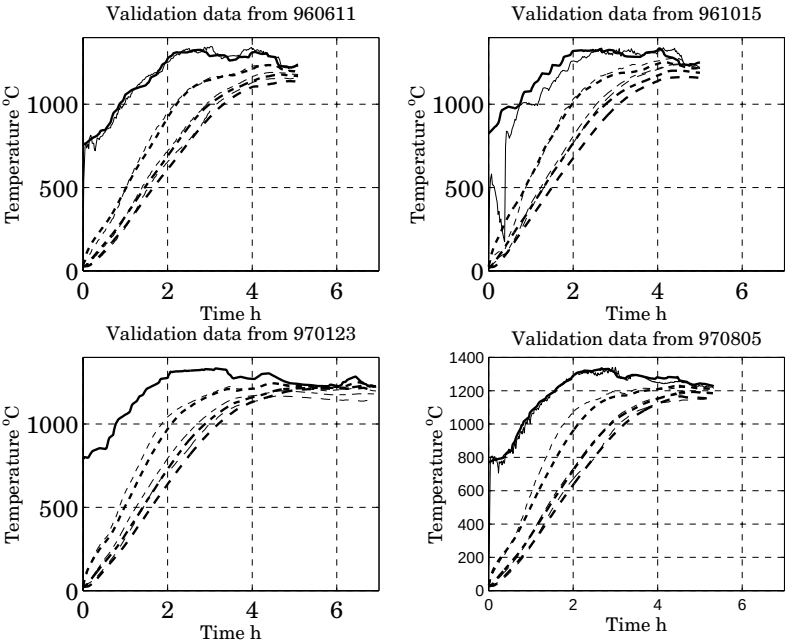

Figure 10.11 Validation results for the PDE (10.9). Note the good agreement for "960611" and "970805" where atmosphere temperature T_a, and wall temperature T_t are in good agreement.

transport system represented by λ_b and T_b is smaller than in the ODE case. The explanation for this could be that in the FEM case the heat transport through the slab is modeled explicitly, while this has to be done artificially in the ODE case. This will lead to a what seems like a heat loss to from the center in the ODE case.

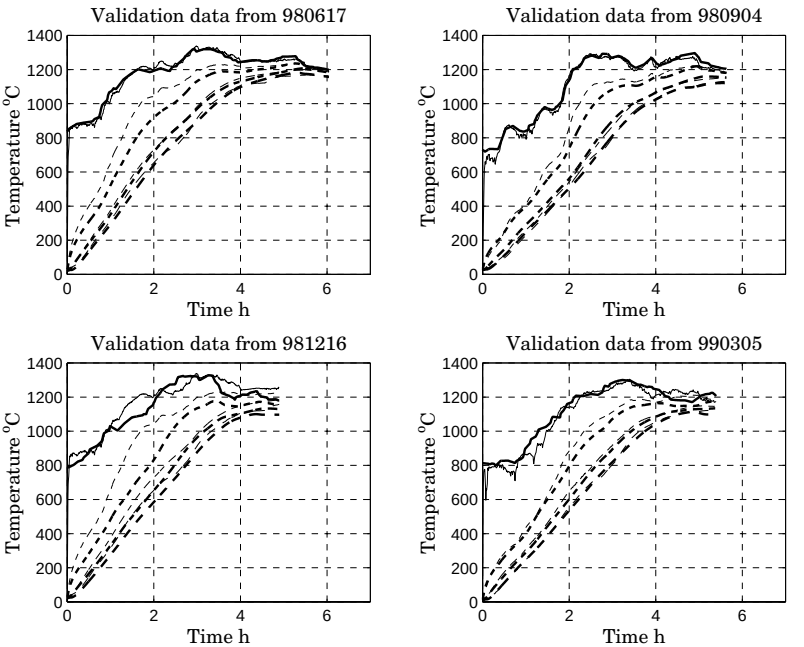

Figure 10.12 Validation results for the PDE (10.9). Note the good agreement for "980617" and "980904" where atmosphere temperature T_a, and wall temperature T_t are in good agreement.

10.3 Conclusions

We are now finished building models for the slab temperature control problem. We have found that the temperature measurements used for zone temperature control can be represented by independent linear first order systems with a reasonable accuracy and that the other temperature measurements in the zones can be represented as linear functions of temperature control measurements.

Two models for the slab temperatures have been built and identified. The first model is a nonlinear ODE which is used for modeling the slab center temperature and the second model is a PDE which is used for modeling the slab top, center, and bottom temperatures. In both cases good agreement is obtained during identification and validation which has been carried out using 9 data sets collected over several years at The Danish Steel Works Ltd. One prerequisite for obtaining a good prediction of the slab temperature is that the calculated furnace temperature is correct, this is especially the case with the PDE model. The results indicate that the furnace can be regarded as a time invariant process which was not clear before the system identification.

The coefficients obtained from the ODE and PDE identification give a bit different pictures of the heating process. The results of the PDE identification is believed to be the most reliable and it is concluded that the coefficients from the the ODE identification are biased due to the assumptions used when deriving the model.

11

Temperature Control—Design

The purpose of this chapter is to design algorithms for the control of the slab temperatures. First we will use the identification results from Chapter 10 to build a nonlinear state space model for all slabs in a furnace control zone. Then we will design a linear control law similar to that of the FOCS system, the purpose of the design is optimization of the furnace control system at The Danish Steel Works Ltd. The final part of the chapter contains a design of a nonlinear control algorithm for the furnace control problem—the performance of the linear and the two nonlinear algorithms will be compared in Chapter 12 using computer simulations.

11.1 The Control Problem

We want to control the temperatures of the slabs in the reheat furnace no. 2 at The Danish Steel Works Ltd. The furnace is divided into 4 furnace temperature control zones, see Figure 8.1, and we control the i'th slab temperature of the j'th zone T_t^j by varying the furnace temperature set points T_m^j and hereby the furnace temperature profile T_t of the control zones, see Figure 8.2. The furnace temperatures are controlled by varying the fuel flow to the burners. The main task of control system is to minimize the effects of the varying slab velocity v_s, which can be seen as a measurable disturbance.

As mentioned in Section 8.3 we will consider the control of the slab temperatures separately for each zone and the problem is reduced to controlling the temperatures of the n_j slabs in each of the four furnace zones.

To simplify the notation in the following we assume that the material properties and thickness of all slabs in the zone are identical, it is straight forward to remove this assumption when necessary. Throughout this chap-

ter $i = 1, \cdots, n_j$ is used for slab index in the zone and $j = 1, \cdots, 4$ is used as zone number.

We build the model for all slabs in a control zone using the ODE model in Section 10.2. Assuming that the zone contains n_j slabs and defining the state vector for zone j

$$T^j(t)^T = \begin{bmatrix} T_1^j(t) & T_2^j(t) & \dots & T_{n_j}^j(t) \end{bmatrix}$$

we obtain the following state space model from (10.7)

$$\begin{aligned} \frac{dT^j}{dt} &= G(T^j)(F(T^j) + U(T_t)) \\ \frac{dx_j}{dt} &= \mathbf{1} v_s(t) \end{aligned} \tag{11.1}$$

where

$$\begin{aligned} G(T^j) &= \begin{bmatrix} g(T_1^j) & 0 & \dots & 0 \\ 0 & g(T_2^j) & \ddots & \vdots \\ \vdots & \ddots & \ddots & 0 \\ 0 & \dots & 0 & g(T_{n_j}^j) \end{bmatrix} \\ F(T^j)^T &= \begin{bmatrix} f(T_1^j) & f(T_2^j) & \cdots & f(T_{n_j}^j) \end{bmatrix} \\ U(T_t)^T &= \begin{bmatrix} u(x_1^j, T_m^j) & u(x_2^j, T_m^j) & \cdots & u(x_{n_j}^j, T_m^j) \end{bmatrix} \\ x^j(t)^T &= \begin{bmatrix} x_1^j(t) & x_2^j(t) & \cdots & x_{n_j}^j(t) \end{bmatrix} \\ \mathbf{1}^T &= \begin{bmatrix} 1 & 1 & \cdots & 1 \end{bmatrix} \end{aligned} \tag{11.2}$$

where we have used that

$$T_t(x,t) = p(x_i^j) T_m^j(t)$$

where p is the linear interpolation of the thermocouple measurements defined by (10.6), and T_m^j is the furnace temperature measurement used for controlling the furnace temperature.

In (11.1) and (11.2) v_s is the velocity of the slabs, x_i^j is the position of the i'th slab in the j'th zone, see Figure 8.2. The elements of (11.2) are

$$\begin{aligned} f(T_i^j) &= -\varepsilon_t \sigma \left(T_i^j(t)\right)^4 - (\lambda_t - \lambda_b) T_i^j(t) - T_b \lambda_b, \ i = 1, \dots, n_j \\ g(T_i^j) &= \frac{1}{h \rho(T_i^j) c_p(T_i^j)} \\ u(x_i^j, T_m^j) &= \varepsilon_t \sigma p^4(x_i^j) \left(T_m^j(t)\right)^4 + \lambda_t p(x_i^j) T_m^j(t) \end{aligned} \tag{11.3}$$

The material parameters ρ and c_p are shown in Figure 10.6. Furthermore, ε_t, λ_t, λ_b, and T_b are the parameters found in the ODE system identification described in Section 10.2.

The mechanics of the model (11.1) are as follows: when a new slab enters zone j it is assigned states T_1^j and x_1^j, and the state numbers of the other slabs in zone j are increased by one. When a slab leaves the zone, the states $T_{n_j}^j$ and $x_{n_j}^j$ are removed from the system. Since the slabs have different lengths these two events are independent.

11.2 Design of FOCS Controller

In the following we will go through the design of the slab temperature controller of the FOCS system. The design has two purposes, it should be used

- for adjustment of the parameters of the existing FOCS system at The Danish Steel Works Ltd.
- for comparison and introduction for the nonlinear deign presented later in this chapter

The controller structure is already given by the system at The Danish Steel Works Ltd., see Figure 11.1. The figure illustrates that the slab temperature controller C_S^j for the j'th zone sets the reference to the furnace temperature controller which again controls the fuel flow to the burners of zone j.

The main purpose of the slab temperature control system is to minimize the heating error for zone j

$$e_L^j(t) = \sum_{i=1}^{n_j} r_L^j(i)(T_i^j(t) - T_r(x_i^j)) = r_L^j T^j - r_L^j T_r(x^j)$$

where T_r is the heating curve, and r_L^j is a vector of nonnegative weights for the temperature deviation of zone j. The design variables of the system are

- **The heating curve T_r.** The slab temperature reference T_r starts at room temperature and ends at the desired final slab temperature. The heating curve is a function of slab position x.
- **The feedforward tables.** The tables specify the furnace temperature set points as a function of the slab speed v_s. This makes sense since v_s can be considered as a measurable disturbance of the slab temperature control system.

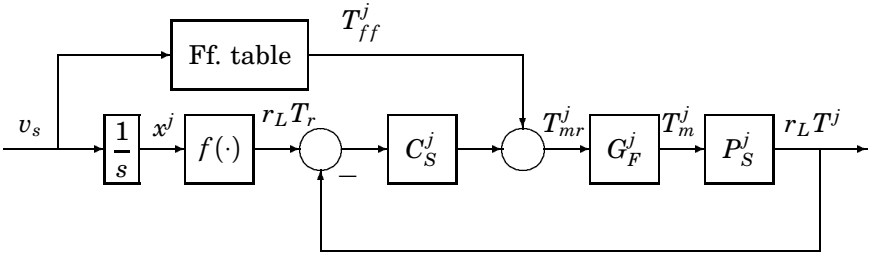

Figure 11.1 The controller structure for the FOCS system consists of PI controllers for the weighted slab temperature $r_L^j T^j$, and furnace temperature T_m^j. T_{ff}^j is the temperature reference from the feedforward tables, and T_{mr}^j is the furnace tempeature reference from the slab tempeature controller. G_F^j is the closed loop transfer function of the furnace temperature control system of zone j, C_S^j is the transfer function of the slab temperature controller for zone j, and P_S^j is the transfer function relating the furnace temperature and the weighted slab temperature $r_L^j T^j$ of zone j.

- **The PI coefficients.** Based on the slab temperature deviation from the heating curve the PI-controllers C_S^j determines a correction of the furnace temperature reference from the feedforward tables.

In the following we will first determine the heating curve and feedforward tables. We will then design the PI-controllers for the slab temperature deviation from the heating curve.

Heating Curve and Feedforward Tables

We start the controller design with a discussion of the heating curve and the feedforward tables, which are parts of the classical approach to the solution of the slab temperature control problem. The heating curve is a reference trajectory for the slab temperatures which sets the temperature reference for the slabs as they are transported through the furnace with speed v_s. The feedforward tables contain the furnace temperature set points necessary to follow the slab heating curve, for an example see Table 11.1. The tables assumes constant slab speed.

The reference slab center temperature T_r is normally chosen as a function of slab position x_i^j instead of time t. In the case where the slabs are moving with constant nominal speed v_{s0} there is no difference, but when a stop occurs the dependence on slab position ensures that rise in temperature reference is stopped and is first started when the slabs start moving again. The dependence on x therefore prevents premature heating of the slabs.

A natural way of choosing the heating curve is to use the stationary

solution of the differential equation for T_l^j when the slabs move through the furnace with the nominal velocity v_{s0}. The advantage of this approach is that in the nominal case the furnace temperatures T_m^j can be kept constant. It is also an advantage in the linear controller design, as we will see later on. In the case where $v_s = 0$ the differential equation for the heating curves reduces to a static equation which can be used for determining the zone temperatures necessary to keep the slabs hot during stops. In the following we only generate heating curve and feedforward tables for the nontrivial case where $v_{s0} > 0$. As we will see later it is not certain that the slab temperatures will stay on the heating curve during the stops.

To generate the constant velocity solution to the differential equation for the slab temperature T_l^j we define the differential equation for the heating curve T_r in zone j as

$$\begin{aligned}
\frac{dT_r}{dt} &= \frac{dT_r}{dx}\frac{dx}{dt} = \frac{dT_r}{dx}v_{s0} = g(T_r)(f(T_r) + u(x, T_{m0}^j)) \\
&\Downarrow \\
\frac{dT_r}{dx} &= \frac{1}{v_{s0}} g(T_r)(f(T_r) + u(x, T_{m0}^j)) \\
\frac{dx}{dt} &= v_{s0} \\
T_r(0) &= T_{in}
\end{aligned} \tag{11.4}$$

where T_{in} is the initial slab temperature, and T_{m0}^j is the constant furnace temperature that ensures that the slab temperatures follow the heating curve. The nominal slab speed v_{s0} is chosen corresponding to a residence time of 6.4 hours corresponding to $v_{s0} = 0.002$ m/s. The residence time is normally 5 hours at The Danish Steel Works Ltd. The reason for the choice of a larger residence time for calculating the heating curve T_r is that the furnace is operated partially as a batch furnace, for further details please refer to the discussion in Chapter 13.

We now have to find the furnace temperature setpoints T_{m0}^j for the four zones, $j = 1, 2, 3, 4$. To reduce the temperature gradient of the slabs and to ensure a buffer of hot slabs when the furnace is subjected to elevated speeds, we choose to keep the slab temperature T_l^j at the desired final temperatures in zones 3 and 4. The simulations of the PDE for the slab temperature in Chapter 12 and the experiences from the implementation of the control strategy show that this is sufficient for ensuring a satisfactory mean temperature and temperature gradient. The remaining freedom we use for minimizing the energy losses of the furnace, which are discussed in Section 8.4.

We choose to use the ODE model (10.7) for generating the heating curve. The reason for not using the PDE model (10.9) is that the identification results show that the ODE gives more reliable results, and that the ODE is easier to handle. The PDE is used for verifying the heating quality after the heating curve is generated.

Based on this discussion we choose the performance criterion

$$\min_{T_{m0}^j} \int_0^l T_t(\tau)d\tau = \min_{T_{m0}^j} \sum_{j=1}^{4} \int_0^{l_z^j} T_{m0}^j p\left(\tau + \sum_{i=1}^{j-1} l_z^j\right) d\tau \tag{11.5}$$

where l is the total length of the furnace and, l_z^j is the length of zone j. The criterion is used for minimizing the heat losses by convection and the heat losses through the stack, see Section 8.4.

The constraints of the optimization problem are

$$\begin{aligned} &\frac{dT_r}{dx} = \frac{1}{v_{s0}} g(T_r)(f(T_r) + u(x, T_{m0}^j)) \\ &|T_r(x) - T_{out}| = 0, \; x \in \left[\sum_{j=1}^{2} l_z^j, \sum_{j=1}^{4} l_z^j\right] \\ &T_{m_{min}}^j \leq T_{m0}^j \leq T_{m_{max}}^j \end{aligned} \tag{11.6}$$

where T_{out} is the desired final slab temperature and T_r is the solution to the differential equation. $T_{m_{min}}^j$ and $T_{m_{max}}^j$ are the limits for the furnace temperatures T_m^j in zone j. The limits are a result of temperature limits for the furnace protection and the identification of the furnace temperature model in Section 10.1.

The heating curve T_r is found by solving the optimization problem (11.5) subject to the constraints obtained from (11.6) using the function `constr` in MATLAB. The result is shown in Figure 11.2. Note that the obtained heating curve ensures later heating compared with the existing one, this should ensure energy savings due to the decrease of the furnace temperatures at the charge end, remember the heat losses through the stack, see Section 8.4. This will be evaluated when looking at the experimental results in Chapter 13.

In the FOCS system the feedforward tables are used for determining an open loop value of the furnace temperatures dependent on the slab velocity v_s. The feedforward temperature is determined by linear interpolation of the table values. The feedforward value is corrected by a feedback control of the slab temperature, the design of the feedback control is discussed later in this section.

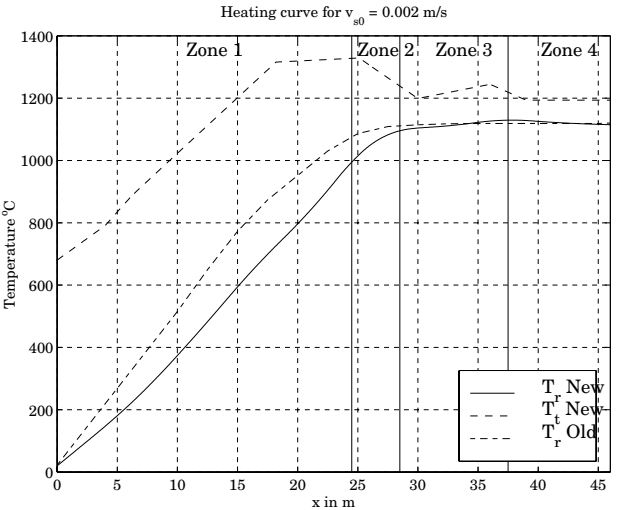

Figure 11.2 New and existing heating curves T_r for the control zones of the reheat furnace with an initial temperature T_{in} of 20°C and a final temperature T_{out} of 1120°C. Note that the new heating curve ensures significantly later heating than the existing one. The heating curve is used as a slab temperature reference as a function of the slab positions x.

It is, in general, not possible to have the same heating curves for two different slab speeds $\tilde{v}_{s0}$ and v_{s0} since this implies that

$$\frac{dT_r}{dx} = \frac{1}{v_{s0}} g(T_r)(f(T_r) + u(x, T^j_{m0})) = \frac{1}{\tilde{v}_{s0}} g(T_r)(f(T_r) + u(x, \tilde{T}^j_{m0}))$$
$$\Downarrow$$
$$u(x, \tilde{T}^j_{m0}) = \left(\frac{\tilde{v}_{s0}}{v_{s0}} - 1\right) f(T_r) + \frac{\tilde{v}_{s0}}{v_{s0}} u(x, T^j_{m0})$$

which is not possible to obtain with a constant T^j_{m0}. Given a nominal speed different than v_{s0} we therefore choose the furnace temperatures that minimizes the distance to the heating curve, this is done by solving the optimization problem

$$\min_{T^j_{mi}} \|T_r - \tilde{T}_r\|_\infty$$

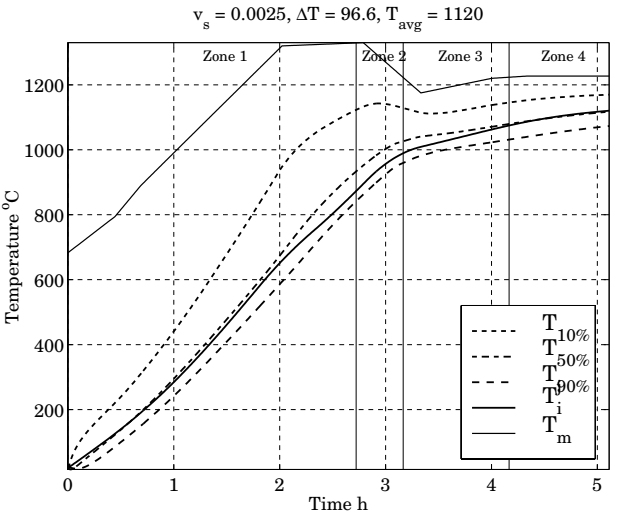

Figure 11.3 Result of finding feedforward temperatures for the nominal residence time of 5 hours corresponding to $v_s = 0.0025$ in the feedforward table. In the figure ΔT denotes the temperature gradient and T_{avg} denotes the average temperature of the FEM simulations at the time of discharge. The FEM simulation shows that the temperature gradient is on the high side, around 97°C but the experiments show that no problems occur during rolling.

subject to the constraints

$$\frac{d\tilde{T}_r}{dx} = \frac{1}{v_{si}} g(\tilde{T}_r)(f(\tilde{T}_r) + u(x, T^j_{mi}))$$
$$T^j_{m_{min}} \leq T^j_{mi} \leq T^j_{m_{max}}$$

The problem is solved for five nominal speeds v_{si} between 0.0017 m/s and 0.005 m/s. Once more `constr` in MATLAB is used for determining the optimal temperatures for the feedforward table. In the optimization the temperatures of zones 3 and 4 are constrained to be larger than 1220°C and 1200°C to ensure a minimal amount of flow and thereby pressure in the last part of the furnace. The maximal temperature of zone 4 is furthermore set to 1240°C to avoid too large temperature gradients of the slabs. The result of the optimization is presented in Figures 11.3, 11.4, and Table 11.1. Note here that speeds over 0.0025 m/s are not feasible, they are only included here since the appear in the tables of the FOCS system at The Danish Steel Works Ltd. The high speeds can only be used for 200 mm slabs.

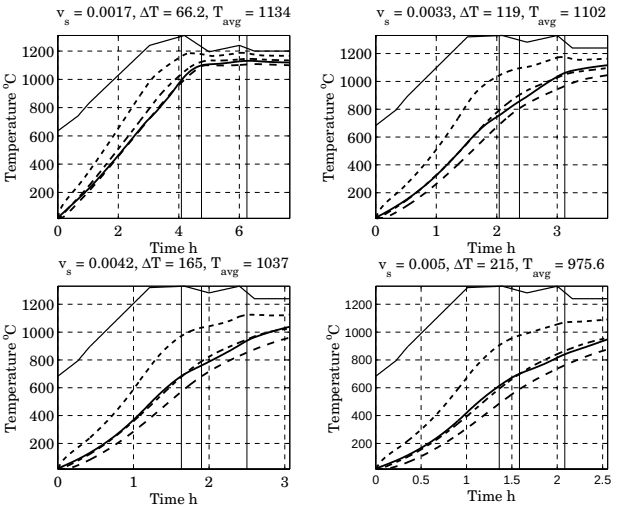

Figure 11.4 Results of the determination of the zone temperatures for the nominal velocities of the feedforward tables. In the figure ΔT denotes the temperature gradient and T_{avg} denotes the average temperature of the FEM simulations at the time of discharge. It is seen that the temperature gradients are not acceptable for slab velocities over $v_s = 0.0025$. The curve marking is the same as used in Figure 11.3.

m/s	0.0017	0.0025	0.0033	0.0042	0.0050
Zone 1	1227°C	1320°C	1320°C	1320°C	1320°C
Zone 2	1308°C	1330°C	1330°C	1330°C	1330°C
Zone 3	1240°C	1220°C	1330°C	1330°C	1330°C
Zone 4	1200°C	1227°C	1240°C	1240°C	1240°C

Table 11.1 New feedforward table with temperature setpoints for the four furnace control zones. The setpoints are given for five different slab speeds. The feedforward table is used for generating an open loop temperature setpoint in the FOCS system.

At zero slab velocity the furnace temperatures are lowered to values specified by a separate table containing multiplication factors for the furnace temperatures at the beginning of the stop. These tables will not be considered here.

Finding the Controller Coefficients

When controlling the temperature of the slabs it is normally desired that they follow the heating curve T_r which defines the control error for the i'th

slab as $T_i^j - T_r(x_i^j)$. It is natural to consider the temperature deviations of the slabs leaving the zone more important than the other slab temperature deviations, this is handled by introducing individual weight terms $r_L^j(i)$ for the slab temperature deviations. We now define the error function for zone j

$$e_L^j(t) = \sum_{i=1}^{n_j} r_L^j(i)(T_i^j(t) - T_r(x_i^j)) \tag{11.7}$$

In the FOCS system four different choices of linear weight functions are possible. We here choose the variant that gives equal weight to all the slabs in a zone, the reason for this is that the experiences from the experiments in Chapter 13 show that the heating of the cold slabs entering are as important as the temperature of the slabs leaving the zone. To keep the design simple we choose the same weight function r_L^j for all four control zones

$$r_L^j(i) = \frac{1}{n_j},\ i = 1, \dots, n$$

Note that this choice of weight function yields $\sum r_L^j(i) = 1$. Since the zone always is filled with slabs this choice of weight ensures a constant gain of the model of the slabs of a zone, as we will see later.

Looking at the control error $Y_i^j = T_i^j - T_r(x_i^j)$ we obtain the differential equation from (11.1)

$$\begin{aligned}\frac{dY_i^j}{dt} &= \frac{dT_i^j}{dt} - \frac{dT_r}{dt} \\ &= g(T_i^j)(f(T_i^j) + u(x_i^j, T_m^j)) - \frac{v_s(t)}{v_{s0}} g(T_r)(f(T_r) + u(x_i^j, T_{m0}^j))\end{aligned} \tag{11.8}$$

Linearization of this equation around the heating curve T_r yields

$$\frac{dY_i^j}{dt} = a(x_i^j)Y_i^j(t) + b(x_i^j)(T_m^j(t) - T_{m0}^j) + k(x_i^j)(v_s(t) - v_{s0})$$

where

$$
\begin{aligned}
a(x_i^j) &= \frac{\partial}{\partial T_i^j}\left[g(T_i^j)(f(T_i^j)+u(x_i^j,T_{m0}^j))\right]\Big|_{T_i^j=T_r(x_i^j)} \\
&= g(T_r(x_i^j))'(f(T_r(x_i^j))+u(x_i^j,T_{m0}^j)) \\
&\quad - g(T_r(x_i^j))(4\varepsilon_t\sigma T_r^3(x_i^j)+(\lambda_t-\lambda_b)) \\
b(x_i^j) &= \frac{\partial}{\partial T_m^j}\left[g(T_r(x_i^j))u(x_i^j,T_m^j)\right]\Big|_{T_m^j=T_{m0}^j} \\
&= g(T_r(x_i^j))(4\varepsilon_t\sigma p(x_i^j)(T_{m0}^j)^3+\lambda_t p(x_i^j)) \\
k(x_i^j) &= \frac{\partial}{\partial v_s}\left[-\frac{v_s(t)}{v_{s0}}g(T_r(x_i^j))(f(T_r(x_i^j))+u(x_i^j,T_{m0}^j))\right]\Big|_{v_s=v_{s0}} \\
&= -\frac{1}{v_{s0}}(f(T_r(x_i^j))+u(x_i^j,T_{m0}^j)
\end{aligned}
$$

f, g, and u are defined in (11.3). Since g is based on tables it is differentiated numerically. We note that we have linearized around a trajectory that is a stationary solution to the nonlinear differential equation for the slab temperature T_i^j. This is a classical approach in nonlinear system theory. The fact that the heating curve is generated as a stationary solution to the differential equation simplifies the linearization considerably.

Joining the linearized models for all slabs in zone j and introducing Y^j as the vector of slab temperature errors for zone j we end up with a linear state space model of order n_j.

$$
\begin{aligned}
\dot{Y}^j(t) &= A^j(x^j)Y^j(t)+B^j(x^j)(T_m^j(t)-T_{m0}^j)+K^j(x^j)(v_s(t)-v_{s0}) \\
e_L^j(t) &= C^jY^j(t)
\end{aligned}
$$

A^j has diagonal structure and B^j, C^j, and K^j are vectors

$$
\begin{aligned}
A^j(x^j) &= \begin{bmatrix} a(x_1^j) & 0 & \dots & 0 \\ 0 & a(x_2^j) & \ddots & \vdots \\ \vdots & \ddots & \ddots & 0 \\ 0 & \dots & 0 & a(x_{n_j}^j) \end{bmatrix} \\
B^j(x)^T &= \begin{bmatrix} b(x_1^j) & b(x_2^j) & \cdots & b(x_{n_j}^j) \end{bmatrix} \\
C^j &= \begin{bmatrix} r_L^j(1) & r_L^j(2) & \cdots & r_L^j(n_j) \end{bmatrix} \\
K^j(x)^T &= \begin{bmatrix} k(x_1^j) & k(x_2^j) & \cdots & k(x_{n_j}^j) \end{bmatrix}
\end{aligned}
$$

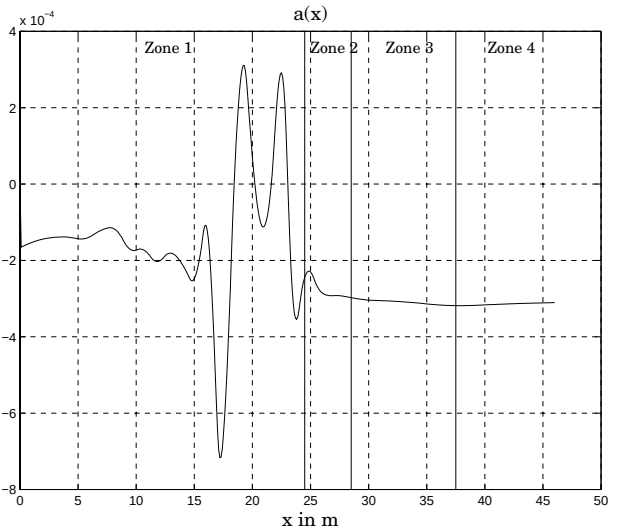

Figure 11.5 Variation of the pole location of a linearization of the nonlinear differential equation for the slab temperature.We assume that the slab temperature T_i^j follows the temperature reference curve T_r. The pole location is shown as a function of slab position x.

Plots of a and b are shown in Figures 11.5 and 11.6, respectively. We note that the values of a equals the eigenvalues of A^j and they become positive due to an internal energy release caused by the phase transformation of the steel. Note that k is the effect of the slab movement with velocity v_s on the error Y_i^j.

Looking at the plot for a in Figure 11.5 and the plot for b in Figure 11.6 we see that the eigenvalues of A and the values of B are constant for zone 4 and the system is therefore neither controllable or observable here. This indicates that a reduction of the number of states in the linearized system might be appropriate.

It is clear from Figures 11.5 and 11.6 that the values of a and b vary with the position of the slab x_i^j. We here cope with this problem by application of averaging. Consider the case where the furnace speed v_s is constant and the slab lengths are identical and a multiple of the zone length l_z^j. We follow a slab through a furnace control zone and when the slab leaves the zone its state is assigned to the new slab entering the zone. It can be realized that the slab temperature control can be seen as

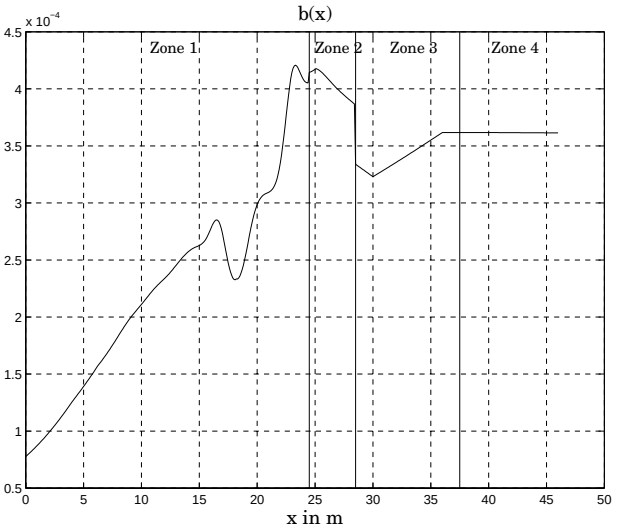

Figure 11.6 Variation of the gain of a linearization of the nonlinear differential equation for the slab temperature. We assume that the slab temperature T_i^j follows the temperature reference curve T_r. The variation is shown as a function of slab position x.

a periodic problem since

$$a(t) = a(t + t^j)$$
$$b(t) = b(t + t^j)$$
$$k(t) = k(t + t^j)$$

where t^j is the time it takes the slab to pass through zone j. The term k is not used here, but the influence of the slab speed v_s is included by the feedforward tables described earlier in this section.

Inspired by averaging theory [Åström and Wittenmark, 1995] we want to approximate the system. Introduce the averaged slab temperature error for the i'th slab in zone j

$$\overline{Y}_i^j = \frac{1}{t^j} \int_0^{t^j} Y(t)\, dt = \frac{v_{s0}}{l_z^j} \int_0^{t^j} Y(t)\, dt$$

and $\bar{Y}^j$ as the vector of averaged slab temperature errors for zone j. Setting $T_m^j - T_{m0}^j = C_S^j(p) C^j \overline{Y}^j$ where $C_S^j(p)$ is the transfer function of the

linear slab temperature controller for zone j we reformulate the differential equation to

$$\begin{aligned}\frac{d\overline{Y}_i^j}{dt} &= \frac{v_{s0}}{l_z^j}\int_0^{t^j} a(t)\,dt\,\overline{Y}_i^j(t) + \frac{v_{s0}}{l_z^j}\int_0^{t^j} b(t)\,dt C_S^j(p)\,C^j\overline{Y}^j(t)\\ &= \frac{1}{l_z^j}\int_0^{l_z^j} a(x)\,dx\,\overline{Y}_i^j(t) + \frac{1}{l_z^j}\int_0^{l_z^j} b(x)\,dx\,C_S^j(p)C^j\overline{Y}_i^j(t)\\ &= \overline{a}^j\overline{Y}_i^j(t) + \overline{b}^j\,C_S^j(p)C^j\overline{Y}^j(t)\end{aligned}$$

where l_z^j is the length of zone j and p is the differential operator. The advantages of the averaging are many, we are able to cope with the positive values of a, and as we will see in the following it is straight forward to design the PI-controllers of the FOCS system for the averaged system. Note that the averaged parameters are not dependent on the slab velocity v_s, they are, however, only guaranteed to be relevant near the heating curve T_r.

Representing each slab in the j'th zone by its averaged linear system we end up with a system matrix A^j with identical eigenvalues and the state space representations for the zones can be reduced to the first order system

$$P_S^j(s) = \frac{C^j\overline{B}^j}{s-\overline{a}^j} = \frac{\sum_1^{n_j} r_L^j(i)\overline{b}^j}{s-\overline{a}^j} = \frac{\overline{b}^j}{s-\overline{a}^j} \tag{11.9}$$

where $\overline{b}^j$ and $\overline{a}^j$ are found by averaging over the zone. We can also see this as we control the slabs temperatures of the zone as the mean temperature of one big piece of steel. Note that due to the special choice of weight function r_L^j the slab lengths do not affect (11.9). The values found in the averaging are

$$\begin{bmatrix}\overline{b}^1\\ \overline{b}^2\\ \overline{b}^3\\ \overline{b}^4\end{bmatrix} = \begin{bmatrix}2.3\cdot 10^{-4}\\ 4.0\cdot 10^{-4}\\ 3.5\cdot 10^{-4}\\ 3.7\cdot 10^{-4}\end{bmatrix}$$

$$\begin{bmatrix}\overline{a}^1\\ \overline{a}^2\\ \overline{a}^3\\ \overline{a}^4\end{bmatrix} = \begin{bmatrix}-1,4\cdot 10^{-4}\\ -2.7\cdot 10^{-4}\\ -3.1\cdot 10^{-4}\\ -3.1\cdot 10^{-4}\end{bmatrix}$$

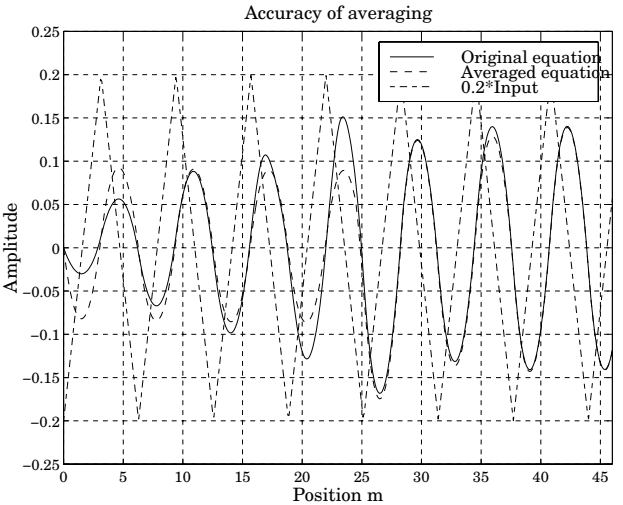

Figure 11.7 Check of validity of averaging. The original linearized system with the time varying coefficients and the averaged equation (11.9) are simulated with a sawtooth wave as input. We note that there is a reasonable agreement between the responses of the original and the averaged system.

Note that all the averaged systems are stable. To verify the dynamic properties of the averaging of the system around the heating curve the original system with the time varying coefficients and the averaged system are simulated with a sawtooth wave as input. The result is shown in Figure 11.7.

The controller structure of the FOCS system is shown in Figure 11.1, it has two PI-controllers, one for the furnace temperature T_m^j and one for the weighted slab temperature $r_L^j T^j$. The averaging analysis implies that $r_L^j T^j = \overline{T}^j$ and we have the linear first order transfer function (11.9) from the furnace temperature T_m^j to the controlled variable. The disturbances of the system—the variations of v_s—enter the system through the reference T_r, see Figure 11.1. This makes the linear controller design a servo problem, see [Åström and Wittenmark, 1997]. Note that the temperature found using the feedforward tables T_{ff}^j is related to a change of the reference T_r. As we will see later this gives a pretty good reaction to the disturbances introduced by the slab movement.

An investigation of the furnace temperature control shows that the performance of these controllers are satisfactory and we therefore choose to keep the existing controller structure for this algorithm.

The transfer functions of the slab and furnace temperature controllers are given by

$$C_F^j(s) = K_{pF}^j + K_{iF}^j \frac{1}{s}$$
$$C_S^j(s) = K_{pS}^j + K_{iS}^j \frac{1}{s}$$

Neglecting dynamics of the fuel and air valves, which are considerably faster than the system dynamics, we end up with the second order closed loop transfer for the furnace and slab temperatures

$$T_m^j(s) = G_F^j(s) T_{mr}^j(s) = \frac{a_2^j (K_{pF}^j s + K_{iF}^j)}{s^2 + (a_2^j K_{pF}^j - a_3^j)s + a_2^j K_{iF}^j} T_{mr}^j(s)$$
$$\overline{T}^j(s) = G_S^j(s) r_L^j T_r(s) = \frac{\overline{b}^j (K_{pS}^j s + K_{iS}^j)}{s^2 + (\overline{b}^j K_{pS}^j - \overline{a}^j)s + \overline{b}^j K_{iS}^j} r_L^j T_r(s)$$

where it has been assumed that the dynamics of the transfer function for the furnace temperature G_F^j are fast compared to the dynamics of G_S^j and therefore can be neglected in the second equation. Since the open loop time constants of the furnace zone temperature, see Section 10.1, is a factor 10 faster than the time constants for the slab temperature this is considered a valid approximation.

Aiming at closed loop time constants half as long as the open loop time constants and a damping factor of 0.7 for the slab temperature yields the following equations for the controller coefficients.

$$K_{iS}^j = -\frac{4(\overline{a}^j)^2}{\overline{b}^j}$$
$$K_{pS}^j = -\frac{1.8\overline{a}^j}{\overline{b}^j}$$

A simulation of a standard slab velocity disturbance, see Section 12.3, is shown in Figure 11.8. The simulations have been carried out using the full nonlinear model for the reheat furnace described in Chapter 12. It is seen that the stop gives a rather large error in the slab temperatures leaving the zone, but also that the PI-controller uses large control effort to counteract the disturbance.

The final question in the linear design is the variation of the slab dimensions. Since the material parameters of (11.3) are $g = 1/(\tilde{h}\rho c_p)$ we

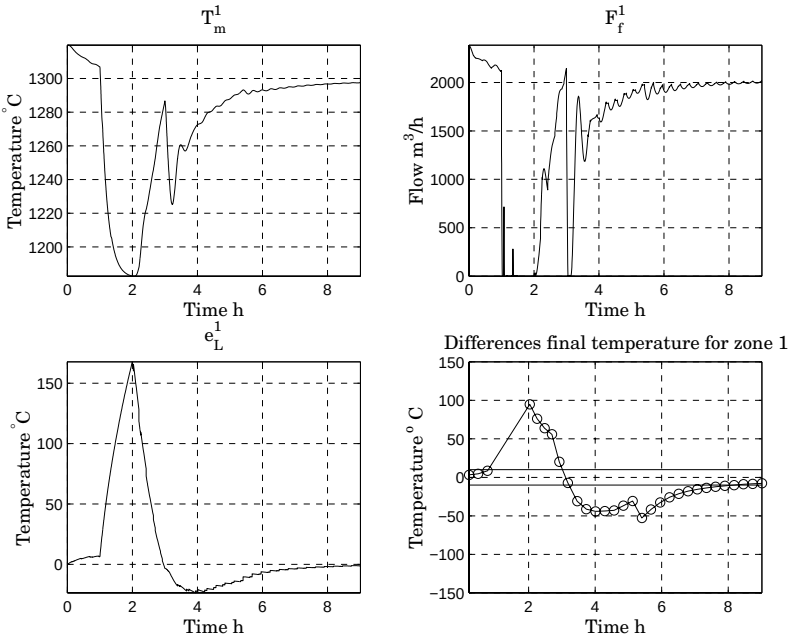

Figure 11.8 Response of the slab temperature control of zone 1 to a step disturbance in the slab velocity v_s when the slab temperatures are controlled using the PI-controller and feedforward table. The slab velocity is changed from its nominal value 0.002 m/s to zero at $t = 1$, to 0.0025 m/s at $t = 2$ and back to the nominal value at $t = 3$, see Figure 12.2. The plots show the reactions of the slab temperature controller to the disturbance. We see that the slabs leaving the zone get approximately 100°C too hot, but this is taken care of later by zones 2 to 4. The responses are kept within the permissible limits of the fuel flow F_f^1 and furnace temperature T_m^1. The control error is defined by $e_L^1 = r_L^1 Y^1$. The circles in the plot in the lower right corner show the temperatures of the slabs leaving the zone. The bend on the curve at t = 5.5 hours is the first slab which has entered the zone after the stop. The horizontal lines around $Y_i^j = 0$ marks a heating error of ±10°C.

see that approximatively

$$\overline{a}_i \propto \frac{1}{h}$$
$$\overline{b}_i \propto \frac{1}{h}$$

which make the gain and pole of (11.9) inversely proportional to the slab thickness h. The characteristic equation of the closed loop system becomes

approximatively

$$s^2 + \frac{\tilde{h}}{h}(\overline{b}^j K_{ps} - \overline{a}^j)s + \frac{\tilde{h}}{h}\overline{b}^j K_{is} = 0$$

which is stable for all positive values of h by Routh's stability test. The different thicknesses are handled in the FOCS system by having a separate heating curve for each slab thickness. Note that a different heating curve for slabs of a different thickness might affect the result, since it will affect the values of $\overline{a}^j$ and $\overline{b}^j$.

11.3 Design of Nonlinear Controller

When controlling the slab heating it is natural to start thinking about the possibility of controlling the slab energy content. Unfortunately, the slab energy content given by $h\rho c_p T_i^j$ is not a monotonic function of temperature T_i^j, due to the variations of ρ, and especially c_p. Instead it turns out to be feasible to control the slab enthalpy h_s which we define by

$$h_s(T_i^j) = \int_0^{T_i^j} h\rho(\tau)c_p(\tau)d\tau. \tag{11.10}$$

Using this variable for the slab temperature control yields, beside the nice interpretation, a simplification of the nonlinear equations we want to control. A plot of the enthalpy as generated on the basis of the heating curve of Figure 11.2 is shown in Figure 11.9.

In the following we will design a nonlinear controller for controlling (11.10), where the slabs are expected to follow the enthalpy curve in Figure 11.9 as they are transported through the furnace. This follows the same lines as the linear controller in Section 11.2. This concept we call *enthalpy control*. In the nonlinear design we will adopt the existing furnace temperature controller and neglect the dynamics of the furnace temperature, as in the linear design.

Choosing the enthalpy (11.10) as output of the nonlinear state space equation (11.1) we end up with the system

$$\begin{aligned} \frac{dT^j}{dt} &= G(T^j)(F(T^j) + U(T_t)) \\ e_V^j(T) &= \tfrac{1}{2}\sum_{i=1}^{n_j} r_{V_i}^j (E_i^j)^2 \end{aligned} \tag{11.11}$$

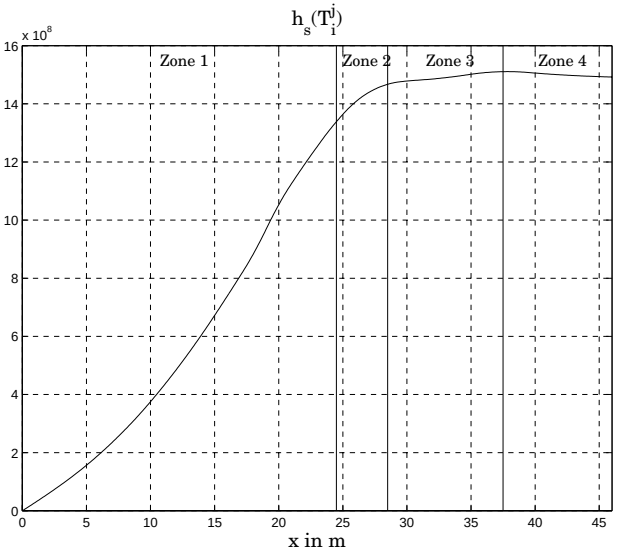

Figure 11.9 Enthalpy curve for the control zones of the reheat furnace with an initial temperature of 20°C and a final temperature of 1120°C. The enthalpy curve is based on the heating curve in Figure 11.2 and (11.10).

where r_V^j is the error weight for the enthalpy controller, h_s is defined by (11.10) and

$$E_i^j(x_i^j, T_i^j) = h_s(T_i^j) - h_r(x_i^j).$$

The weights of r_V^j now can be chosen freely. The enthalpy reference h_r which depends on slab position x_i^j, is defined as

$$h_r(x_i^j) = \int_0^{T_r(x_i^j)} h\rho(\tau)c_p(\tau)\,d\tau$$

Many other choices of error functions than the quadratic one used in (11.11) are possible, it is chosen here because it works well in practice and we can use it for proving a stability result later on.

Using the nonlinear geometric methods for investigating the controllability and observability, see [Nijmeijer and van der Schaft, 1991], of (11.11) is unfortunately not feasible due to the repeated differentiation of g which is only given by numerical data. A sufficient condition for a system to be locally controllable is that the linearized system is controllable,

see [Nijmeijer and van der Schaft, 1991]. As seen from the discussion in Section 11.2 this is not always the case. Using the linearized model we, furthermore, see that a sufficient condition for lack of (state) controllability is that two slab temperatures T_i^j and T_k^j are equal—this can, for instance, happen during longer stops if the furnace temperature profile p is the same for x_i^j and x_k^j. This indicates that it can be difficult to control the furnace in these situations.

Looking at the linearization in Section 11.2 we see that the linearized system is not always observable in a neighborhood around the heating curve and we can therefore not derive sufficient conditions for observability either. Again we see that during stops where the slab temperatures become equal we can get problems with the observability of the nonlinear system.

Investigating the methods suited for nonlinear controller design it turns out that *feedback linearization* is well suited for controlling the slab temperatures. Given a reference trajectory for the slab enthalpy h_r the main idea is to make the control error behave like the linear system

$$\frac{d}{dt}e_V^j = -c_1^j e_V^j - c_0^j \int_0^t e_V^j(\tau)\, d\tau \tag{11.12}$$

which we choose to have the same dynamics as the linearized system of Section 11.2. Note that we have introduced an integral state in (11.12) which will ensure that the error e_V^j converges to zero in the presence of offsets in (11.12). This is along the same ideas as the *tracking problem* described in [Isidori, 1989], but there no integrator is used and furthermore (11.11) is not affine in the input u due to the variation of p with the slab positions x_i^j. We therefore have to solve the problem by other means.

The first thing we note is that it is not possible to use the integrator in (11.12), since $e_V^j \geq 0$ the value of the integral will always be increasing, instead we introduce the equation

$$\frac{d}{dt}e_V^j = -c_1^j e_V^j - c_0^j \sum_{i=1}^{n_j} r_{V_i}^j E_i^j \int_0^t E_i^j(\tau)\, d\tau \tag{11.13}$$

and now the integrands can take positive as well as negative values, and

(11.13) is usually still close to (11.12). Rewriting (11.13) yields

$$\frac{d}{dt}e_V^j = \sum_{i=1}^{n_j} r_{V_i}^j 2\dot{E}_i^j E_i^j = -c_1^j e_V^j - c_0^j \sum_{i=1}^{n_j} r_{V_i}^j E_i^j \int_0^t E_i^j(\tau)\, d\tau \qquad (11.14)$$

$$\Downarrow \qquad (11.15)$$

$$\sum_{i=1}^{n_j} r_{V_i}^j E_i^j \left(2\dot{E}_i^j + c_1^j E_i^j + c_0^j \int_0^t E_i^j(\tau)\, d\tau \right) = 0$$

which implies that the characteristic equations of the slab enthalpy errors E_i^j all have the characteristic equation

$$s^2 + \frac{1}{2}c_1^j s + \frac{1}{2}c_0^j = 0$$

when the signs of E_i^j are the same, which typically is the case when the system is subjected to large disturbances, when the controller action is important. To obtain the same dynamics in the large adjustments as the linear controller in these cases we choose $c_0^j = 8\overline{\alpha}^j$ and $c_1^j = 0.707 \cdot 8\overline{\alpha}^j$, where $\overline{\alpha}^j$ are the averaged poles of the linearized system in Section 11.2.

The differential equation for the enthalpy error E_j^i is

$$\begin{aligned}\frac{d}{dt}E_i^j &= \frac{d}{dt}h_s(T_i^j) - \frac{d}{dt}h_r(T_r(x_i^j)) \\ &= (f(T_i^j) + u(x_i^j, T_m^j)) - \frac{v_s}{v_{s0}}(f(T_r()x_i^j) + u(x_i^j, T_{m0}^j))\end{aligned} \qquad (11.16)$$

Note that the material properties g are not present in (11.16), this is the advantage of using the enthalpy h_s as controlled output instead of the temperature T_i^j. Using the fact that u depends on T_m^j as in (11.3) gives a fourth order polynomial for T_m^j when (11.16) and (11.13) are combined

$$\alpha_1 \left(T_m^j(t)\right)^4 + \alpha_2 T_m^j(t) = \alpha_3 \qquad (11.17)$$

where

$$\begin{aligned}
\alpha_1 =& 2\varepsilon_t \sigma \sum_{i=1}^{n_j} r_{V_i}^j p^4(x_i^j) E_i^j \\
\alpha_2 =& 2\lambda_t \sum_{i=1}^{n_j} r_{V_i}^j p(x_i^j) E_i^j \\
\alpha_3 =& 2\sum_{i=1}^{n_j} r_{V_i}^j E_i^j \left[-f(T_i^j) + \frac{v_s(t)}{v_{s0}} (f(T_r(x_i^j)) + u(x_i^j, T_{m0}^j)) \right] \\
& - c_1^j e_V^j - c_0^j \sum_{i=1}^{n_j} r_{V_i}^j E_i^j \int_0^t E_i^j(\tau)\, d\tau
\end{aligned}$$

which can be done numerically by using for instance `fzero` in MATLAB. Note that f in α_3 represents the temperature losses, $v_s/v_{s0}(f+u)$ can be seen as a feedforward from the slab speed and $c_1^j e_V^j + c_0^j \sum r_{V_i}^j E_i^j \int E_i^j$ is the feedback part of the control law. We conclude that the nonlinear control law has the features of the linear control law, but this time they are automatically built-in.

The next question that arises it the stability of the control law. Using the Lyapunov function

$$V(E^j, \int E^j) = e_V^j + \frac{1}{2} c_0^j \sum_{i=1}^{n_j} r_{V_i}^j \left(\int_0^t E_i^j(\tau) d\tau \right)^2$$

with the time derivative

$$\begin{aligned}
\dot{V}(E^j, \int E^j) &= \dot{e}_V^j + c_0^j \sum_{i=1}^{n_j} r_{V_i}^j E_i^j \int_0^t E_i^j(\tau) d\tau && (11.18) \\
&= -c_1^j e_V^j && (11.19)
\end{aligned}$$

where E^j is a vector containg the enthalpy errors E_i^j for zone j. Since $V \to \infty$ as $(E_i^j, \int E_i^j) \to \infty$ we have by the *Global Invariant Set Theorem* in [Slotine and Li, 1991] that $(E_i^j, \int E_i^j)$ converges to the largest invariant set where $\dot{V} = 0$. This is given by

$$M = \left\{ x \mid (x_1, \ldots, x_{n_j}) = 0,\ (x_{n_j+1}, \ldots, x_{2n_j}) \in R^{n_j} \right\}$$

and we therefore conclude that $E_i^j \to 0$ as $t \to \infty$. The control system is therefore globally asymptotically stable. Note that we only have guarantee

for stability when (11.17) is solvable. The solvability issue investigated in the following.

In equation (11.17) we see that α_1 and α_2 are positive and since the left hand side is a monotonically increasing function of T_m^j we conclude that (11.17) will have a unique solution if and only if α_3 is positive. This is introduced by the physical limitation $T_m^j \geq 0$—it is not possible to cool the slabs by reducing the temperature below 0°K.

The conclusion is that the system is globally asymptotically stable when the slab temperatures T_i^j are near the heating curve T_r. When too large deviations are present it is not sure that (11.17) is solvable. The large deviations can, for instance, happen during stops or excessive furnace speeds. This is to some extent parallel to the controllability problems of the linearized system.

The performance of the nonlinear control law (11.17) is investigated by implementing the nonlinear state space model (11.1) and the control law (11.17) in MATLAB. The result of a step disturbance is shown in Figure 11.10. The simulations have been carried out using the full nonlinear model for the reheat furnace described in Chapter 12. For the nonlinear equations we use the weight function

$$r_V^j = \frac{1}{\sum_{i=1}^{n_j} r_{V_i}^j} [\, 1 \quad \cdots \quad 1 \quad 2 \quad 5 \quad 10 \quad 20 \quad 50 \quad 100 \,]$$

Note that the final slab temperatures converges faster towards the specified value for the nonlinear controller, the price paid is somewhat larger variations of the fuel flow F_f^1. Note that the nonlinear system is within ±20°C after about 4.5 hours, while the PI-controller reaches this level at approximately 6.5 hours.

11.4 Conclusions

In this chapter we have designed both a linear and one nonlinear control law for the slab temperature control problem. The linear design includes a description of a new way of generating a heating curve, which is the temperature reference, and the feedforward tables which are used as feedforwards from the slab velocity. In the following section a new design method for design of a PI control law for the slab temperatures is described. This is done by linearizing the nonlinear model for the slab temperature around the heating curve and reducing the model order. The linear design is based on the controller structure of the existing furnace control system at The Danish Steel Works Ltd.

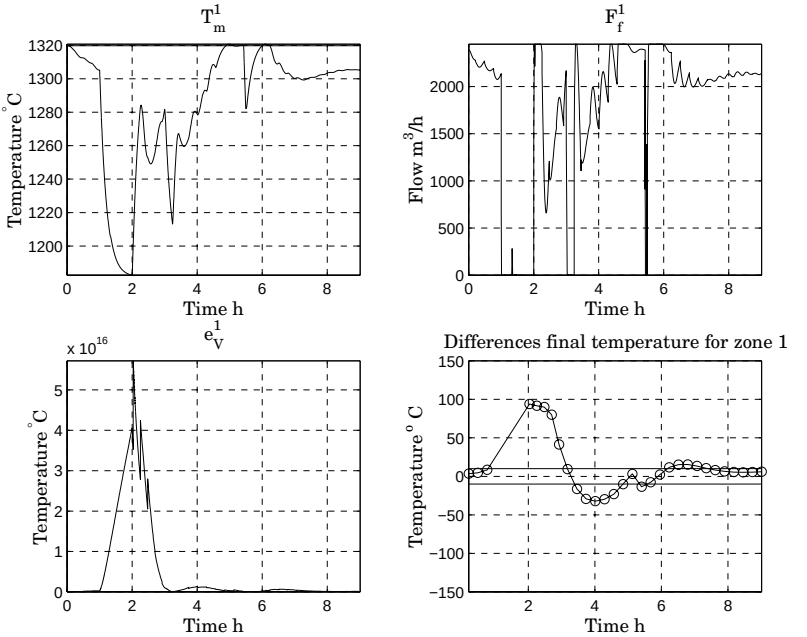

Figure 11.10 Response of the slab temperature control of zone 1 to a step disturbance in the slab velocity v_s when the slab temperatures are controlled using the enthalpy controller. The slab velocity is changed from its nominal value 0.002 m/s to zero at $t = 1$, to 0.0025 m/s at $t = 2$ and back to the nominal value at $t = 3$, see Figure 12.2. The plots show the reactions of the slab temperature controller. The responses are kept within the permissible limits of the fuel flow F_f^1 and furnace temperature T_m^1. e_V^1 is the enthalpy error for zone 1. The circles in the plot in the lower right corner show the temperatures of the slabs leaving the zone. The horizontal lines around $Y_i^j = 0$ marks a heating error of ± 10°C. This figure should be compared to Figure 11.8.

The nonlinear control law, which is a new control algorithm for the slab temperature problem, is designed using feedback linearization. In the design the slab temperature is to follow a given enthalpy reference curve dependent on the slab position. The enthalpy reference is found using the heating curve from the linear design. Integral control action is used in nonlinear control law and the closed loop dynamics of the nonlinear controller is chosen to be similar to the closed loop dynamics of the linear design. It is shown that the nonlinear controller is globally asymptotically stable, given the equation for determining the furnace temperatures is solvable, and that the controller output is unique, if a solution exists.

It is interesting to note that the design of the nonlinear control law is

straight forward while the linear controller design is requires more work. On the other hand the linear control law is straight forward to implement while the nonlinear control law requires a solver for the nonlinear equation (11.17). The performances of the two control laws is investigated using computer simulations based on the full nonlinear model and a standard disturbance in the slab velocity. The simulations show that the response speed of the nonlinear controller is significantly faster than the response speed of the linear controller, the price paid is somewhat larger variations of the control signal.

A more complete comparison of the two controller concepts is given in the next chapter, there more detailed simulations will be carried out and the performance of the control systems will be investigated.

12

Temperature Control—Simulations

The purpose of this chapter is to evaluate and compare the performance and robustness of the PI-controller and the enthalpy controller designed in Chapter 11. The evaluation is done through computer simulations using MATLAB.

We will first describe the simulation program and the cases be to simulated. This is followed by an investigation of the robustness to parameter variations, the response to a standard disturbance, and finally a simulation of the real case when the furnace does production.

12.1 Implementation of Simulation Model and Control Laws

The purpose of the simulations is verifications of the control laws and it should therefore be possible to simulate the furnace operation with different slab lengths (we neglect the thickness variations) and varying slab speed. We should furthermore be able to simulate the slab heating as the slabs are transported through the four furnace zones.

The simulations cover the center track of the three furnace tracks and the inputs to the simulation programs are

- A vector of slab lengths. They can either be 2 m or a uniformly distributed sequence with values in the interval $[1.5, 2.5]$ m
- Slab speed, this is either the test function also used in the evaluation of the controller design in Chapter 11 or time series taken from the pig runs.

The outputs from the simulation program are the time series for

- The fuel flows F_f^j for each furnace zone.

- The furnace temperature T_m^j for each furnace zone.
- The slab temperatures T_i^j computed using the ODE model for all the slabs that passes through the furnace.
- The slab temperatures $T_{10\%}$, $T_{50\%}$, and $T_{90\%}$, computed for a chosen critical slab using the PDE model.

All are functions of time t. The same inputs and outputs are used for both the PI-controller and the nonlinear controller.

The limitations of the temperature control system are the fuel flows F_f^j—they can not be smaller than zero or larger than a given limit for each zone. Using the model derived in Section 10.1 the limitations in fuel flow lead to upper and lower limits of the furnace temperatures T_m^j. There is furthermore given limitations for the maximal permissible furnace temperatures to protect the furnace construction.

The simulation program should handle the following main tasks

- Material tracking, using the slab lengths and slab speed, the program should keep track of the slabs in the furnace zones.
- Simulation of furnace temperature, using the linear model for the furnace temperatures derived in Section 10.1.
- Simulation of slab temperature, using the nonlinear ODE model for the slab temperatures derived in Section 10.2
- Control of furnace temperature, using the PI-control algorithm for the furnace temperatures.
- Control of slab temperatures, using the PI-controller or the nonlinear controller mentioned in Sections 11.2 and 11.3.

Given the slab lengths and the slab speed the simulation program first determines at which times slabs enter and leave the four furnace zones. The simulation for each zone is stopped and started each time a slab enters or leaves the zone. When the simulation is stopped the important variables are stored and the initial values are determined with the new constellation and the simulation is restarted with the new number of slabs in the zone. The simulation is handled by first simulating the entire run for zone 1, and then simulating zone 2, with the final temperatures of zone 1 as initial values etc. It is assumed that the slabs are 20°C when they enter zone 1.

The models and the controllers are described by a set of differential equations which is solved using the built-in function `ode45`. When the simulations of all zones are finished the PDE model derived in Section 10.2 is used for computing the temperatures for the slabs with the shortest

residence time in the furnace. This slab is expected to have the largest temperature gradient since there has been a short time interval available for heat conduction through the slab. Note that the residence time is determined by the furnace operator and it can therefore not be affected by the controllers.

The implementation of the furnace model and the slab temperature models (11.1) is straight forward, the only modification is the extension of zone 1 also to include zone 0 which is the dark zone without burners before zone 1, see Figure 8.1. This is possible since the temperatures of zone 0 are well correlated with the temperatures of zone 1.

To maintain simplicity it is chosen to implement the controllers as continuous time differential equations, it would, however, be straight forward to convert the control algorithms to discrete time. One possibility with the nonlinear controller would be to use a sampling time which is short compared to the furnace time constants and to keep the furnace temperature references constant between the sampling instants.

The implementation of the PI-controller is done by specifying the differential equation for the controller and by introduction of tracking to prevent integrator windup, see [Åström and Wittenmark, 1997]. The time constant for the tracking system is chosen to the same value as the integral time. The feedforward from the slab speed is implemented as a table, and the feedforward value is found by linear interpolation of the table values. During stops the feedforward value is set to the lower limit for the furnace temperature. It should be noted that this is a simplification of the function in the FOCS system where the furnace temperatures are ramped down from the furnace temperatures T_m^j when the stop occurs using a table with multiplication factors depending on the stop time, which in some cases might be unknown.

The equation for the nonlinear control algorithm (11.17) is solved by first computing the sign of the left side of the equation minus the right side at the maximal and minimal furnace temperatures. If the two expressions have different signs the equation has a zero in the feasible furnace temperature interval. In this case the solution is found using the function `fzero` in MATLAB. The analysis in Chapter 11 shows us that this solution is unique. If both expressions are negative it is not possible to obtain a sufficiently high temperature to solve the equation and the furnace temperature reference is set to the maximal permissible value. Along the same lines the furnace temperature reference is set to the lowest possible value if both terms are positive. A condition for solving the equation is that $|\sum_i E_i^j|$ is larger than a specified limit, this is introduced to avoid problems with solvability of the nonlinear equation when E^j is close to zero. In the nonlinear case the temperature reference newer gets outside the specified interval and we here choose to block the integrator when

saturation occurs, instead of tracking the integral part.

As mentioned in Section 11.2 the existing controller parameters are used for controlling the furnace temperatures. The simulations indicate that the furnace temperature controller settings do not have a major impact on the slab temperature control. This is sensible since the furnace temperature dynamics are much faster than the slab temperature dynamics.

12.2 What to Investigate in Simulations?

Before carrying out the simulations it is important to realize that the operation of the furnace is dictated by practical considerations and not by guidelines for optimal furnace operation. This implies that the furnace typically is operated at a high speed approximately 45 minutes and then rests 15 minutes or more when slabs from furnace no. 1 are rolled. The large variations in slab speed makes the evaluation of the dynamic performance and the temperature gradients especially important in our case.

The simulations presented in the following will be used for investigating the robustness and the performance of the control algorithms. Three main cases are considered

- The robustness, what happens when the parameters of the slab temperature model varies.
- The propagation of a standard disturbance, see Figure 12.2, through the furnace, the same case used for evaluation in the controller design in Chapter 11, but now we look at all four zones.
- Doing production, here we use a recorded slab speed and different slab lengths.

The simulation of the standard disturbance is used as an idealized introduction to the simulation with the real slab speed. The advantage of this approach is that the standard disturbance is more regular and the consequences of the speed variation are more straight forward to analyze.

12.3 Robustness

Since it is hard to verify the robustness of the nonlinear system analytically we choose to do a simple investigation of parameter variations using the simulation program. The parameters that can be expected to vary are

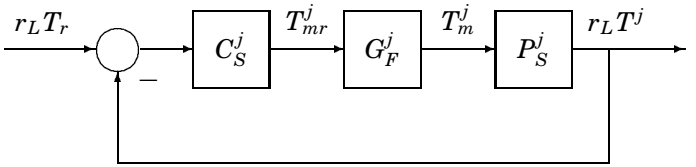

Figure 12.1 Block diagram of controller configuration, where C_S^j is the slab temperature controller for zone j, G_F^j is the closed loop transfer function from the furnace temperature reference T_{mr}^j to the furnace temperature T_m^j, and P_S^j is the model for the slab temperatures. In the robustness test the parameters of P_S^j are varied. The feedforward is not shown in the figure since it does not affect the stability. Note that the block diagram covers the case for the PI-controller, the block diagram for the nonlinear controller is similar.

ε_t, λ_t, λ_b, and T_b of the nonlinear ODE (11.1). In the simulations we vary each parameters $\pm 20\%$ one at the time, see Figure 12.1.

The sensitivity to the parameter variations for the two controllers is evaluated by looking at the responses for the control error e for zone 1 when subjected to the disturbance in slab velocity shown in Figure 12.2. No significant impact on the dynamics is seen and we therefore conclude that the slab temperature controllers are not sensitive to variations in the four Specified parameters.

12.4 A Stop

The purpose of this simulation is to investigate the effect of a stop on the slab temperatures in the four furnace zones. This is done by simulating the complete furnace model with a constant slab length of 2 m and the slab velocity shown in Figure 12.2. During the first hour the velocity disturbance represents that the furnace is operated at nominal speed, and then a stop occurs where the slab velocity is zero. After the stop the slabs of the furnace are hotter than specified by the heating curve and it is therefore possible to operate the furnace at a speed larger than nominal for one hour. After this the furnace speed is reduced to its nominal level.

The fuel flows when the furnace is subjected to the the velocity disturbances are shown in Figures 12.3 and 12.5, while the errors in the slab temperatures as they leave the zone are shown in Figures 12.4 and 12.6.

The simulations show that the error is largest in zone 1—the problem here is that the zone contains more than 10 slabs which all should

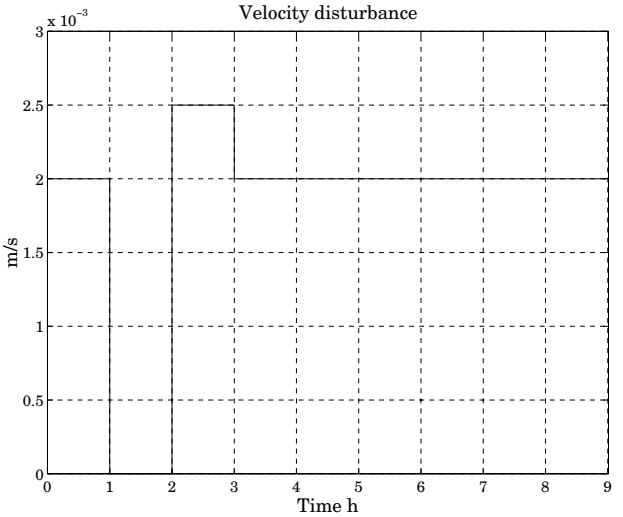

Figure 12.2 Velocity disturbance used to evaluate the controller performance and in the investigation of the sensitivity of parameter variations. Initially the slab speed v_s has the nominal value 0.0020 m/s, after 1 hour the production is stopped for 1 hour and the velocity becomes zero. After the stop the furnace speed is increased to 0.0025 for 1 hour to partially compensate for the production loss and finally the slab speed is set back to its nominal level.

be heated to different temperatures, the result is that the slabs get too hot during the stop and too cold after the slabs start moving again. The pattern for zone 2 is similar to the one for zone 1, but it is more complex due to a temperature error in the incoming slabs from zone 1. One could say that the error is filtered through the furnace zones. The impact on zones 3 and 4 is smaller since all slabs in these zones should have the same temperature and the only disturbance is therefore the temperature error of the incoming slabs.

Comparing the performance of the two controllers we note that the magnitudes of the errors are similar. It seems like the nonlinear controller reacts a bit slower on the stop, but on the other hand reacts faster when the slab movements are started again. In zone 4 the nonlinear controller has a smaller temperature error Y_i^j than the FOCS-controller when the slabs leave the zone. The price paid for this are the larger variations of the fuel flow in zones 3 and 4. One major difference is the response times where the nonlinear controller is able to control the slab temperatures to the correct value at 6.5 hours, see Figure 12.6, which is significantly shorter faster than the FOCS-controller which reaches zero error at 8.5

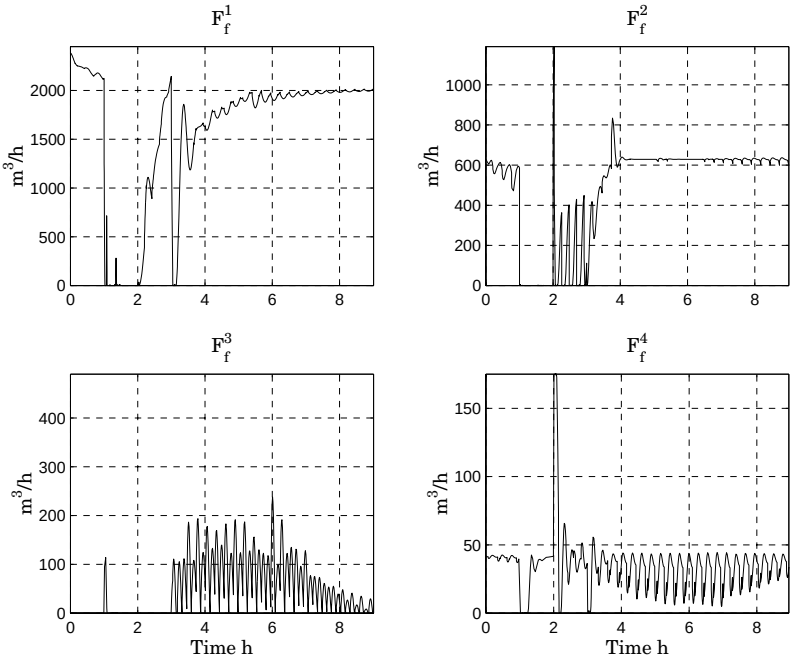

Figure 12.3 Effect of the velocity disturbance shown in Figure 12.2 on the fuel flows F_f^j of the four zones when the slab temperatures are controlled using the PI-controller. Note the oscillations, which are the result of cold slabs entering the zone and hot slabs leaving the zone.

hours, see Figure 12.4.

12.5 Production

We will now investigate the controller performance with varying slab lengths and the recorded slab velocity from the pig runs. The first step is to take a look on the slab speed which is shown in Figure 12.7. We see that the slab movements are close to pulses and it is difficult to use this signal for the furnace temperature feedforward. It is therefore chosen to filter the velocity by using a FIR-filter computing the mean velocity over the last 30 minutes, see Figure 12.7.

Looking at the slab temperatures in Figures 12.8 and 12.12 and the results in Table 12.1 we note that the slab temperatures becomes too large for the FOCS-controller. The final temperatures are also more accurate

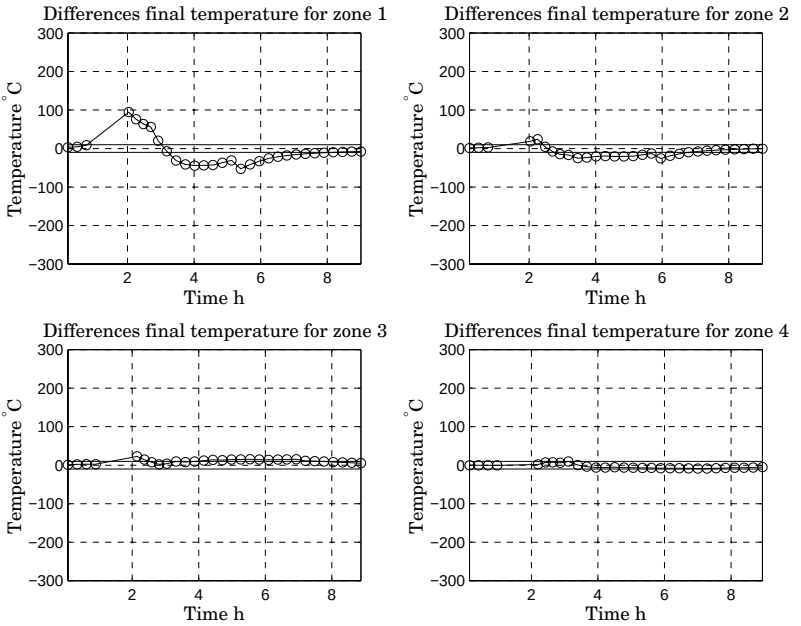

Figure 12.4 Effect of the velocity disturbance shown in Figure 12.2 on the final temperature errors Y_i^j of the four zones when the slab temperatures are controlled using the PI-controller. It is seen that the disturbance has large impact in zones 1 and 2, while it has smaller influence in zones 3 and 4. The horizontal lines around $Y_i^j = 0$ marks a heating error of ± 10°C.

for the nonlinear controller. This affects the energy consumption which is approximated by the integral of the fuel flow to the burners $\int F_f^j dt$ in the j'th zone. The energy consumption are shown in the titles of Figures 12.9 and 12.13 and we see that the energy consumptions are larger for the FOCS-controller in zones 1,2, and 3. For zone 4 the energy consumption is larger for the nonlinear controller. The total energy consumption for all zones for the FOCS-controller is 1.59×10^8 m^3 while it is 1.53×10^8 m^3 for the nonlinear controller, this indicates that the nonlinear controller uses less energy for heating the slabs, probably due to the faster reaction to disturbances.

Looking at the errors of the final temperatures in Figures 12.10 and 12.14 we see that the performance in zones 1 and 2 are similar of the two controllers, the reason probably being that the performance is limited by saturation. Comparing the errors of zones 3 and 4 we see that the nonlinear controller has a significantly better performance compared to

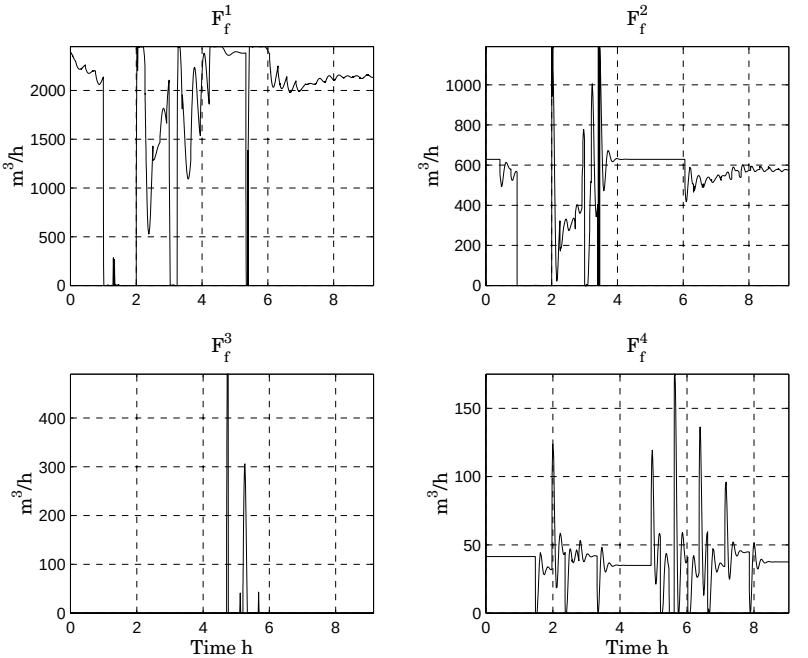

Figure 12.5 Effect of the velocity disturbance shown in Figure 12.2 on the fuel flows F^j of the four zones when the slab temperatures are controlled using the enthalpy controller. Note the oscillations, which are the result of cold slabs entering the zone and hot slabs leaving the zone. The reason for the flow of zone 3 being zero most of the time is that the slabs already are heated to the specified temperature in zone 2 and the working point for the linear model for the furnace temperature. This figure should be compared with Figure 12.3.

the FOCS-controller. The mean value of the heating error in zone 4 is $\mu^4 = -8.22$ for the FOCS-controller and $\mu^4 = 1.52$ for the nonlinear controller while the standard deviation for the nonlinear controller in zone 4 is less than 50% compared to the standard deviation for the FOCS-controller. The price paid is again larger variations of the fuel flows F_f^j as seen from Figures 12.9 and 12.13.

The FEM simulations of the critical slab with the shortest residence time in the furnace are shown in Figures 12.11 and 12.15 show that the critical slab heated using the FOCS-controller has a heating error of -6°C and a temperature gradient ΔT of 77.7°C, while the critical slab heated using the nonlinear controller has a temperature error of 7°C and a temperature gradient ΔT of 74.9°C. We conclude that the performance in this direction is equal for the FOCS-controller and the nonlinear controller.

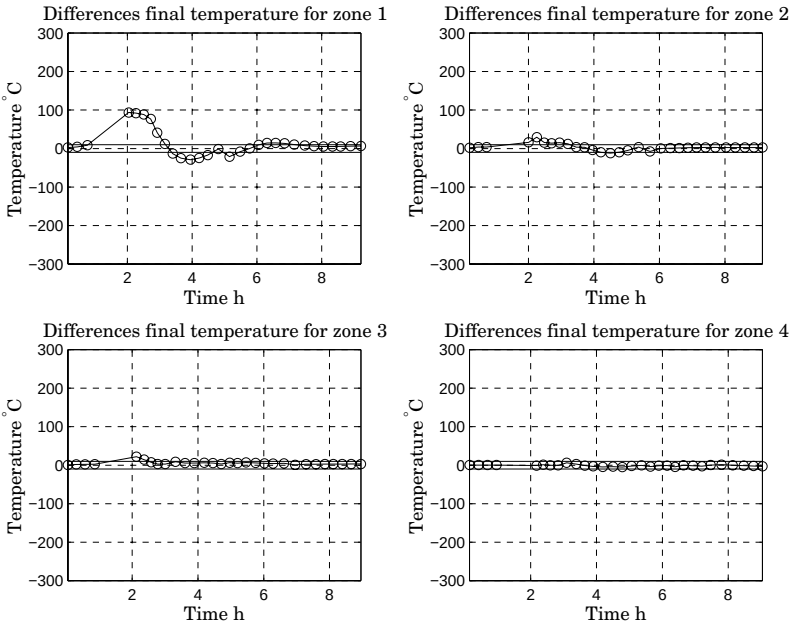

Figure 12.6 Effect of the velocity disturbance shown in Figure 12.2 on the final temperature errors Y_i^j of the four zones when the slab temperatures are controlled using the enthalpy controller. It is seen that the disturbance has large impact in zones 1 and 2, while it has smaller influence in zones 3 and 4. The horizontal lines around $Y_i^j = 0$ marks a heating error of ± 10°C. This figure should be compared with Figure 12.4.

The temperature gradient will be discussed further in Chapter 13.It has not been possible to detect any influence of the varying slab length, the conclusion here is that this is handled well by the normalization of the error weights r_L^j and r_V^j.

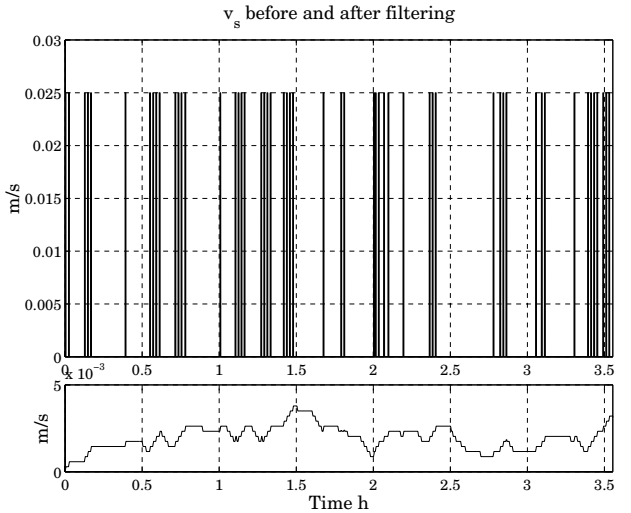

Figure 12.7 Slab velocity v_s before and after filtering. The top plot shows the velocity before filtering and the bottom plot the velocity after filtering. The slabs are moved forward in steps of 0.5 m and each movement takes 20 s. The filtered velocity is obtained by computing the mean velocity over the last 30 minutes.

	FOCS-controller	Nonlinear controller
(μ^1, σ^1)	$(-73.1,\ 71.7)$	$(-77.5,\ 68.0)$
(μ^2, σ^2)	$(-68.4,\ 59.5)$	$(-70.9,\ 56.6)$
(μ^3, σ^3)	$(19.4,\ 14.5)$	$(12.2,\ 11.0)$
(μ^4, σ^4)	$(-8.22,\ 11.5)$	$(1.52,\ 5.41)$

Table 12.1 Table of mean values μ^j and standard deviations σ^j for the FOCS-controller and the nonlinear controller of zone j. The values are for the deviations of the final temperature found when simulating the furnace doing production.

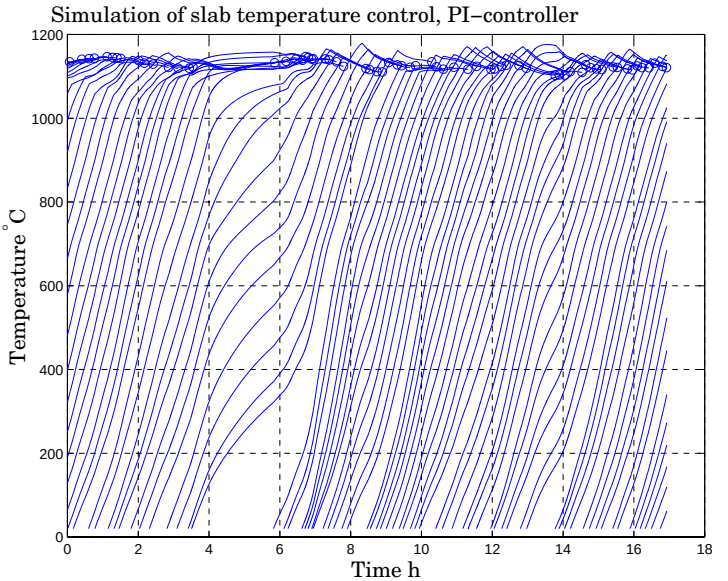

Figure 12.8 Slab temperatures T_t^j controlled by the FOCS-controller as they are transported through the furnace. Note the reactions during and right after the stop beginning around $t = 4$ h.

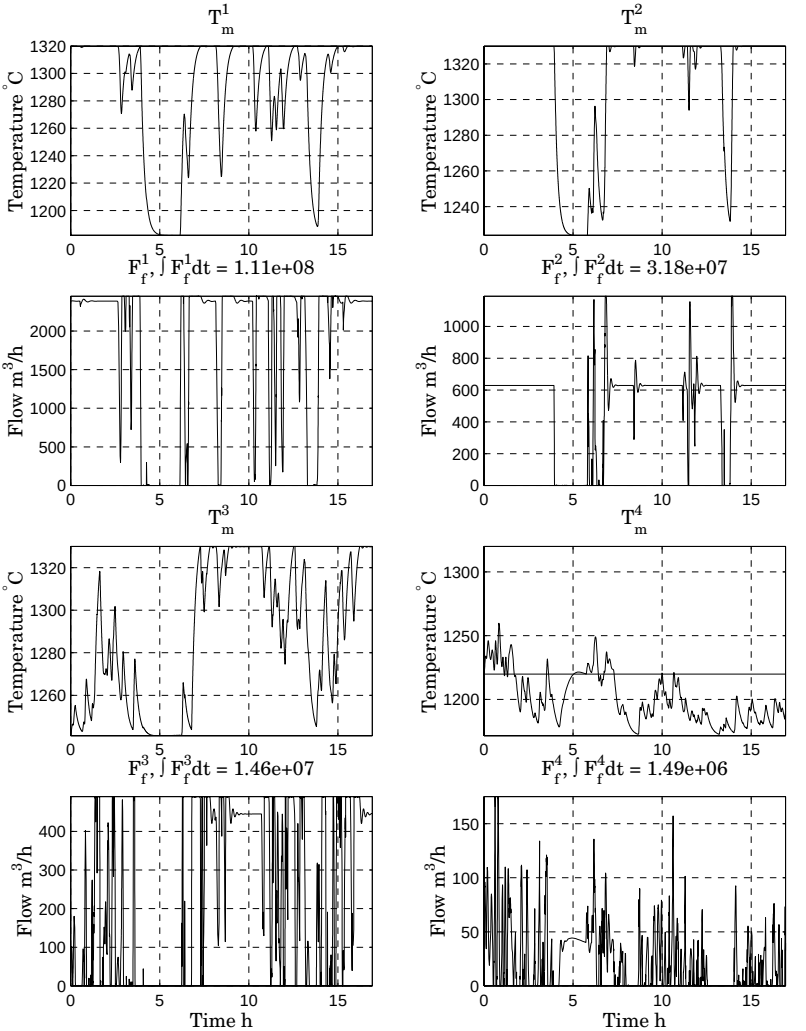

Figure 12.9 Fuel flows F_f^j and furnace temperatures T_m^j when the slab temperatures are controlled using the FOCS-controller.

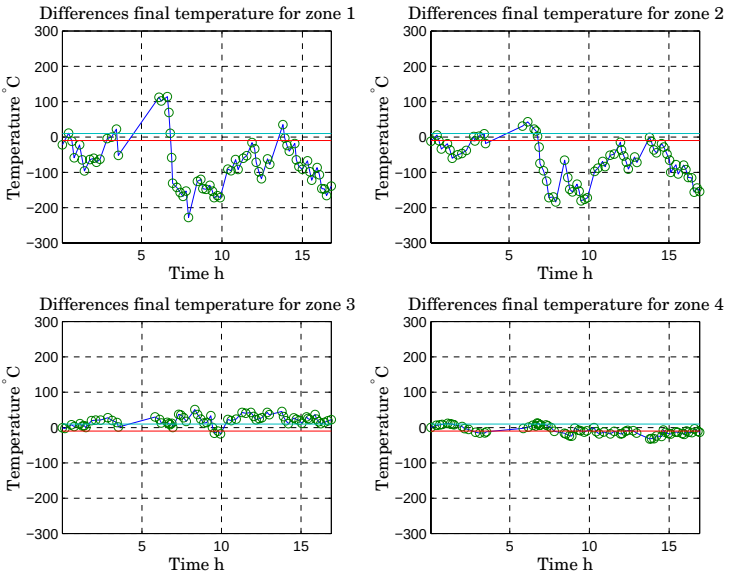

Figure 12.10 Final temperature errors Y_i^j for the four zones when the slab temperatures are controlled by the FOCS-controller. The mean value and the standard deviation of the error in final temperatures are shown in Table 12.1. The horizontal lines around $Y_i^j = 0$ marks a heating error of ± 10°C.

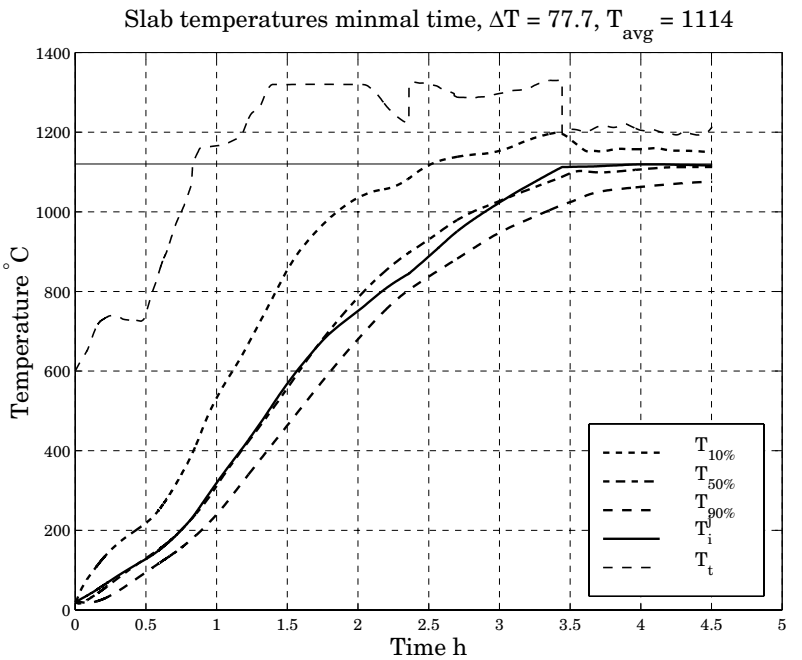

Figure 12.11 FEM simulation of the propagation of the slab temperature for the slab with the shortest residence time in the furnace when controlled by the FOCS-controller. In the figure $T_{10\%}$, $T_{50\%}$, and $T_{90\%}$ are the temperatures 10%, 50%, and 90% below the upper surface,respectively computed using the PDE model for the slab temperature. T_t is the furnace temperature and T_i^j is the slab temperature computed using the nonlinear ODE for the slab temperature.

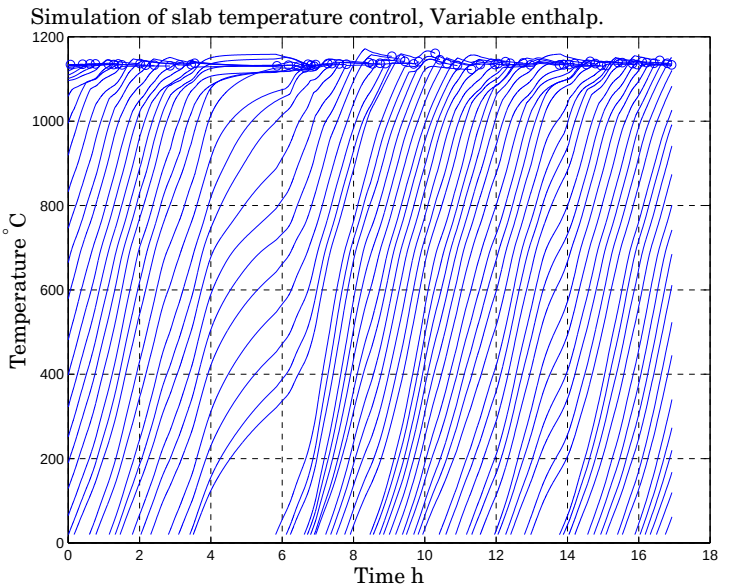

Figure 12.12 Slab temperatures T_i^j controlled by the nonlinear controller as they are transported through the furnace. Note the reactions during the stop beginning at $t = 4$ h. This figure should be compared with Figure 12.8.

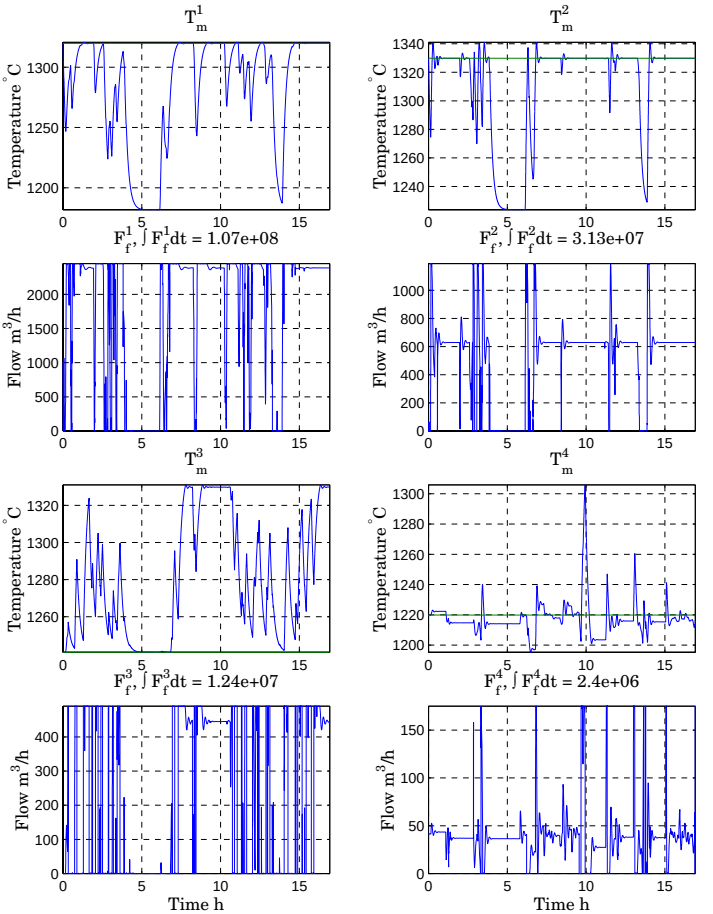

Figure 12.13 Fuel flows F_f^j and furnace temperatures T_m^j when the slab temperatures are controlled using the nonlinear controller. This figure should be compared with Figure 12.9.

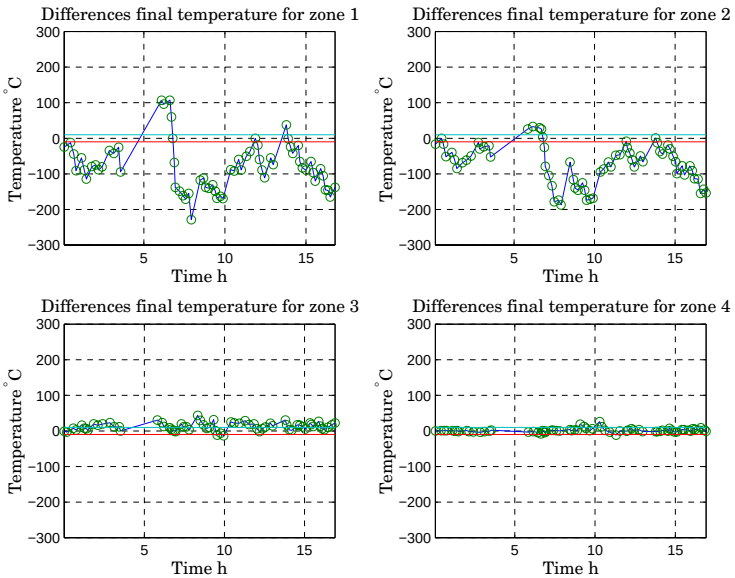

Figure 12.14 Final temperature errors Y_i^j for the four zones when the slab temperatures are controlled by the nonlinear controller. The mean value and the standard deviation of the error in final temperatures are shown in Table 12.1. The horizontal lines around $Y_i^j = 0$ marks a heating error of ±10°C. This figure should be compared with Figure 12.10.

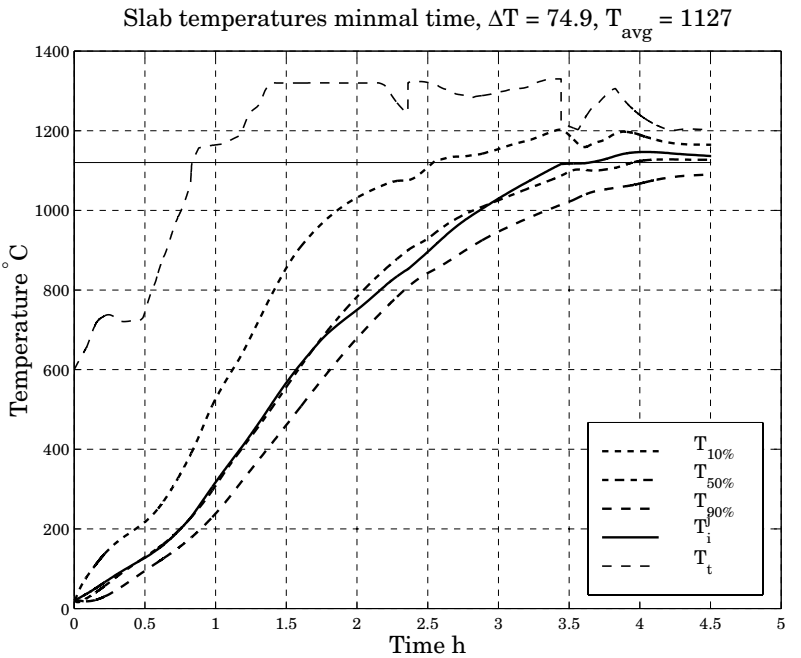

Figure 12.15 FEM simulation of the propagation of the slab temperature for the slab with the shortest residence time in the furnace when controlled by the nonlinear controller. In the figure $T_{10\%}$, $T_{50\%}$, and $T_{90\%}$ are the temperatures 10%, 50%, and 90% below the upper surface,respectively computed using the PDE model for the slab temperature. T_t is the furnace temperature and T_l^J is the slab temperature computed using the nonlinear ODE for the slab temperature. This figure should be compared with Figure 12.11.

Conclusions

We have now investigated the performance and robustness of the FOCS-controller and the nonlinear controller for the slab temperatures. The robustness is investigated by simulating the 16 cases found by varying the four parameters of the model by $\pm 20\%$ for each controller. The parameter variations do not affect the dynamics of the response significantly and we therefore conclude that the system is not especially sensitive to parameter variations.

The performances of the controllers are investigated by first subjecting the four zones to the standard velocity disturbance and simulating the system with a slab speed obtained from the pig runs. The responses to the standard disturbance show that the slab temperature error of zones 1 and 2 are large, while the errors of zones 3 and 4 are small. The magnitude of the errors are the same for the two controllers, but the response speed of the nonlinear controller is superior to the response speed of the linear controller. The price paid is larger variations of the control signal for the nonlinear controller.

The performances of the controllers when subjected to real slab speeds and varying slab lengths show that both controllers are able to control the slab temperatures with good accuracy. The performances of the two controllers are similar for zones 1 and 2, while the nonlinear controller is superior for zones 3 and 4. The simulations also indicate that the energy consumption for the nonlinear controller is smaller than the energy consumption of the FOCS-controller. The FEM simulations show that the temperature gradients for a critical slab heated using the two control algorithms are practically equal.

13

Temperature Control—Experimental Results

In this chapter the results and experiences of the redesign of the FOCS temperature control system at The Danish Steel Works Ltd. are presented. The parameters used for the redesign are the heating curve, feedforward tables, and controller coefficients found in Chapter 11. To find out what to expect from the implementation the performance of the new and existing FOCS parameters are evaluated using the simulation program described in Chapter 12 before the implementation.

In the following we will first use computer simulations to compare the performance of the FOCS system with the new parameters to the performance of the system with the old parameters. This will prepare us for the evaluation of the experimental results. Then the experiences from the implementation of the new parameters are described and the results are presented. The last part of the chapter describes what remains to be done in the redesign of the FOCS system.

13.1 Comparison of New and Existing Parameters

Before we start the implementation of the new parameters we compare the performance of the FOCS system with the existing parameters to the performance of the system with the new parameters shown in Chapter 12.

The main difference between the existing and the new adjustments are

- The heating curve for the existing system specify that the slabs should reach the specified final temperature after zone 1. The new

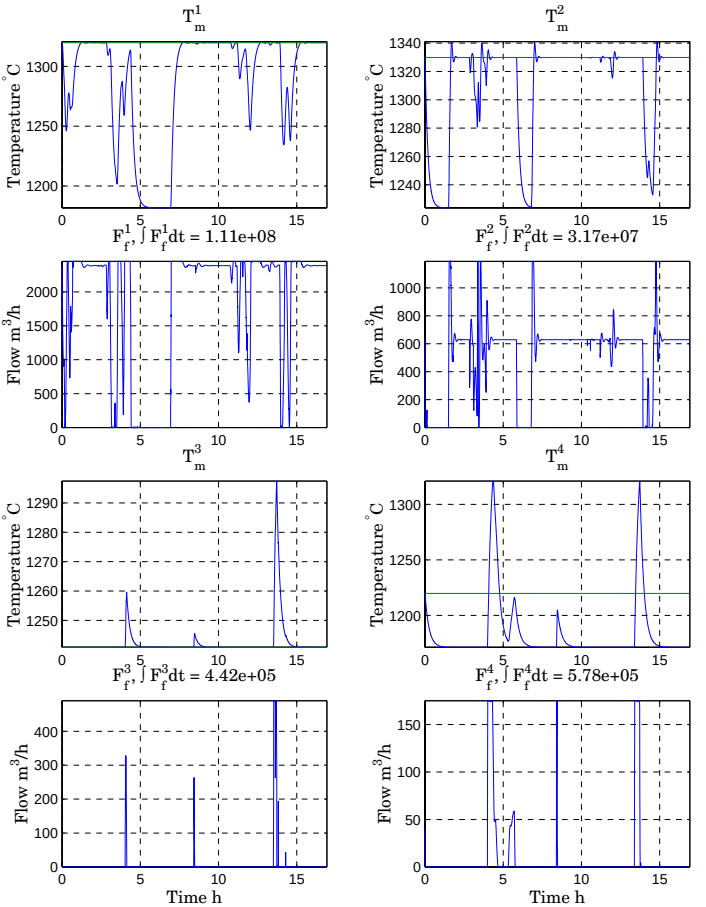

Figure 13.1 Fuel flows F_f^j and furnace temperatures T_m^j when the slab temperatures are controlled using the PI controller with the old parameters, heating curve, and feedforward tables. This figure should be compared with Figure 12.9.

heating curve specifies that this should happen after zone 2, see Section 11.2.

- The existing feedforward tables specifies almost identical temperatures for the different speeds. The new feedforward tables contain significantly different zone temperatures for the specified nominal speeds.

- Comparing the new and existing controller coefficients we see that

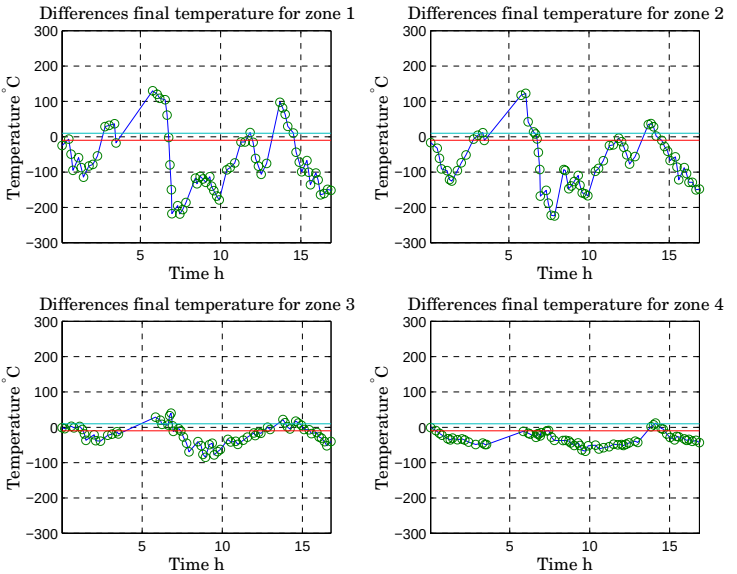

Figure 13.2 Final temperature errors Y_i^j for the four zones when the slab temperatures are controlled by PI controller with the old parameters, heating curve and feedforward tables. In the following we have μ^j and σ^j as the mean value and the standard deviation of the error for zone j respectively. The results are $\mu^1 = -67.2$, $\sigma^1 = 88.0$, $\mu^2 = -69.1$, $\sigma^2 = 73.0$, $\mu^3 = -19.9$, $\sigma^3 = 27.7$, $\mu^4 = -33.2$, $\sigma^4 = 17.7$. The horizontal lines around $Y_i^j = 0$ marks a heating error of ± 10°C. This figure should be compared with Figure 12.10 and Table 12.1.

the new proportional gain is a factor 2 higher than the existing gains and that the new integral gains are more than a factor 10 lower than the existing ones.

The results of the simulations are shown in Figures 13.1 and 13.2.

Comparing Figures 13.1 and 13.2 for the existing controller parameters to Figures 12.9 and 12.10 for the new parameters we see that the errors for the new parameters are significantly smaller than with the existing ones. This is a result of the new feedforward tables and controller coefficients—other simulations show that the existing coefficients results in a poorly damped response. The later heating due to the new heating curve will result in a larger temperature gradient, but the FEM simulations indicate that it will only yield an increase of approximately 2°C which is not considered as a significant change. The total energy consumption of all four zones is 1.44×10^8 m^3 is significantly lower than the FOCS-controller with the new parameters, but note that slab temperatures of zones 3 and 4 are significantly lower than specified for the FOCS-controller with the old settings.

13.2 Results and Experiences

Several new experiences were gained when the new parameters were implemented. First of all the heating curve is very critical. Three different heating curves have been implemented. The two first heating curves ending after zone 3 and in the middle of zone 3 was implemented before the heating curve presented in Chapter 11 but none of them worked well. This indicates that the present heating curve is the limit of what is feasible for proper furnace operation.

During the experiments the author realized that the furnace was operated partially as a batch furnace. The reason for this practice is that the furnace no. 1, a pusher furnace with smaller capacity, can only be operated 15 minutes consecutive minutes every hour, which leaves 45 minutes to operation of furnace no. 2.

The result of this practice is that furnace no. 2 is operated at an elevated speed for approximately 45 minutes and then rests for approximately 15 minutes. The furnace will only be able to deliver hot slabs at the elevated speed if the slabs of zones 3 and 4 are at the specified temperature when the furnace operation starts after the break. The fact that the capacities of zones 3 and 4 are small compared to zones 1 and 2 amplifies this effect. This is one of the explanations for why the old heating curve ends after zone 1 and why the author was forced to adjust the new heating curve to end after zone 2, in practice zones 1, 2, and 3 are used as buffers of hot steel at high slab speeds. Zone 3 is then used as the last resort if the slabs fail to follow the heating curve due to a too large slab speed.

It is not possible for the furnace to heat the slabs at the average speed as specified by either the old or the new heating curve. Actually, the heat-

ing curve is computed using an average residence time of 6.4 hours, see Section 11.2. This is done to ensure that a buffer of hot slabs is created whenever the furnace is stopped.

When implementing the feedforward tables the temperatures of zones 3 and 4 were adjusted to obtain a higher furnace temperature. The adjustment was done to obtain a larger furnace pressure in the end of the furnace, which is an advantage according to the operators' experience. This is in good agreement with the heat losses from the slab bottom surface in the last part of the furnace described in Section 10.2.

Using the latest pig runs a systematic error of −20°C was found in the final temperature of the FOCS system and the desired temperature was therefore adjusted form 1120°C to 1140°C to counteract this offset. The control algorithm was furthermore modified to use the center temperature for temperature control instead of the mean temperature, since the pig runs showed that the latter value is not correct in the first part of the heating interval.

When implementing the controller parameters the author realized that coupling between slab temperature and furnace temperature is significant when cold slabs enter the zone. This was seen from the fact that if zone 1 reacted too late, when cold slabs entered the zone, it was not possible to obtain a proper zone temperature even at full fuel flow. The result was improper heating of the slabs. Since the coupling between slab temperature and zone temperature is not included in the model this problem was not revealed by the simulations. The operators were aware of this fact and complained about the reaction with the old settings of the control system, which after a stop first reacted when zone 1 were half filled with cold slabs.

The reason for the delayed response of zone 1 was that the slab temperature controller was allowed to reduce the furnace temperature specified by the feedforward tables by 100°C when computing the set point for the furnace temperature controller. Due to the batch oriented operation of the furnace the delay temperatures are kept high to ensure heating of the slabs during the stops. The result was that the slab temperature controller reduced the furnace temperature down to its lowest permissible limit and when cold slabs entered the zone the integral part kept down the furnace temperature reference until the error went below zero—which occurred when the zone was half filled with cold slabs. This is probably the reason for the old heating curve being rather extreme, since this ensures hot slabs despite the slow reaction of the slab temperature controller of zone 1. The reaction of the other furnace zones are of less importance since they are shorter and have smaller capacity, and therefore the reaction of zone 1 is critical compared to the reaction of the other furnace zones.

When the new parameters were implemented the lower output limit of

the slab temperature controller was adjusted form −100°C to −60°C and this, together with the new controller parameters with a much smaller integral gain and a double as large proportional gain yielded an instantaneous reaction of zone 1 when cold slabs entered the zone. Note that the faster behavior of the controller was predicted by the simulations of the furnace operation. However, for zone 3 we decreased the maximal permitted adjustment from −50°C to −20°C and increased the integral time from approximately 500 s to 2500 s to obtain an immediate reaction when cold slabs entered the zone despite the other slabs in the zone being too hot. This is similar to the desired control action of zone 1.

The faster response of the slab temperature control system made it possible to use the new heating curve, which results in a later heating and therefore ought to lead to a smaller energy consumption. The slab temperatures follow the heating curve better than before and the temperatures after a stop are now closer to the heating curve than before. At the same time the operators are now satisfied with the reaction of the furnace control system and the furnace capacity is increased.

It is unfortunately hard to obtain dynamic plots from the FOCS system, but it is possible to obtain slab temperatures, slab weight, and discharge time from the production control systems. The result of the experiments are shown in Figures 13.3, 13.4, and 13.5.

The plot of the slab temperatures at time for discharge in Figure 13.3 shows that the mean temperature has not been affected significantly by the experiments, the reasons for the rather large value (approximately 1160°C) is a systematic error of 20°C of the slab temperature calculation and the high furnace temperatures in zones 3 and 4 to ensure proper furnace pressure.

The temperature gradients shown in Figure 13.4 shows that the gradients has been large at two instants in February 1999. This corresponds with the two non optimal heating curves mentioned in the beginning of this section. Note that the temperature now are at the previous level, despite the later heating curve.

The plot of the discharged tons per day from furnace no. 2 shows a significant increase of discharged tons in the beginning of March 1999. Considering the transient of the filter this corresponds well with the time for the implementation new heating curve and controller coefficients, which took place between March 4th and March 11th. Before the adjustments the production level is between 1350 tons/day and 1700 tons/day and after the adjustments it is increased to lie between 1550 tons/day and 1900 tons/day. Bearing in mind the short time interval for evaluation of the performance this indicates an increase in productivity of approximately 10%.

In 1998 the average natural gas consumption was 37.3 m^3/ton, in

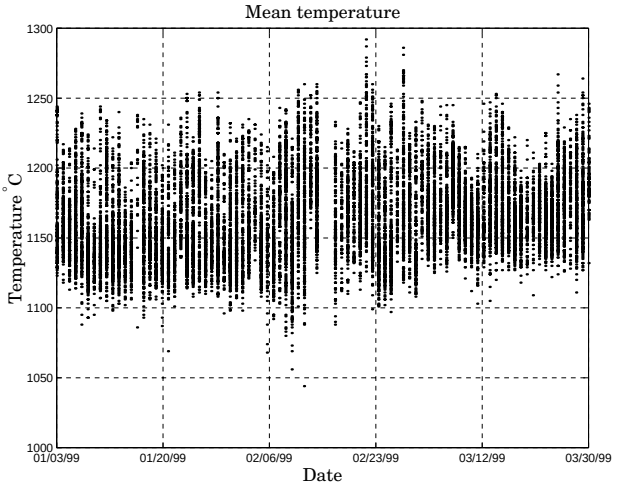

Figure 13.3 Mean temperature of the slabs discharged from furnace no. 2 at The Danish Steel Works Ltd. from January 3rd to March 30 1999. The slab temperatures are obtained from the temperature calculation of the FOCS system. Note the American date format.

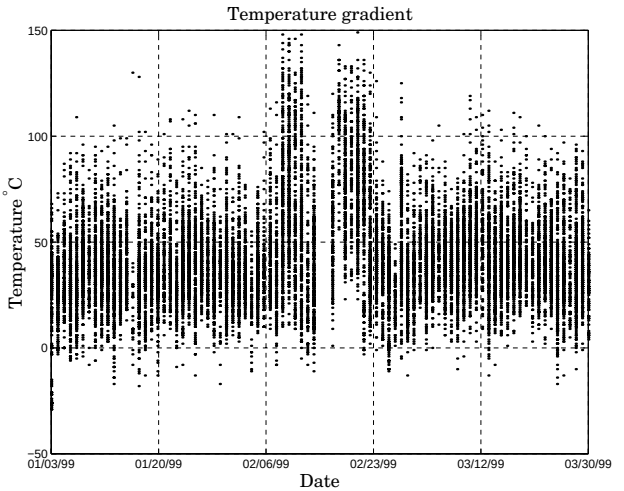

Figure 13.4 Temperature gradient of the slabs discharged from furnace no. 2 at The Danish Steel Works Ltd. from January 3rd to March 30 1999. The slab temperatures are obtained from the temperature calculation of the FOCS system. Note the American date format.

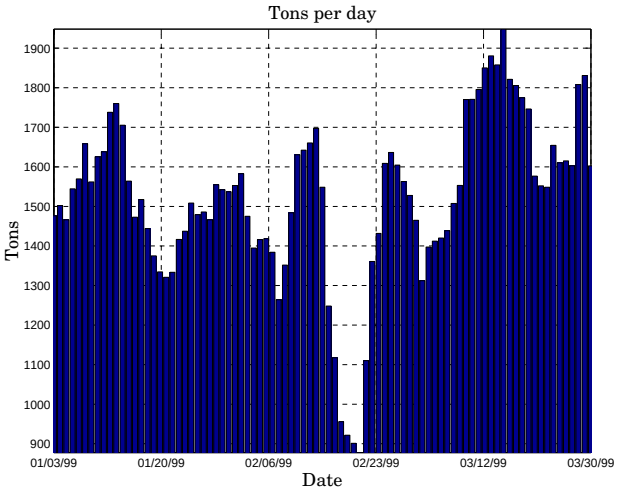

Figure 13.5 Slab weight per day discharged from furnace no. 2 at The Danish Steel Works Ltd. from January 3rd to March 30 1999. The data are filtered using a FIR filter computing the mean value over 7 days. Note the American date format.

January 1999 it was 42.2 m^3/ton, in February 1999 it was 38.1 m^3/ton, and in March 1999 it was 36.3 m^3/ton. The author has been warned that the energy consumption of the furnace varies considerably and we therefore only dare to conclude that the new settings of the FOCS system not has caused the energy consumption to increase drastically.

13.3 What Is Left?

At the time being (April 1999) it still remains to adjust the heating strategy for 200 mm slabs, which has not been discussed, the reason being that the heating of the 260 mm slabs is the critical case with respect to furnace capacity. The strategy with for the 200 mm slabs should be coordinated with the strategy for the 260 mm slabs, to obtain a unified heating strategy for the two slab thicknesses.

Another thing which remains to be tuned is the delay strategies. Here the solution to the differential equation for the heating curve (11.4) for $v_{s0} = 0$ can be used for obtaining the temperatures necessary to keep the energy content of the slabs in a zone at a constant level during a stop. The models for the furnace temperatures (10.5) can be used for determining the zone temperatures for different stop times.

13.4 Conclusions

This chapter contains a description of the implementation of the heating curve, feedforward table and controller parameters of the FOCS system derived in Chapter 11.

Simulation results indicate that the new parameters yields a better control of the slab temperatures, and this is verified when implementing the controller coefficients, feedforward tables, and heating curve. The implementation, however, also shows that saturation is a problem when cold slabs enter a zone, and this is not revealed by the simulations.

The main result of the implementation is that an increase in the response speed of zone 1 has resulted in a larger furnace capacity and that a more energy economical heating curve can be used. The furnace operators are very satisfied with the new setting and investigations show that the mean value and temperature gradient of the slabs are unaffected by the new settings, but that the furnace capacity seems to have been increased by approximately 10%. It does not seem like the adjustments have caused the energy consumption of the furnace to increase.

Remaining work on the adjustment of the FOCS system consists of design of a heating strategy for 200 mm slabs and the tuning of the delay tables used during stops.

14

Conclusions

The title of this thesis is "Modeling and Control of Plate Mill Processes" and two such processes have been modeled and controlled, namely the rolling mill and the reheat furnace. It is time to give the concluding remarks on the work done, the obtained results, and the experience gained during the work. The chapter will be ended by suggestions for how the work can be continued.

14.1 What Has Been Done?

The two first chapters of the thesis contain a description and analysis of the thickness control problem. It is here concluded that the main disturbances of the system is hardness variations of the plates and the task of the thickness control is to keep the plate thickness constant despite these disturbances. The classical solution is analyzed and it is concluded that it can't handle asymmetric hardness variations and that the estimation of the controlled output introduces stability problems.

In the modeling of the rolling mill a dynamical and multivariable model for the thickness control system is derived. The model consists of a nonlinear model for the hydraulic thickness control actuators and a linear multivariable model for the rolling stand. Since the plate thickness is not measured during rolling an observer is developed for estimation of the plate thickness. The data collection is carried out by measuring the key variables of the rolling mill during normal production and then measuring the plate thickness afterwards using a specially designed measurement device. Afterwards, the data sets are joined by formulating and solving an optimization problem. This has given a unique set of data for the system identification.

The parameters of the model for the rolling mill are found using the collected data. A set of constant nominal parameters are found for the hydraulic positioning systems, where good agreement between model and

data is obtained. Due to variations in the plate hardness during rolling there is poor agreement between model and data when time invariant methods are used for the system identification. The hardness variations are included in the extra signal available for the observer, and therefore good agreement between model and data is obtained in this case.

The model is used for designing a nonlinear multivariable thickness control algorithm. The algorithm is evaluated using computer simulations and it is found that the new controller is able to handle the asymmetric case and gives a more accurate thickness control compared to the existing control system. The new control strategy is also found to be stable for the relevant parameter variations. The performance is also acceptable for the different material characteristics of the steel plate found in the system identification.

The next part of the thesis concerning slab temperature control is started with a description of the reheat furnace where it is concluded that the main disturbance in the furnace operation is variations of the slab speed. The task of the slab temperature control problem is to ensure a high furnace throughput, and a proper heating quality while keeping the energy consumption at a minimum.

The data collection for the modeling of the slab temperature is carried out by the pig, which is a transportable data collection device used for measuring the slab temperature. While the pig is transported through the furnace the key furnace variables are collected by the slab temperature control system. The data are used for identifying three models for the reheat furnace: a linear model for the furnace temperatures, a nonlinear ODE model for the slab temperature, and a nonlinear PDE model for the slab temperature distribution. Fair agreement is obtained for the furnace model while good agreement is obtained for the two slab temperature models.

A new way of obtaining parameters for the slab temperature control system at The Danish Steel Works Ltd. is described in the thesis. The slab temperature controller design is started by generating the heating curve, which is the slab temperature reference to be followed as the slabs are transported through the furnace. From the heating curve and model for the slab temperatures a feedforward table is generated. Furthermore, a first order model for the slab temperatures is generated using linearization and averaging. The linear model is used for finding parameters for the PI-regulators controlling the slab temperatures. In the final part of the controller design a nonlinear controller is designed using the nonlinear ODE for the slab temperatures and it is shown that the nonlinear controller is globally asymptotically stable.

The robustness against parameter variations and the performance of the linear and nonlinear controller are investigated using computer simu-

lations. The simulations show that none of the controllers are sensitive to parameter variations and that the performance of the nonlinear controller is superior to the performance of the linear controller. The price paid is faster variations of the control signal.

The heating curve, feedforward tables, and the controller parameters found in the design have been implemented in the slab temperature control system at The Danish Steel Works Ltd. The new controller parameters have introduced a faster reaction of the furnace when cold slabs are charged into the furnace after a stop, this leads to increased furnace capacity. The faster reaction also have made a later heating possible which should give a reduction in the furnace energy consumption. The furnace operators are very satisfied with the performance of the slab temperature control system and the experimental results indicate a 10% increase in furnace capacity, with unchanged mean temperatures and temperature gradients. Data from the reheat furnace no. 2 indicate that the energy consumption has not been increased by the adjustments.

14.2 Results

The results of the work in this thesis are models and controllers for the rolling mill and reheat furnace derived using data from the processes at The Danish Steel Works Ltd.

For the rolling mill the model for the hydraulic systems is nonlinear and is more or less standard, the contribution of the work presented here is that the model is derived using real data from a rolling mill. The model for the mill frame and plate is new and it covers the multivariable nature of rolling process, this model is also derived using real data from the mill.

The thickness controller is a second order multivariable nonlinear control law, able to handle the nonlinearity of the hydraulic systems and asymmetric material conditions of the plates. The controller can be simplified to PI controller for a first implementation, if necessary. To have a multivariable controller ready for implementation better data are needed for a more complete investigation of the multivariable nature of the rolling process.

Three models have been derived for the reheat furnace. A simple model for furnace temperature and two advanced models for the slab temperature. All models are derived using data from the reheat furnace at The Danish Steel Works Ltd. The furnace model is used for the computer simulations, and the first model for the slab temperature can be used for evaluating the slab center temperature, while the other can be used for evaluating the slab temperature gradients, which are important for proper operation of the rolling mill

For the slab temperature control problem we have two designs. The first design is a PI-controller with the same structure as the slab temperature controller at The Danish Steel Works Ltd. This design has been verified using experiments. The second design is a nonlinear controller based on the nonlinear model for the slab center temperature. If a model is available this controller is easier to design and the simulations indicate a better performance, but a nonlinear solver is required to implement the control law.

As mentioned in Chapter 1 the reheat furnace and the rolling mill are two quite different processes. The author has, however, experienced several factors common for the control of the two processes

- Given proper data and the necessary time it has been possible to derive models with few parameters that give reasonable predictions of the process behavior. The models have been used for tuning the control algorithms and experimental results from the furnace control system show a performance improvement.
- Even if advanced controllers are used in this thesis it seems like the existing PI controllers after the optimization does a job almost equally good. This especially seems to be the case with the furnace control system.
- The knowledge gained in the work with the modeling and control of a process is valuable in other contexts. One example is the discovery that the slabs are only cooled in the last part of the furnace when deriving the PDE model for the slab temperature and another example is the measurement of the thickness variations introduced by the cold zones of the roller tables of the rolling mill.

As a final comment on the work done it should be mentioned that in the thickness control the main effort lies in the derivation and identification of the multivariable model for the rolling mill since these models were not available when the work on the thickness control was started. The initial situation for the temperature control problem was that both data and models already were available for the slab temperature control. Since implementation, and experiments, furthermore, were possible in this case this is the reason for the controller design being the main subject in the slab temperature control part of the thesis.

14.3 Future Work

If the work presented in this thesis should be continued several open points are available for future work

- **Improvement of the rolling mill model**. The crucial thing here is to obtain data with better excitation. This could be done by special experiments and would make a better determination of, for instance, the multivariable structure and friction between roll pack and rolling stand possible.
- **Implementation of simplified thickness control law**. Using the mean value of the plate thickness the multivariable thickness algorithm can be turned into a nonlinear SISO PI-controller. The implementation of this controller has been going on for a while, the hardware is implemented an the program is being developed.
- **Continuation of work with FOCS system**. This work is actually already going on in connection with a project done by MEFOS where an adaption algorithm for the FOCS temperature estimator will be implemented at The Danish Steel Works Ltd. . The measurement is obtained from radiation pyrometers near the rolling mill.
- **Implementation of a nonlinear slab temperature controller**. It seems that the nonlinear controller giver better results and is easier to design. It would be interesting to implement it and see if the controller also works better in practice.
- **Implementation of multivariable plate thickness controller**. This is planned to be a part of an ECSC project starting medio 1999. The plan is to implement the thickness control law on the rolling mill at The Danish Steel Works Ltd. It is necessary to improve the multivariable models for the rolling mill before the control law is implemented.
- **Development of an advanced furnace model**. As pointed out several places in the thesis the linear model of the furnace temperature could be improved considerably. An important part to include is the interaction between the furnace temperature and the temperature of the slabs.

The author plans continue the work on one or more of the above items and hopes that it will be as much fun as doing the work presented in this thesis.

15

Bibliography

ABILDGAARD, O. (1991): *Issues in Unified Optimization of Systems and Controllers*. PhD thesis, Control Engineering Institute, Technical University of Denmark.

ANDERSSON, M. (1994): *Object-Oriented Modeling and Simulation of Hybrid Systems*. PhD thesis, Department of Automatic Control, Lund Institute of Technology.

ASADA, Y. *et al.* (1986): "New feedforward gauge control method for cold tandem mills." *IFAC Proceedings of the 1986 Automation in Mining Mineral and Metal Processing Conference*.

ÅSTRÖM, K. J. and P. EYKHOFF (1971): "System identification – a survey." *Automatica*, **7**, pp. 123 – 162.

ÅSTRÖM, K. J. and B. WITTENMARK (1995): *Adaptive control*. Addison-Wesley Publishing Company.

ÅSTRÖM, K. J. and B. WITTENMARK (1997): *Computer-Controlled Systems*, third edition. Information and System Sciences Series. Prentice-Hall.

ATORI, H. *et al.* (1992): "Application of two-degree-of-freedom control system to automatic gauge control." *American Control Conference*.

BAEHR, H. D. and K. STEPHAN (1996): *Wärme- und Stoffübertragung*, 2 edition. Springer Verlag.

BENGTSSON, G. (1994): *Manual for μ-controller*. First Control Systems AB, Västerås, Sweden.

BRYANT, G. F., P. D. SPOONER, and J.M.CALEY (1975): "Design of tandem mill dynamic control schemes." *Proceedings of the 5th IFAC World Congress*.

CHOI, S. G., M. A. JOHNSON, and M. J. GRIMBLE (1994): "Polynomial LQG control of back-up-roll eccentricity gauge variations in cold rolling mills." *Automatica*, **30:6**, pp. 975–992.

CRANDALL, S. H., N. C. DAHL, and T. J. LARDNER (1978): *An Introduction to the Mechanics of Solids*. McGraw Hill.

CUMMING, I. G. (1972): "On-line identification of a steel mill." *Automatica*, **8**, pp. 531 – 541.

DAVIES, D. A. *et al.* (1983): "Control of gage, width, profile and shape on rautatuukki's 3.6-meter plate mill." *Iron and Steel Engineer*, December.

DESOER, C. A. and M. VIDYASAGAR (1975): *Feedback Systems: Input-Output Properties*. Academic Press.

EDWARDS, W. J. (1978): "Design of entry strip thickness controls for tandem cold mills." *Automatica*, **14**, pp. 429–441.

EDWARDS, W. J. *et al.* (1987): "Roll eccentricity control for strip rolling mills." *Proceedings of the IFAC 10th Triennial World Congress*.

FERGUSON, J. J. *et al.* (1986): "Modern hot-strip mill thickness control." *IEEE Transactions on Industry Applications 1986*, September/October.

FODA, S. and P. AGATHOKLIS (1992): "Control of the metal rolling process. a multidimensional system approach." *Journal of the Franklin Institute*, **329:2**, pp. 317–332.

FONTANA, P., A. BOGGIANO, A. FURINGHETTI, G. CABARAS, and C. A. SIMONCINI (1983): "An advanced computer control system for reheat furnaces." *Iron and Steel Engineer*, pp. 55 – 83.

FUJII, S. and M. SAITO (1975): "A new mathematical model for plate mill control." *Proceedings of the 5th IFAC World Congress*.

GINZBURG, V. B. (1984): "Dynamic characteristics of automatic control system with hydraulic actuators." *Iron and Steel Engineer*.

GOU, R.-M. (1991): "Evaluation of dynamic characteristics of hagc system." *Iron and Steel Engineer*, July.

GRIFFITHS, E. (1953): *Physical constants of some commercial steels at elevated temperatures*. Butterworths Scientific Publications, London, UK.

GRIMBLE, M. J. and M. A. JOHNSON (1988): *Optimal Control and Stocastic Estimation. Theory and Applications.*, vol. II, chapter 13.4 Gauge Control and the Back-up Roll Eccentricity Problem. John Wiley & Sons.

GUO, R.-M. (1994): "Material damping effect in cold rolling process." *Iron and Steel Engineer*, December.

GUSTAVSSON, I. (1975): "Survey of applications of identification in chemical and physical processes." *Automatica*, **11**, pp. 3–24.

H. E. PIKE, J. and S. J. CITRON (1970): "Optimization studies of a slab reheating furnace." *Automatica*, **6**, pp. 41 – 50.

HANSEN, E. B. (1993): *Variationsregning (Eng: Calculus of Variations)*. Polyteknisk Forlag.

HARVEY, C. A. and G. STEIN (1978): "Quadratic weights for asymptotic regulator properties." *IEEE Transactions on Automatic Control*, **AC-23:3**, pp. 378 – 387.

HOLLANDER, F. and S. P. A. ZUURBIER (1982): "Design, development and performance of on-line computer control in a 3-zone reheating furnace." *Iron and Steel Engineer*, January, pp. 44 – 52.

HUZYAK, P. and T. L. GERBER (1984): "Design and application of hydraulic gap control systems." *Iron and Steel Engineer*, August.

ISIDORI, A. (1989): *Nonlinear Control Systems*, second edition. Springer-Verlag.

JOHANSSON, R. (1993): *System Modeling and Identification*. Prentice Hall.

KAILATH, T. (1980): *Linear Systems*. Prentice-Hall.

KITAMURA, A. *et al.* (1987): "Recursive identification technique for roll eccentricity control." *IFAC Proceedings of the 10th Triennial World Congress*.

KOKAI *et al.* (1985): "Factors affecting the accuracy of plate tickness and their influences on plate flatness." *Transactions ISIJ*, **25**.

KUSTERS, A. and G. A. J. M. VAN DITZHUIJZEN (1994): "MIMO system identification of slab reheating furnace." *Proceedings of the IEEE Conference on Control Applications*, **3**, pp. 1557 – 1563.

LEDEN, B. (1985): "Processtyrning af ämnesvärmningsugnar." Technical Report. MEFOS.

LEDEN, B. (1986): "A control system for fuel optimization of reheating furnaces." *Scandinavican Journal of Metallurgy*, **15**, pp. 16 – 24.

LEDEN, B. (1999): *User's manual STEELTEMP-IE©*. MEFOS, Luleå.

LJUNG, L. (1991): *System Identification Toolbox*. The MathWorks, Inc.

MEIROVITCH, L. (1980): *Computational Methods in Structural Dynamics*. Sijthoff & Noordhoff.

MIDDLETON, R. H. and G. G. GOODWIN (1990): *Digital Control and Estimation. An Unified Approach.*, chapter 15 An Industial Case Study. Prentice Hall.

MIZUNO, K. (19??): "Multivariable nonlinear control system design for multistand rolling mill." *Hitachi Review*.

MOORE, B. C. (1976): "On the flexibility offered by state feedback in multivariable system beyond closed loop eigenvalue assignment." *IEEE Transactions on Automatic Control*, October, pp. 689 – 692.

NAKAGAWA, S. *et al.* (1990): "Gauge control system for hot strip finishing mill." In *Proceedings of the IEEE Conference on Decision and Control*, vol. 3.

NIJMEIJER, H. and A. VAN DER SCHAFT (1991): *Nonlinear Dynamic Control Systems*. Springer-Verlag.

PAUL, F. W. (1975): "A mathematical model for evaluation of hydraulic controlled cold rolling mills." *Proceedings of the 5th IFAC World Congress*.

PEDERSEN, L. M. (1993): "Plate thickness control of hot rolling mills." Technical Report ISRN LUTFD2/TFRT--7513--SE. Department of Automatic Control, Lund Institute of Technology.

PEDERSEN, L. M. (1994): "Identification of hydraulic system on rolling mill." In *Preprints ot the 10th IFAC Symposium on System Identification*, vol. 3, pp. 337 – 342.

PEDERSEN, L. M. (1995a): "Modeling and identification of hot rolling mill." In *Proceedings of 1995 American Control Conference*, vol. 5, pp. 3674 – 3678.

PEDERSEN, L. M. (1995b): "Multivariable thickness control of a hot rolling mill." Licentiate Thesis ISRN LUTFD2/TFRT--LUFTD2/TFRT--3214--SE--SE. Department of Automatic Control, Lund Institute of Technology, Sweden.

PEDERSEN, L. M. (1996): "Multivariable model for a hot rolling mill." The Control of Profile and Flatness. The Institute of Materials. For a copy of this reference, please contact the author.

PEDERSEN, L. M. (1998): "Slab temperature control for reheating furnaces." Technical Report ISRN LUTFD2/TFRT--LUTFD2/TFRT--7581--SE--SE. Department of Automatic Control, Lund Institute of Technology, Sweden.

PEDERSEN, L. M. and B. WITTENMARK (1996): "Multivariable controller design for hot rolling mill." In *Proceedings of the 13th Trennial IFAC World Congress*, vol. M, pp. 475 – 480. IFAC.

PEDERSEN, L. M. and B. WITTENMARK (1998a): "Multivariable controller design for hot rolling mill." *IEEE Journal of Control Systems Technology*.

PEDERSEN, L. M. and B. WITTENMARK (1998b): "On the reheat furnace control problem." In *Proceedings of 1998 American Control Conference*.

PEDERSEN, L. M. and B. WITTENMARK (1998c): "Optimization of thickness control system." In *Reglermöte '98*. Lund.

PEDERSEN, L. M. and B. WITTENMARK (1998d): "Thickness control for a plate mill." In *Automation in Mining, Mineral, and Metal Processing*. IFAC.

PEDERSEN, L. M. and B. WITTENMARK (1999): "Development of advanced furnace control algorithm." *Steel Technology International*, pp. 149 – 152.

PICHLER, R. and R. LANGER (1989): "Automation concept for the control of reheating furnaces in rolling mills." *Metallurgical Plant and Technology*, pp. 68 – 75.

RICHTER, F. (1973): *Die wichtigsten physikalischen Eigenshaften von 52 Eisenwerkstoffen*, vol. 8. Verlag Stahleisen M. B. H., Düsseldorf, Germany.

RIXIN, L. and N. BAOLIN (1992): "Mathematical model for dynamic operation and optimum control of pusher type slab reheating furnace." *Industrial Heating*, March, pp. 60 – 62.

ROBERTS, W. L. (1983): *Hot Rolling of Steel*, vol. 10 of *Manufacturing Engineering and Materials Processing*. Marcel Dekker.

SAITO, M. *et al.* (1981): "High-accuracy plate thickness control." *Proceedings of the IFAC 8th Triennial World Congress*.

SCHURKO, R. J., C. WEINSTEIN, M. K. HANNE, and D. J. PELLECCHIA (1987): "Computer control of reheat furnaces: A comparison of strategies and applications." *Iron and Steel Engineer*, May, pp. 37 – 42.

SIEGEL, R. and J. R. HOWELL (1992): *Thermal Radiation Heat Transfer*, third edition. Taylor & Francis.

SLOTINE, J.-J. E. and W. LI (1991): *Applied Nonlinear Control*. Prentice Hall, Inc.

STEIN, G. (1979): "Generalized quadratic weights for asymptotic regulator properties." *IEEE Transactions on Automatic Control*, **AC-24:4**, pp. 559 – 565.

STONE, M. D. (1969): "Backup roll bending – for crown and gauge control." *Iron and Steel Engineer*, December, pp. 69 – 87.

TEOH, E. K., G. C. GOODWIN, W. J. EDWARDS, and R. G. DAVIES (1984): "An improved strip thickness controller for a rolling mill." *Proceedings of the IFAC 9th Triennial World Congress, vol. 4.*

TROSTMANN, E. (1987): *Hydraulisk Styring (Eng: Hydraulic Control).* Instituttet for Styreteknik, DTH.

WOOD, G. E. *et al.* (1977): "Mill modulus variation and hysteresis – their effect on hot strip mill agc." *Iron and Steel Engineer*, January.

YAMASHITA, A., Y. MISAKA, N. HASE, and R. TAKAHASHI (1976): "Development of feedformward agc for 70" hot strip mill at Kashima Steel Works." *The Sumitomo Search, no. 16*, November, pp. 34–39.

YEH, T.-H. *et al.* (1991): "The development of new backup roll eccentricity compensation system for the plate mill." *China Steel; Technical Report.*

ZELTKALNS, A. *et al.* (1977): "Force sensing in rolling mills." *Iron and Steel Engineer*, January.

Notations

A cross sectional area of roll pack, 43
A^j system matrix for linearized slab temperature model, 138
A_1 area in hydraulic system corresponding to p_1, 35
A_2 area in hydraulic system corresponding to p_2, 35
A_3 area in hydraulic system corresponding to p_3, 35
A_4 area of grease piston, 35
A_c, B_c, C_c, D_c state space matrices for model for rolling stand, 49
B^j input matrix for linearized slab temperature model, 138
C^j output matrix for linearized slab temperature model, 138
C_F^j furnace temperature controller for zone j, 143
C_S^j slab temperature controller for zone j, 140
C_v transfer function for traditional thickness controller, 26
E Young's modulus for steel, 43
E^j vector of enthalpy errors for zone j, 149
E_i^j control error for slab i in zone j for nonlinear controller, 146
E_z^j thermal energy content of furnace zone j, 112
F column vector of heat losses from slab, 129
F matrix used for calculating f_c, 50
F_f^j fuel flow of the burners of zone j, 108
G diagonal matrix of material properties of slab, 129
G_F^j closed loop transfer function for furnace temperature for zone j, 143
G_S^j closed loop transfer function for furnace temperature for zone j, 143
G_h transfer function for hydraulic systems controlled by C_z, 25
G_t transfer function of thickness control system, 27
I second moment of area for the work roll, 43
K mill spring coefficient, 24
K^j input matrix for v_s for linearized slab temperature model, 138
K_{iF} integral gain of furnace temperature controller, 143
K_{iS} integral gain of slab temperature controller, 143
K_{pF} proportional gain of furnace temperature controller, 143

K_{pS} proportional gain of slab temperature controller, 143
L state feedback matrix for new thickness controller, 85
P_S^j averaged system for slab temperatures of zone j, 141
P_s supply oil pressure for hydraulic systems, 34
Q weighting matrix for states in eigenspace design, 87
Q_1 flow into left side of oil cylinder, 34
Q_2 flow into right side of oil cylinder, 34
R weighting matrix for control signal in eigenspace design, 87
T temperature profile of slab in thickness direction, 102
T^j state vector of the slab temperatures of zone j, 129
T_a furnace atmosphere temperature near slab top surface, 108
T_b temperature below slab bottom surface, 102
T_i^j center temperature of the i'th slab in the j'th zone, 128
T_m^j furnace zone control temperature of the j'th zone, 101
T_r heating curve, 131
T_s temperature of furnace surroundings, 104
T_t profile of furnace roof temperature, 101
$T_{10\%}$ slab temperature 10% of slab thickness from top surface, 109
$T_{50\%}$ slab temperature 50% of slab thickness from top surface, 109
$T_{90\%}$ slab temperature 90% of slab thickness from top surface, 109
T_{avg} mean temperature of FEM simulations at discharge time, 135
T_{ff}^j setpoint from feedforward tables for zone j, 142
T_{in} initial slab temperature, 132
T_{m0}^j nominal furnace temperatures, 132
$T_{m_{max}}^j$ upper furnace temperature limit for zone j, 133
$T_{m_{min}}^j$ lower furnace temperature limit for zone j, 133
T_{mr}^j furnace temperature reference for zone j, 131
T_{out} desired final slab temperature, 133
U column vector of heat inputs to slab, 129
Y^j vector of temperature errors for zone j, 138
Y_i^j temperature error of the i'th slab in zone j, 137
ΔT temperature gradient of FEM simulations discharge time, 135
$\Gamma_1, \ldots, \Gamma_6$ matrices found in the modeling of the rolling stand, 48
Φ matrix used for calculating v_c and v_e, 52
β_1, β_2 solution of equation for finding the eigenfunctions ϕ_1 and ϕ_2, 46
δ Kronecker function, 48
$\dot{m}_s$ air mass flow through stack, 104
ε function used in state transformation to obtain u, 44
ε_t it the emissivity of slab top surface, 102
η scaling factor for $\overline{P}_s$ to find p_2, 37
G_{v_c} transfer function relating thickness difference to position difference, 70

$\grave{\omega}_n$ undamped natural frequency for $\grave{G}_{v_c}$, 82
$\grave{f}$ difference between north and south rolling forces, 73
$\grave{k}_g$ steady state gain for $\grave{G}_{v_c}$, 82
$\grave{v}_c$ half the difference between north and south thickness from model, 70
$\grave{z}$ half the difference between north and south roll positions, 70
$\hat{u}$ approximate solution for u, 46
κ time constant for feedback linearized hydraulic systems, 84
λ heat conduction coefficient of steel, 102
λ_b heat conduction coefficient for bottom surface of slab, 102
λ_j j'th closed loop eigenvalue for rolling stand, 85
λ_t heat conduction coefficient for top surface of slab, 102
μ^j mean temperature error for zone j, 167
μ distance from plate edge for thicknesses used as controlled outputs, 51
ν_1, ν_2 finite right closed loop eigenvectors for rolling stand, 85
$\nu_3, \ldots, \nu_8$ infinite right closed loop eigenvectors for rolling stand, 85
ω_{nh} undamped natural frequency for G_h, 82
$\overline{G}_{v_c}$ transfer function relating mean value of thickness to mean value of positions, 70
$\overline{K}$ estimate of mill deflection coefficient K, 26
$\overline{P}_s$ oil supply pressure transformed to grease side, 36
$\overline{T}$ slab mean temperature, 103
$\overline{T}^j$ output of averaged system for zone j, 142
$\overline{Y}_i^j$ averaged temperature error for slab in zone j, 140
$\overline{\omega}_n$ undamped natural frequency for $\overline{G}_{v_c}$, 82
$\overline{\alpha}^j$ pole for averaged linear slab model in zone j, 141
$\overline{b}^j$ gain from furnace temperature for averaged linear slab model in zone j, 141
$\overline{f}$ mean value of rolling force, 24
$\overline{k}_g$ steady state gain for $\overline{G}_{v_c}$, 82
$\overline{r}$ reference value for $\overline{v}$ in traditional control, 26
$\overline{v}$ mean value of north and south plate thickness, 24
$\overline{v}_c$ mean value of north and south thickness from model, 70
$\overline{v}_e$ estimate of $\overline{v}$, 26
$\overline{v}_{-1}$ mean value of north and south plate thickness for previous pass, 24
$\overline{z}$ mean value of roll positions, 24
$\overline{z}_h$ output of linear model for hydraulic system, 25
$\overline{z}_r$ reference for $\overline{z}$ in traditional thickness control, 25
ϕ_1, ϕ_2 eigenfunctions obtained in the series expansion of u, 45
ρ mass density of steel, 43
σ^j standard deviation of temperature error for zone j, 167
σ Boltzmann's constant, 102

σ scalar control weight in eigenspace design, 87
θ_s prediction error for identification of south hydraulic system, 63
θ_n prediction error for identification of north hydraulic system, 61
φ variable used in analysis of thickness control system, 27
ϖ variation of the outgoing thickness v_d relative to the outgoing thickness v_{d-1}, 42
$\widehat{T}$ variable used in analysis of slab heating, 103
$\xi_1, \ldots, \xi_3$ variables of model for hydraulic systems, 61
$\xi_{n_1}, \ldots, \xi_{n_3}$ variables in the model for the north hydraulic system, 60
$\dot{i}$ i times partial derivation with respect to x, 43
a pole of linearized equation for T_l^j, 138
a_1^j parameter for heat transport due to hot air for zone j, 113
a_2^j parameter for heat input for burners in zone j, 113
a_3^j parameter for heat losses to surroundings for zone j, 113
a_4^j parameter for heat loss due to slab transport for zone j, 113
a_5^j offset for zone j in furnace temperature model, 113
a_m plate hardness used in traditional modeling, 24
a_{hn1} parameter for flow through servo valve in model for north hydraulic system, 37
a_{hn2} parameter for oil compressibility in model for north hydraulic system, 37
a_{hn3} parameter for leak flow in model for north hydraulic system, 37
a_{hs1} parameter for flow through servo valve in model for south hydraulic system, 37
a_{hs2} parameter for oil compressibility in model for south hydraulic system, 37
a_{hs3} parameter for leak flow in model for south hydraulic system, 37
a_{m1} plate hardness, 42
a_{m2} plate damping, 42
a_{m3} parameter of v_r in p_d, 42
b gain from T_m^j of linearized equation for T_l^j, 138
c_0^j integral gain of nonlinear controller for zone j, 147
c_1^j proportional gain of nonlinear controller for zone j, 147
c_p specific heat capacity of steel, 102
e white noise sequence with unit variance, 62
e_L^j linear error function for zone j, 137
e_V^j error function for nonlinear controller, 145
f heat losses of slab, 129
f vector of rolling forces, 23
f_c vector of forces calculated using model for rolling stand, 50
f_n rolling force at north side, 23
f_s rolling force at south side, 23

r_s reference for plate thickness at south edge, 86
r_{l_n} input for feedback linearization of north hydraulic system, 84
r_{l_s} input for feedback linearization of south hydraulic system, 89
t time, 24
t^j average time for the slab to pass through zone j, 140
u heat inputs to slab, 129
u new variable for obtaining homogeneous boundary conditions, 44
v vector of plate thicknesses, 23
v_c vector of thicknesses calculated using rolling stand model, 51
v_d plate thickness across plate width, 40
v_n plate thickness at north edge, 23
v_r rotational speed of work roll, 41
v_s plate thickness at south edge, 23
v_s slab speed, 101
v_z^j total air flow out from zone j, 112
v_{-1n} ingoing plate thickness at north edge, 24
v_{-1s} ingoing plate thickness at south edge, 24
v_{c_n} thickness at north side calculated using model for the rolling stand, 51
v_{c_s} thickness at south side calculated using model for the rolling stand, 51
v_{d-1} ingoing thickness across plate width, 41
v_{e_m} center thickness calculated using observer, 75
v_{e_n} plate thickness at the north edge found using observer, 52
v_{e_s} plate thickness at south edge found using observer, 52
v_{s0} nominal slab speed used for generating heating curve, 131
v_{si} nominal speeds of feedforward table, 135
w plate width, 24
x slab position, horizontal coordinate, 102
x position in width direction for rolling mill, 38
x^j vector of slab positions in zone j, 129
$x_1, \ldots, x_3$ positions for measurement of plate thickness v_d, 55
x_i^j position of the i'th slab in zone j, 111
x_v vector of servo valve positions, 51
x_{vn} position of servo valve glider of north hydraulic system, 34
x_{vrn} control signal for north servo valve, 56
x_{vrs} control signal for south servo valve, 56
x_{vs} position of servo valve glider of south hydraulic system, 51
y position in slab thickness direction, vertical coordinate, 102
y_c states of the model for the rolling stand, 49
y_e estimate of y_c found using observer, 50
y_n measured output for identification of south hydraulic system, 60
y_s measured output for identification of north hydraulic system, 63

y_{h_n} predicted output for identification of south hydraulic system, 61
y_{h_s} predicted output for identification of north hydraulic system, 63
z vector of grease piston positions, 23
z_d roll position across plate width, 40
z_n position of north grease piston, 23
z_s position of south grease piston, 23
z_t maximal value of position of grease piston, 37
z_{h_n} north position found using model for hydraulic system, 37
z_{h_s} south position found using model for hydraulic system, 51